

**UCSF**

**UC San Francisco Electronic Theses and Dissertations**

**Title**

Dissecting the ER stress-induced Apoptotic Pathway

**Permalink**

<https://escholarship.org/uc/item/9bq236rh>

**Author**

Austgen, Kathryn Maureen

**Publication Date**

2011

Peer reviewed|Thesis/dissertation

Dissecting the ER Stress-Induced Apoptotic Pathway

by

Kathryn M. Austgen

DISSERTATION

Submitted in partial satisfaction of the requirements for the degree of

DOCTOR OF PHILOSOPHY

in

Biomedical Sciences

in the

GRADUATE DIVISION

of the

UNIVERSITY OF CALIFORNIA, SAN FRANCISCO

Copyright (2011)

by

Kathryn Maureen Austgen

*I dedicate my dissertation to my best friend and husband, Sean Murphy. We made it! Thank you for keeping me smiling and enjoying all of the amazing things in my life.*

## ACKNOWLEDGEMENTS

First, I want to thank Scott Oakes and Don Ganem. Your tremendous guidance and advice has shaped me into the scientist and person I am today. Thank you for proving that a joint thesis could very easily be successful if everyone just plays nicely. I also want to thank the members of the Oakes lab (Nikki Reyes, John-Paul Upton, Emily Johnson, Debbie Caswell, and Eric Wang) for keeping me sane during my graduate studies with Kezar Pub nachos and wings, Ocean Beach bonfires, happy hours and Beirut tournaments. Also, thank you to the Ganemites (Michael Armanini, Carolina Arias, Priya Bellare, Sabine Bisson, Sanjay Chandriani, Henry Chang, Meghan Holdorf, Amy Kistler, Horng-Ru Lin, Alexis Madrid, Monika Martick, Jinjong Myoung, and Yiyang Xu) for being my twelve mini-professors. Thank you for your patience, wisdom, and advice.

Thank you to all of the amazing friends I have made at UCSF. I could not have achieved this without all of you and our endless wine nights and lots of delicious duck fat. You have inspired me to be a woman as gracefully balanced and accomplished as all of you.

To my parents, Peter and Priscilla, I do not tell you enough how much I appreciate your support of my crazy whims and how much it means to me that you are there to pick up the pieces when some of them do not turn out as well as I envisioned. I love you.

Lastly and most important, thank you to my boys, Sean and Walter.

Walter, you are the best snuggler and kisser in the world. Sean, you are my better, happier half. Thank you for supporting me through this and taking a few gray hairs (and losing a few) for the team. I love you with all my heart and am excited to see where life takes us together.

# **Dissecting the ER Stress-Induced Apoptotic Pathway**

by

Kathryn Maureen Austgen

## **ABSTRACT**

The endoplasmic reticulum (ER) is the main site in the cell for the folding and processing of secreted proteins. Various physiological and pathological processes can overwhelm the protein folding capacity of the ER. This condition, referred to as “ER stress,” typically triggers the activation of the Unfolded Protein Response Pathway (UPR). The activation of this pathway results in expansion of the ER, an increase in chaperone proteins, inhibition of cap-dependent translation, and if homeostasis is not reestablished, apoptosis.

ER stress-induced apoptosis, secondary to a buildup of misfolded proteins, leads to cell loss in a number of human degenerative diseases including ALS, Parkinson, and type II diabetes. In contrast, cancer cells and viruses manipulate the cytoprotective aspects of the UPR, aberrantly promoting cell survival. Therefore, understanding how to manipulate the UPR’s cytoprotective/cytotoxic threshold could lead to new treatment approaches for a wide variety of unrelated diseases.

Despite its important role in such a wide variety of diseases, the mechanisms underlying ER stress-induced apoptosis are poorly understood. Utilizing an unbiased biochemical system, I have identified the ER stress-induced

pro-apoptotic effectors that signal Bax and Bak at the mitochondrion, BID and CRK, and the mechanisms behind their activation up irremediable ER stress. In addition, the study of viral manipulation of host machinery has historically provided great insight into cellular biology. Viral infection is a biologically relevant system in which to study the cytoprotective/cytotoxic threshold of the UPR. A large lytic virus, such as Kaposi's Sarcoma Herpes Virus (KSHV or HHV-8), must be able to increase the folding capacity of the ER in order to accommodate the acute influx of viral protein during replication, while coordinately inhibiting the apoptotic consequences of intense ER stress. In this study, I have determined that KSHV inhibits UPR signaling through the IRE1 transmembrane kinase/endoribonuclease during lytic infection and is able to expand the ER through a novel function. These findings reveal new insights into the cytoprotective/cytotoxic regulation of the UPR and novel functions of lytic KSHV. These findings have implications for many diseases aside from viral infection, including type II diabetes, cancer, and neurodegeneration.



## TABLE OF CONTENTS

Chapter 1: Introduction_____	1
References_____	12
Chapter 2: Proto-oncogene CRK is a pro-apoptotic BH3-only transducer of irremediable endoplasmic reticulum stress.	
Background_____	14
Results_____	15
Discussion_____	42
Materials and Methods_____	45
References_____	50
Chapter 3: Identification of the cysteine protease responsible for CRK cleavage upon irremediable endoplasmic reticulum stress.	
Background_____	52
Results and Discussion_____	56
Materials and Methods_____	67
References_____	69
Chapter 4: Lytically replicating Kaposi's Sarcoma Herpes Virus induces XBP1- independent ER expansion.	
Background_____	71
Results and Discussion_____	75
Materials and Methods_____	84
Acknowledgements_____	85

References	86
Chapter 5: Multiple Defects, including premature apoptosis, prevent KSHV replication in murine cells.	
Background	88
Results and Discussion	89
Materials and Method	103
References	106
Chapter 6: Purification and Identification of Glioblastoma secreted factor responsible for NK cell ligand upregulation on primary monocytes.	
Background	109
Results and Discussion	116
Materials and Methods	138
Acknowledgements	139
References	140
Chapter 7: Summary	
Novel components of the ER stress-induced apoptotic pathway	142
KSHV manipulation of the UPR	144
Identification of a novel function of LDH and its role in GBM immune evasion	146
References	148

## LIST OF TABLES

<b>Table 2.1</b> – Tryptic peptides detected by Mass spectrometry_____	20
<b>Table 2.2</b> – Plasmids used in Chapter 2_____	49
<b>Table 3.1</b> – Cathepsin and tissue localization_____	61
<b>Table 6.1</b> – NKG2D ligands_____	111
<b>Table 6.2</b> – Purification and activity concentration of Purification #1_____	121
<b>Table 6.3</b> – Mass spectrometry results of Purification #2_____	129
<b>Table 6.4</b> – LDH isoenzymes_____	133

## LIST OF FIGURES

<b>Figure 1.1:</b> The Unfolded Protein Response_____	2
<b>Figure 1.2:</b> IRE1 $\alpha$ RNase signaling outputs_____	4
<b>Figure 1.3:</b> Intrinsic Apoptosis_____	6
<b>Figure 1.4:</b> Kaposi's Sarcoma Clinical Presentation_____	8
<b>Figure 1.5:</b> KSHV Genome_____	9
<b>Figure 2.2:</b> Model of Cytochrome c releasing assay_____	17
<b>Figure 2.2:</b> Presence of CcRA in <i>bax</i> <sup>-/-</sup> <i>bak</i> <sup>-/-</sup> MEF S100_____	17
<b>Figure 2.3:</b> Purification and identification of CcRA_____	19
<b>Figure 2.4:</b> <i>Crk</i> <sup>-/-</sup> MEFs are resistant to ER stress-induced apoptosis_____	21
<b>Figure 2.5:</b> CRKI and/or CRKII restore <i>crk</i> <sup>-/-</sup> MEF sensitivity to ER stress-induced apoptosis_____	23
<b>Figure 2.6:</b> Characterization of stable CRKII <i>crk</i> <sup>-/-</sup> MEF rescue_____	24
<b>Figure 2.7:</b> Overexpression of CRK sensitizes wild-type MEFs to ER stress-induced apoptosis_____	25
<b>Figure 2.8:</b> CRKII (Y221) dephosphorylation_____	28
<b>Figure 2.9:</b> CRKII (Y221) dephosphorylation is PTP1B-independent_____	29
<b>Figure 2.10:</b> CRKII is cleaved upon irremediable ER stress_____	31
<b>Figure 2.11:</b> CRKI is cleaved upon irremediable ER stress_____	32
<b>Figure 2.12:</b> CRK senses and executes apoptosis downstream of ATF6 _____	34
<b>Figure 2.13:</b> A cysteine protease cleaves CRK upon ER stress_____	36
<b>Figure 2.14:</b> CRK is cleaved at D110 upon ER stress_____	37

<b>Figure 2.15:</b> Pro-apoptotic CRK is BAX/BAK-dependent _____	39
<b>Figure 2.16:</b> CRK is a sensitizing BH3-only protein _____	41
<b>Figure 2.17:</b> Mutagenesis of CRK BH3 domain _____	42
<b>Figure 3.1:</b> CRK is cleaved upon irremediable ER stress _____	53
<b>Figure 3.2:</b> CRK is cleaved by a cysteine protease _____	54
<b>Figure 3.3:</b> CRK is not cleaved by caspase 2 upon ER stress _____	57
<b>Figure 3.4:</b> Cathepsin detected in mass spec analysis of purified cytosolic extract _____	58
<b>Figure 3.5:</b> E64 inhibits CRK cleavage and ER stress-induced apoptosis _____	59
<b>Figure 3.6:</b> Cathepsin cleavage of CRK _____	63
<b>Figure 3.7:</b> Subcellular localization of cathepsin B following ER stress _____	65
<b>Figure 4.1:</b> IRE1/XBP1 pathway _____	73
<b>Figure 4.2:</b> XBP1 transcriptional targets _____	73
<b>Figure 4.3:</b> XBP1 overexpression induces ER expansion _____	74
<b>Figure 4.4:</b> XBP1 required for ER expansion _____	74
<b>Figure 4.5:</b> No XBP1 splicing during KSHV lytic replication _____	76
<b>Figure 4.6:</b> ER expansion occurs during KSHV lytic cycle _____	78
<b>Figure 4.7:</b> BODIPY-BFA quantitation of ER expansion during lytic cycle _____	79
<b>Figure 4.8:</b> KSHV actively inhibits XBP1 slicing during lytic cycle _____	80
<b>Figure 4.9:</b> Screen for KSHV-encoded inducer of ER expansion #1 _____	81
<b>Figure 4.10:</b> Screen for KSHV-encoded inducer of ER expansion #2 _____	82
<b>Figure 5.1:</b> KSHV infection efficiency of mouse and human cells _____	91
<b>Figure 5.2:</b> Ratio of latent gene transcripts during latent infection _____	92

<b>Figure 5.3:</b> Lytic reactivation by ectopic RTA expression_____	92
<b>Figure 5.4:</b> Lytic mRNA transcript levels in RTA-induced cells_____	93
<b>Figure 5.5:</b> Lytic reactivation with HDAC inhibitors_____	93
<b>Figure 5.6:</b> Lytic transcription pattern and viral DNA replication_____	95
<b>Figure 5.7:</b> Murine cells undergo premature apoptosis upon KSHV lytic replication_____	97
<b>Figure 5.8:</b> Anti-apoptotic mRNA transcript levels_____	98
<b>Figure 5.9:</b> Genetic inhibition of apoptosis permits viral DNA replication in murine cells_____	100
<b>Figure 6.1:</b> Model of tumor cell recognition and killing by natural killer (NK) cells _____	111
<b>Figure 6.2:</b> GBM tumor cells express NKG2D ligands_____	115
<b>Figure 6.3:</b> Model of NK cell evasion by GBM_____	116
<b>Figure 6.4:</b> Purification scheme #1_____	117
<b>Figure 6.5:</b> Purification 1: Phenyl Sepharose column_____	118
<b>Figure 6.6:</b> Purification 1: Gel Filtration column_____	119
<b>Figure 6.7:</b> Purification 1: Mono S column_____	119
<b>Figure 6.8:</b> Purification 1: Mono Q column_____	120
<b>Figure 6.9:</b> Purification 1: Silver stain of activity-containing fractions_____	121
<b>Figure 6.10:</b> Purification 2: Hydroxyapatite scout for BSA removal_____	123
<b>Figure 6.11:</b> Purification 2: Hydroxyapatite gradient scout for BSA removal _____	123
<b>Figure 6.12:</b> Purification 2: Verification of Hydroxyapatite gradient_____	124

<b>Figure 6.13:</b> Purification scheme #2	125
<b>Figure 6.14:</b> Purification 2: Hydroxyapatite BSA removal columns	126
<b>Figure 6.15:</b> Purification 2: Final Hydroxyapatite BSA removal column	127
<b>Figure 6.16:</b> Purification 2: MonoQ Column	127
<b>Figure 6.17:</b> Purification 2: Silver stain of ULBP1h-containing fractions	128
<b>Figure 6.18:</b> Enzymatic function of LDH	132
<b>Figure 6.19:</b> LDH1 and LDH5 induce ULBP1 and MICB	134
<b>Figure 6.20:</b> Purification scheme #3	136
<b>Figure 6.21:</b> LDH present in MICBh-containing fractions	137
<b>Figure 7.1:</b> Model of pro-apoptotic CRK mechanism	143
<b>Figure 7.2:</b> Model of potential XBP1-independent ER expansion mechanisms	145
<b>Figure 7.3:</b> Model of NK cell evasion by glioma cells	147

## CHAPTER 1

### Introduction

The endoplasmic reticulum (ER) is the main site in the cell for the folding and processing of secreted proteins. Various physiological and pathological processes can overwhelm the protein folding capacity of the ER (15, 20). This condition, referred to as “ER stress,” typically triggers the activation of the Unfolded Protein Response Pathway (UPR), an evolutionarily conserved signaling transduction pathway that allows communication between the ER and nucleus. The activation of this pathway results in expansion of the ER, an increase in chaperone proteins, inhibition of cap-dependent translation, and if homeostasis is not reestablished, apoptosis (20).

ER stress-induced apoptosis, secondary to a buildup of misfolded proteins, leads to cell loss in a number of human degenerative diseases including amyotrophic lateral sclerosis (ALS), Parkinson, and type II diabetes (15, 18, 20). In contrast, cancer cells and viruses manipulate the cytoprotective aspects of the UPR, aberrantly promoting cell survival (2, 6, 12). Therefore, understanding how to manipulate the UPR’s cytoprotective/cytotoxic threshold could lead to new treatment approaches for a wide variety of unrelated diseases.

The mammalian UPR is a complex pathway comprised of three branches (Fig. 1.1). Upon ER stress, this pathway is initiated by ER transmembrane proteins IRE1 (inositol requiring enzyme 1), PERK (ER resident transmembrane protein kinase), and ATF6 (activating transcription factor 6) (21). Accumulated



misfolded proteins induce the oligomerization and activation of IRE1, PERK, and ATF6 by directly binding their luminal domains and/or by displacing the ER chaperone, BIP (4).

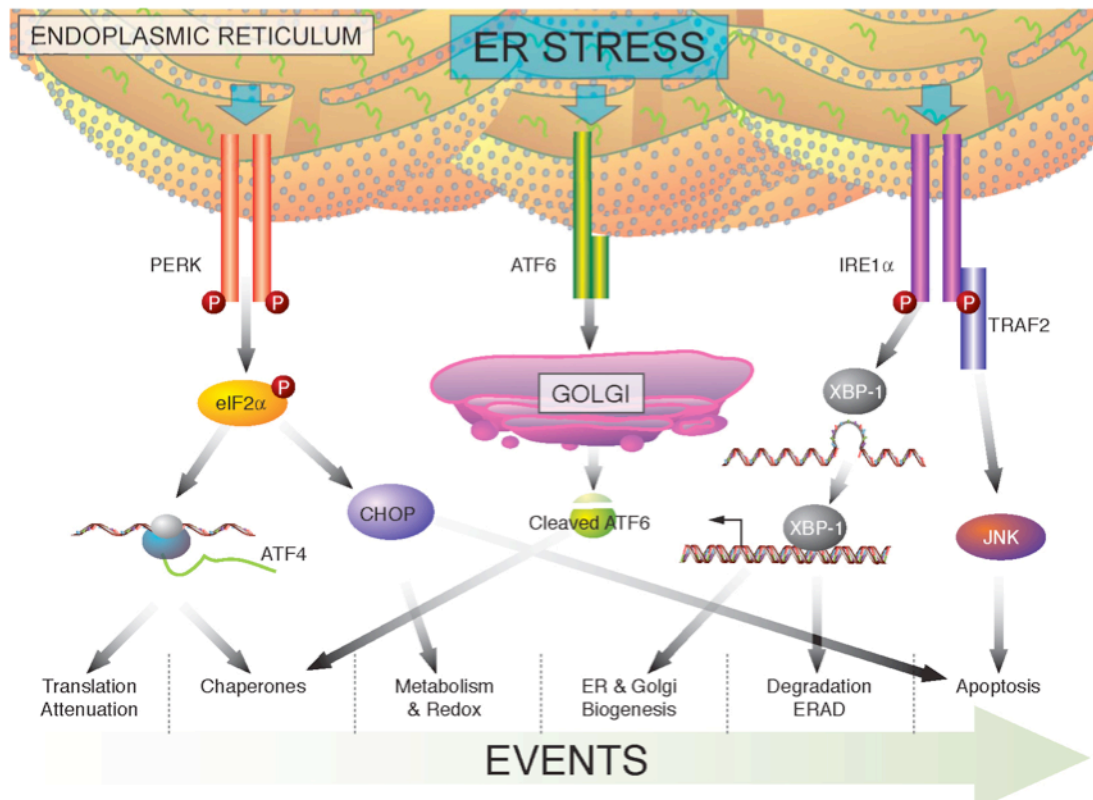


**Fig. 1.1.** The Unfolded Protein Response (UPR). ER transmembrane receptors, IRE1, PERK, and ATF6, sense ER stress and initiate the unfolded protein response to re-establish protein folding homeostasis. This is accomplished through the cytoprotective outputs of the UPR including; translation attenuation, chaperone upregulation, ERAD activation, and ER expansion. However, if ER stress is prolonged, the UPR initiates apoptosis through poorly understood mechanisms.

Ire1 $\alpha$  is a ser/threonine receptor protein kinase with endoribonuclease activity and is the most conserved branch of the UPR. In the presence of ER stress, Ire1 $\alpha$  homo-oligomerizes, which induces a conformational change that results in autophosphorylation. This autophosphorylation activates the

endoribonuclease activity, which splices and removes an unconventional intron from XBP1 mRNA (4). The spliced XBP1 message is translated into an active transcription factor that increases the protein folding capacity of the ER by upregulating genes encoding ER chaperones, ER biogenesis enzymes (10), and ER-associated protein degradation (ERAD) components (11). Furthermore, upon irremediable ER stress, IRE1 $\alpha$  degrades ER-localized transcripts, thereby decreasing the folding demand on the ER (Fig. 1.2). This mRNA decay function of IRE1 $\alpha$ 's RNase domain seems to be primarily cytotoxic through degrading transcripts that encode chaperones and other proteins required for protein secretion. The latter output may tip the UPR cytoprotective/cytotoxic threshold in favor of apoptosis. This hypothesis supports previous data implicating a pro-apoptotic role of IRE1 $\alpha$  (14). *Ire1*<sup>-/-</sup> MEFs demonstrate greater survival in comparison to wild-type MEFs upon toxic doses of ER stress-inducing agents. In addition, IRE1 overexpression results in BAX/BAK dependent apoptosis through the mitochondrial pathway. Reports also link IRE1 $\alpha$  to pro-apoptotic JNK signaling. These data implicate that the binary functions of IRE1 $\alpha$ 's RNase domain may be a key switch protein initiating the UPR's transition from adaptive to pro-apoptotic.

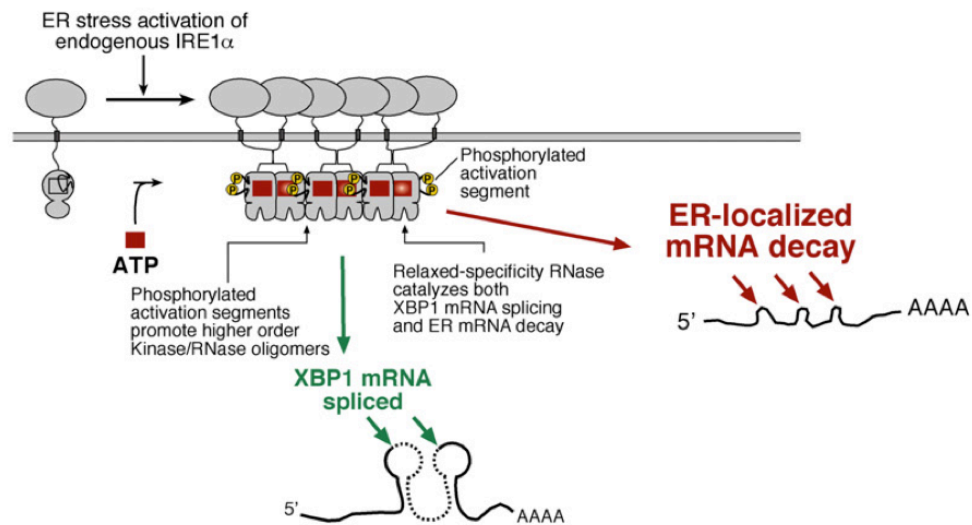


**Fig. 1.2.** IRE1α RNase domain signaling outputs. IRE1α outputs are both cytoprotective and cytotoxic. Upon oligomerization via transphosphorylation, the RNase domain of IRE1α becomes active. It nonconventionally splices XBP1, permitting translation of an adaptive transcription factor upregulating chaperones and inducing ER biogenesis. In contrast, upon irremediable ER stress, IRE1α's RNase domain degrades ER-localized transcripts and through unknown mechanisms initiates the apoptotic pathway. Adapted from Han, D *et al. Cell* 2009.

The UPR also regulates transcription through ATF6. Upon ER stress, ATF6 (p90ATF6) translocates to the golgi apparatus where it is cleaved into an active transcription factor (p50ATF6) by site1 and site2 proteases. p50ATF6 then migrates to the nucleus, where it induces genes encoding ER quality control proteins containing an ER stress response element (ERSE) in their promoter (4). ATF6 outputs are reported as being purely cytoprotective; however, when challenged with ER stress agents, *atf6*<sup>-/-</sup> MEFs are more resistant to ER stress-induced apoptosis than wild-type MEFs (22). While slightly less resistant in comparison to *ire*<sup>-/-</sup> MEFs, these data suggest that ATF6 plays an as yet undefined role in ER stress-induced apoptosis.

The final branch of the UPR, PERK, blocks cap-dependent translation and protein synthesis, thereby reducing the protein load present in the overworked ER. Dimerization of PERK activates its kinase domain to phosphorylate eIF2 $\alpha$  (eukaryotic translation initiation factor 2 alpha). Phosphorylation inhibits eIF2 $\alpha$ , which is required for cap-dependent translation. However, some mRNAs involved in reestablishment of homeostasis contain an internal ribosomal entry site (IRES) present in the 5' untranslated region and are therefore, able to escape phospho-eIF2 $\alpha$  mediated translation inhibition. For example, the transcription factor ATF4 can bypass this inhibition and is upregulated by the abundance of unoccupied translation machinery to induce expression of genes involved in redox reactions and protein secretion (1, 4), increasing the cytoprotective effects of the UPR. It has previously been suggested that PERK-dependent upregulation of the transcription factor CHOP, directly promotes cell death. This explanation is supported by evidence that links CHOP to anti-apoptotic protein downregulation, namely Bcl-2. However, CHOP, via upregulation of GADD34, may play a role in negatively regulating the pro-survival phosphorylation of EIF2 $\alpha$  and subsequent translation attenuation. The latter data suggests CHOP indirectly promotes cell death by negatively regulating adaptive UPR outputs.

Despite its important role in such a wide variety of diseases, the mechanisms underlying ER stress-induced apoptosis are poorly understood. It is known that ER stress-induced apoptosis requires mitochondrial BAX and BAK (20), two pro-apoptotic members of the Bcl-2 family. Oligomerization of these

proteins results in cytochrome *c* release, formation of the apoptosome, and activation of the caspase cascade (26). BAX/BAK oligomerization can occur through binding of pro-apoptotic BH3-only proteins. This event is antagonized by the binding and sequestering of BH3-only proteins by anti-apoptotic factors (e.g. BCL-2, BCL-X<sub>L</sub>, and MCL-1)(26)(Fig. 1.3).

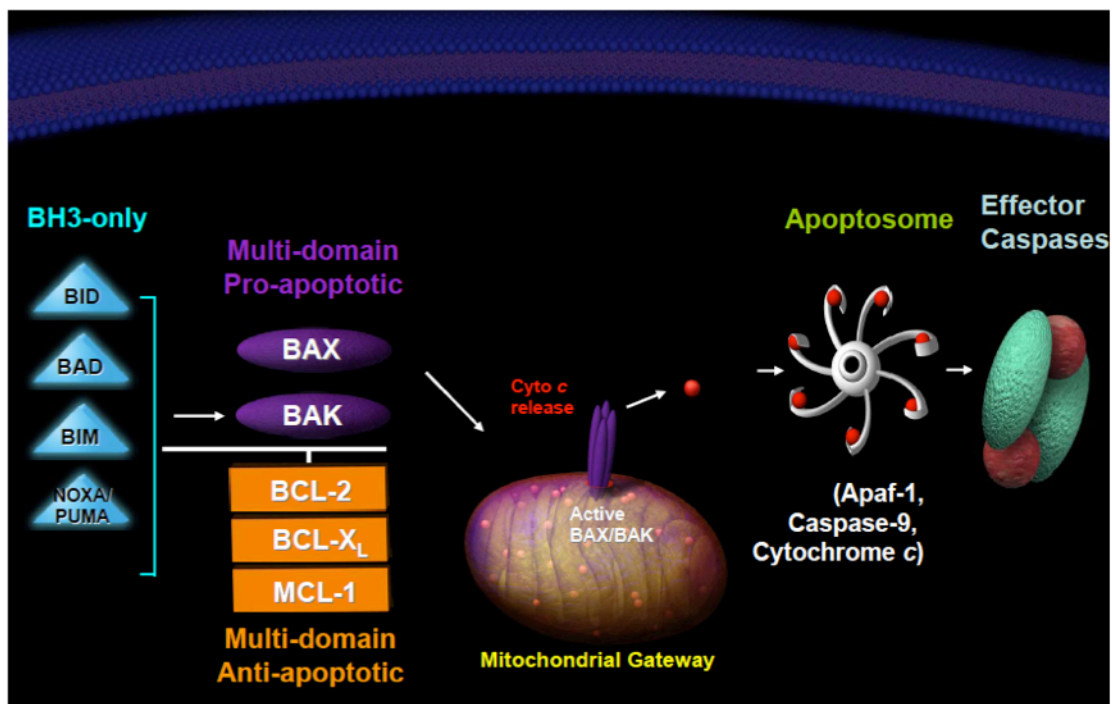


**Fig. 1.3.** Intrinsic Apoptosis. Activation of pro-apoptotic BH3-only proteins (e.g. BID, BAD, BIM, NOXA, PUMA) bind to and induce the oligomerization of BAX and/or BAK at mitochondria. This binding is antagonized by anti-apoptotic proteins (e.g Bcl-2, Bcl-X<sub>L</sub>, MCL-1). Upon oligomerization BAX and/or BAK induce the release of cytochrome *c* from the mitochondria outer membrane. Cytochrome *c*, in addition to Apaf-1 and caspase 9 form the apoptosome. The formation of this complex results in the activation of effector caspases and the destruction of the cell.

While the apoptotic machinery downstream of the mitochondrion is well understood, the signaling pathways connecting it to the ER remain largely unknown. We established a biochemical system to identify the ER stress-induced pro-apoptotic effectors that signal BAX and BAK at the mitochondrion

(Fig 2.1). We have previously found that ER stress activates Caspase-2 to proteolytically cleave BID into an apoptotic signal that then induces mitochondrial BAX/BAK oligomerization (25). BIM has also been implicated in ER stress-induced apoptosis. However, the loss of neither BID nor BIM confers as much resistance as the loss of BAX and BAK. These data suggest that there are likely additional pro-apoptotic signals activated by ER stress. Dissecting the apoptotic signaling pathway connecting ER to mitochondria will provide vital information necessary to produce effective therapies for diseases in which ER stress-induced apoptosis is implicated, but a critical question remains: What event(s) initiates the UPR's switch from cytoprotection to cytotoxicity?

The study of viral manipulation of host machinery has historically provided great insight into cellular biology. Viral infection is a biologically relevant system in which to study the cytoprotective/cytotoxic threshold of the UPR for several reasons. A large lytic virus, such as Kaposi's Sarcoma Herpes Virus (KSHV or HHV-8), must be able to increase the folding capacity of the ER in order to accommodate the acute influx of viral proteins in the ER during replication, while coordinately inhibiting the apoptotic consequences of intense ER stress. Therefore, it is likely that KSHV, like many other Herpes viruses, encodes genes that function to manipulate the UPR to its benefit. To date, little is known about how KSHV regulates the UPR and understanding the mechanisms involved should provide critical insight into the initiating switch for ER stress-induced apoptosis.

KSHV is the epidemiological cause of Kaposi's Sarcoma (KS) and two B cell diseases, primary effusion lymphoma (PEL) and Multicentric Castleman's disease. KS is the most clinically common disease caused by KSHV (Fig 1.4). It is highly associated with immunocompromised patients, including transplant recipients and those diagnosed with HIV. KS belies the name sarcoma, as it is unlike classical sarcomas. Sarcomas are commonly composed of a single cell type derived from mesenchymal tissue. In contrast, KS lesions are of lymphatic endothelial origin and are composed of polyclonal abnormal elongated endothelial cells and are highly vascularized (5). Though similarly to classical tumors, without treatment, KSHV can be fatal (7).

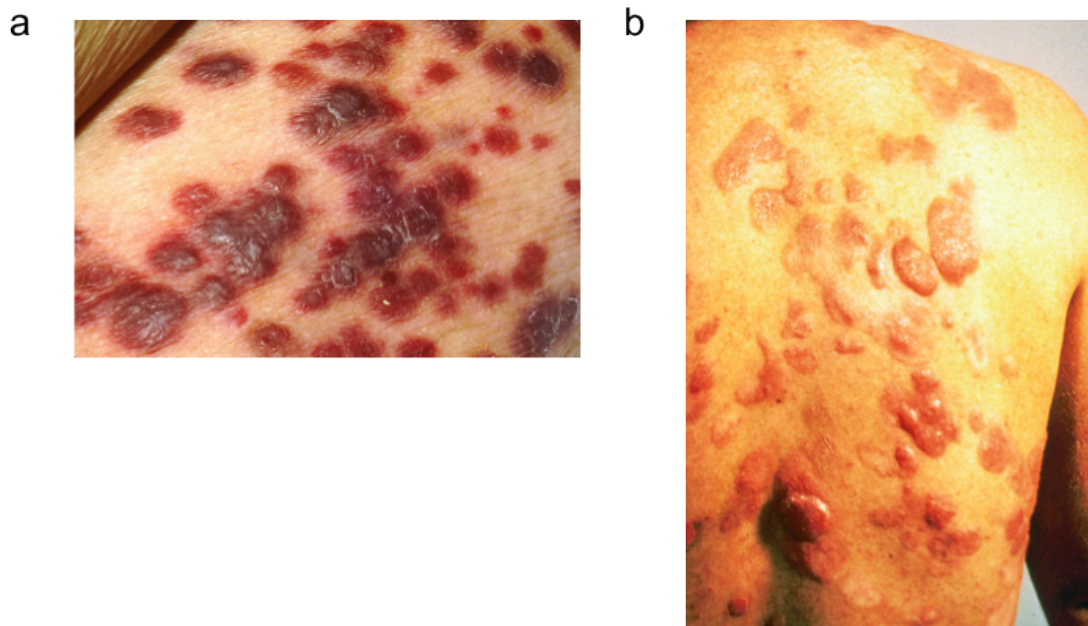


**Fig. 1.4.** Papular cutaneous Kaposi's sarcoma.

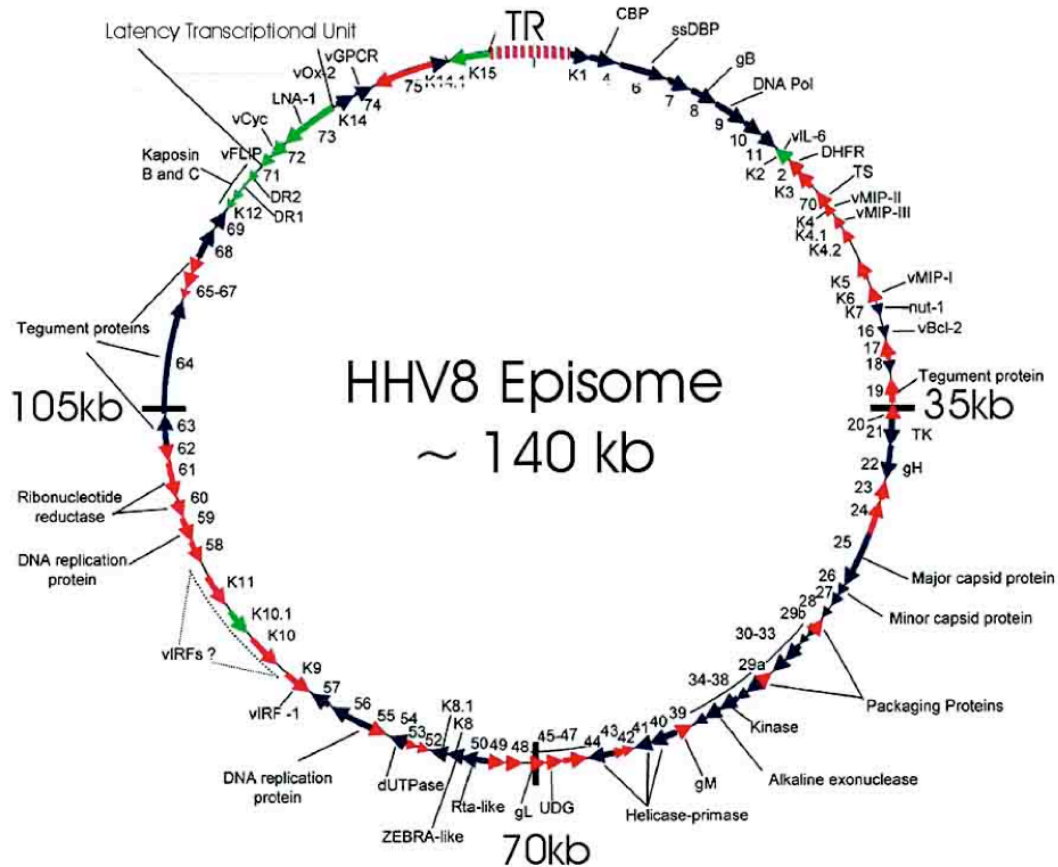


**Fig. 1.5. The genome of KSHV.** Latency genes are shown in green. From Cotter & Robertson, *Frontiers Biosci* 7:358 (2002)

KSHV is a member of the lymphotropic  $\gamma$ -herpesvirus family and is a large double-stranded linear DNA virus (~165kb). The genome encodes at least 90 genes, many with unknown functions (Fig. 1.5). Herpesviruses are capable of two genetic programs, latency and lytic replication. Latency is the default pathway of KSHV, during which the viral genome is transcriptionally repressed, allowing expression of only a handful of genes (~5-8) involved in immune escape and maintenance of the viral episome in proliferating cells (7).

The alternative transcriptional program is lytic replication when infectious virions are produced in the host cell (7). The environmental cues that trigger the



switch from latency to the lytic cycle are poorly understood, but the viral protein responsible for activating transcription of lytic genes is encoded by ORF50, also known as the replication and transcriptional activator (RTA) (8, 16, 17, 23, 27). Within 30 hours of lytic cycle initiation, the majority of the linearized viral genome is transcribed, viral mRNAs encoding transmembrane or secreted proteins are trafficked from the nucleus to ribosomes and translated into the ER, where they are folded, and undergo post-translational modifications (23). In addition to the many protein components of the virion capsid, KSHV encodes multiple glycoproteins involved in immune modulation and viral entry, which require extensive post-translational processing in the ER (23). The massive influx of viral proteins into the ER during this process would be expected to overwhelm the folding capacity of the ER and lead to ER stress-induced apoptosis. In order to successfully complete the assembly of its viral progeny, we predict that KSHV must manipulate the cytoprotective aspects of the UPR, induce ER biogenesis and increase chaperone levels, while coordinately shifting the UPR-dependent apoptotic threshold to permit successful assembly of infectious virions.

As stated previously, little is known about the role of the UPR during KSHV infection. However, studies of other Herpes family members, such as Herpes Simplex 1 (HSV-1), Human Cytomegalovirus (HCMV), and Epstein-Barr virus (EBV) suggest that KSHV likely manipulates the UPR to promote its persistence (REF).

During HSV-1 infection PERK and IRE1 $\alpha$  remain inactive. HSV-1's Glycoprotein B (gB) binds to the luminal domain of PERK, preventing its

activation and subsequent translation attenuation (3, 19). Further investigation is required to elucidate the mechanism inhibiting IRE1 $\alpha$  activation. In contrast, HCMV infection induces PERK and IRE1 $\alpha$  activation as evidenced by ATF4 accumulation and XBP1 splicing. However, HCMV actively inhibits ATF6 cleavage (9, 24). EBV shares the most homology with KSHV of any other herpes virus. EBV manipulates the UPR to perpetuate latent infection. LMP1, a latently expressed oncogene that signals cell growth actively induces PERK. PERK activation upregulates ATF4, which targets the LMP1 promoter (Fig. 1.6) (13). Through this mechanism, EBV has manipulated the UPR to create a positive feedback loop, which perpetuates its infection. Given, the homology and shared function of many herpes genes, it is probable that KSHV similarly manipulates the UPR to its benefit.

A biochemical dissection of the ER stress-induced apoptotic pathway will identify pro-apoptotic components required for communication with the mitochondrial apoptotic machinery. Second, investigation into the role of the UPR during KSHV life cycle will reveal new insights into the cytoprotective/cytotoxic regulation of the UPR and novel functions of KSHV encoded genes. The findings from this study have implications for many diseases aside from viral infection, including type II diabetes, cancer, and neurodegeneration.

## References

1. **Ameri, K., and A. L. Harris.** 2008. Activating transcription factor 4. *Int J Biochem Cell Biol* **40**:14-21.
2. **Bi, M., C. Naczki, M. Koritzinsky, D. Fels, J. Blais, N. Hu, H. Harding, I. Novoa, M. Varia, J. Raleigh, D. Scheuner, R. J. Kaufman, J. Bell, D. Ron, B. G. Wouters, and C. Koumenis.** 2005. ER stress-regulated translation increases tolerance to extreme hypoxia and promotes tumor growth. *EMBO J* **24**:3470-3481.
3. **Cheng, G., Z. Feng, and B. He.** 2005. Herpes simplex virus 1 infection activates the endoplasmic reticulum resident kinase PERK and mediates eIF-2alpha dephosphorylation by the gamma(1)34.5 protein. *J Virol* **79**:1379-1388.
4. **Credle, J. J., J. S. Finer-Moore, F. R. Papa, R. M. Stroud, and P. Walter.** 2005. On the mechanism of sensing unfolded protein in the endoplasmic reticulum. *Proc Natl Acad Sci U S A* **102**:18773-18784.
5. **Dourmishev, L. A., A. L. Dourmishev, D. Palmeri, R. A. Schwartz, and D. M. Lukac.** 2003. Molecular genetics of Kaposi's sarcoma-associated herpesvirus (human herpesvirus-8) epidemiology and pathogenesis. *Microbiol Mol Biol Rev* **67**:175-212, table of contents.
6. **Feldman, D. E., V. Chauhan, and A. C. Koong.** 2005. The unfolded protein response: a novel component of the hypoxic stress response in tumors. *Mol Cancer Res* **3**:597-605.
7. **Ganem, D.** 2006. KSHV infection and the pathogenesis of Kaposi's sarcoma. *Annu Rev Pathol* **1**:273-296.
8. **Gradoville, L., J. Gerlach, E. Grogan, D. Shedd, S. Nikiforow, C. Metroka, and G. Miller.** 2000. Kaposi's sarcoma-associated herpesvirus open reading frame 50/Rta protein activates the entire viral lytic cycle in the HH-B2 primary effusion lymphoma cell line. *J Virol* **74**:6207-6212.
9. **Isler, J. A., A. H. Skalet, and J. C. Alwine.** 2005. Human cytomegalovirus infection activates and regulates the unfolded protein response. *J Virol* **79**:6890-6899.
10. **Lee, A. H., G. C. Chu, N. N. Iwakoshi, and L. H. Glimcher.** 2005. XBP-1 is required for biogenesis of cellular secretory machinery of exocrine glands. *EMBO J* **24**:4368-4380.
11. **Lee, A. H., N. N. Iwakoshi, and L. H. Glimcher.** 2003. XBP-1 regulates a subset of endoplasmic reticulum resident chaperone genes in the unfolded protein response. *Mol Cell Biol* **23**:7448-7459.
12. **Lee, D. Y., J. Lee, and B. Sugden.** 2009. The unfolded protein response and autophagy: herpesviruses rule! *J Virol* **83**:1168-1172.
13. **Lee, D. Y., and B. Sugden.** 2008. The LMP1 oncogene of EBV activates PERK and the unfolded protein response to drive its own synthesis. *Blood* **111**:2280-2289.
14. **Lin, J. H., H. Li, D. Yasumura, H. R. Cohen, C. Zhang, B. Panning, K. M. Shokat, M. M. Lavail, and P. Walter.** 2007. IRE1 signaling affects cell fate during the unfolded protein response. *Science* **318**:944-949.

15. **Lin, J. H., P. Walter, and T. S. Yen.** 2008. Endoplasmic reticulum stress in disease pathogenesis. *Annu Rev Pathol* **3**:399-425.
16. **Lukac, D. M., J. R. Kirshner, and D. Ganem.** 1999. Transcriptional activation by the product of open reading frame 50 of Kaposi's sarcoma-associated herpesvirus is required for lytic viral reactivation in B cells. *J Virol* **73**:9348-9361.
17. **Lukac, D. M., R. Renne, J. R. Kirshner, and D. Ganem.** 1998. Reactivation of Kaposi's sarcoma-associated herpesvirus infection from latency by expression of the ORF 50 transactivator, a homolog of the EBV R protein. *Virology* **252**:304-312.
18. **Marciniak, S. J., and D. Ron.** 2006. Endoplasmic reticulum stress signaling in disease. *Physiol Rev* **86**:1133-1149.
19. **Mulvey, M., C. Arias, and I. Mohr.** 2007. Maintenance of endoplasmic reticulum (ER) homeostasis in herpes simplex virus type 1-infected cells through the association of a viral glycoprotein with PERK, a cellular ER stress sensor. *J Virol* **81**:3377-3390.
20. **Oakes, S. A., S. S. Lin, and M. C. Bassik.** 2006. The control of endoplasmic reticulum-initiated apoptosis by the BCL-2 family of proteins. *Curr Mol Med* **6**:99-109.
21. **Ron, D., and P. Walter.** 2007. Signal integration in the endoplasmic reticulum unfolded protein response. *Nat Rev Mol Cell Biol* **8**:519-529.
22. **Shen, X., R. E. Ellis, K. Sakaki, and R. J. Kaufman.** 2005. Genetic interactions due to constitutive and inducible gene regulation mediated by the unfolded protein response in *C. elegans*. *PLoS Genet* **1**:e37.
23. **Sun, R., S. F. Lin, L. Gradoville, Y. Yuan, F. Zhu, and G. Miller.** 1998. A viral gene that activates lytic cycle expression of Kaposi's sarcoma-associated herpesvirus. *Proc Natl Acad Sci U S A* **95**:10866-10871.
24. **Tirosh, B., N. N. Iwakoshi, B. N. Lilley, A. H. Lee, L. H. Glimcher, and H. L. Ploegh.** 2005. Human cytomegalovirus protein US11 provokes an unfolded protein response that may facilitate the degradation of class I major histocompatibility complex products. *J Virol* **79**:2768-2779.
25. **Upton, J. P., K. Austgen, M. Nishino, K. M. Coakley, A. Hagen, D. Han, F. R. Papa, and S. A. Oakes.** 2008. Caspase-2 cleavage of BID is a critical apoptotic signal downstream of endoplasmic reticulum stress. *Mol Cell Biol* **28**:3943-3951.
26. **Wei, M. C., W. X. Zong, E. H. Cheng, T. Lindsten, V. Panoutsakopoulou, A. J. Ross, K. A. Roth, G. R. MacGregor, C. B. Thompson, and S. J. Korsmeyer.** 2001. Proapoptotic BAX and BAK: a requisite gateway to mitochondrial dysfunction and death. *Science* **292**:727-730.
27. **Xu, Y., D. P. AuCoin, A. R. Huete, S. A. Cei, L. J. Hanson, and G. S. Pari.** 2005. A Kaposi's sarcoma-associated herpesvirus/human herpesvirus 8 ORF50 deletion mutant is defective for reactivation of latent virus and DNA replication. *J Virol* **79**:3479-3487.

# **Proto-oncogene CRK is a pro-apoptotic BH3-only transducer of irremediable endoplasmic reticulum stress**

## **Background**

Excessive demands on the protein folding capacity of the endoplasmic reticulum (ER) cause irremediable ER stress and contribute to cell loss in a number of cell degenerative diseases, including type 2 diabetes and neurodegeneration (7, 12). If unable to resolve ER stress through its homeostatic signaling outputs, the unfolded protein response (UPR) activates the intrinsic mitochondrial apoptotic pathway (15). However, the signals communicating catastrophic ER damage to the mitochondrial apoptotic machinery remain poorly understood.

Irremediable ER stress represents a form of intrinsic cell damage that culminates in activation of the BAX/BAK-dependent mitochondrial apoptotic pathway (15). Homo-oligomerization of BAX and/or BAK consequently results in outer mitochondrial membrane permeabilization and release of pro-death mitochondrial proteins (e.g., cytochrome *c*) into the cytosol, causing activation of effector caspases (2, 9, 19). For many forms of cell injury, including ER stress,

we have a limited understanding of the cellular transducers that relay the information of upstream damage to BAX/BAK oligomerization at mitochondria. To date, the only known BAX and/or BAK activators are members of the pro-apoptotic BH3-only family, a diverse class of polypeptides containing a loosely conserved ~9-12 amino acid BH3 death domain (1, 18)(10). The BH3-only proteins BID, BIM, NOXA and PUMA have been previously implicated in ER stress-induced death(22); however, cells deficient in one or more of these proteins are not completely resistant to this form of apoptosis (8, 25). Therefore, it is highly probable that additional proteins that communicate ER stress to the mitochondrial apoptotic machinery remain to be discovered. To pursue this possibility, we took an unbiased biochemical approach to purify the major ER stress-induced cytosolic pro-apoptotic activity.

## Results

Given their strong resistance to ER stress-induced apoptosis (8, 25), we reasoned the *Bax*<sup>-/-</sup>*Bak*<sup>-/-</sup> mouse embryonic fibroblasts (MEFs) present a unique and powerful tool to trap and identify pre-mitochondrial apoptotic signals activated by ER stress. Therefore, we challenged SV40-transformed *Bax*<sup>-/-</sup>*Bak*<sup>-/-</sup> MEFs with the pharmacological agent Brefeldin A (BFA), which blocks ER-golgi protein transport, to induce irremediable ER stress and initiate the pre-mitochondrial apoptotic program. We prepared cytosolic extracts (S100) from untreated or BFA-treated *Bax*<sup>-/-</sup>*Bak*<sup>-/-</sup> MEFs, then incubated isolated Jurkat

mitochondria with these extracts, and measured the amount of mitochondrial cytochrome *c* released as a readout for pro-apoptotic activity (Fig. 2.1). The S100 of BFA-treated *Bax*<sup>-/-</sup>*Bak*<sup>-/-</sup> cells triggers the release of ~90% of total intra-mitochondrial cytochrome *c* in a BAX/BAK-dependent manner (22), while the S100 fraction from untreated *Bax*<sup>-/-</sup>*Bak*<sup>-/-</sup> MEFs induces negligible (<5%) cytochrome *c* release (Fig. 2.2). Thus, ER stress induces a cytosolic activity capable of releasing mitochondrial cytochrome *c*, which we have termed **Cytochrome *c* Releasing Activity (CcRA)**. We previously found that proteolytically active BID (tBID) is responsible for a portion of this CcRA (~30%), but that the majority of CcRA remains intact in BFA-treated *Bid*<sup>-/-</sup> S100 (22). Therefore, we designed and performed a biochemical purification strategy to isolate additional CcRA factors in the BFA-treated *Bax*<sup>-/-</sup>*Bak*<sup>-/-</sup> S100 (Fig. 2.3a).

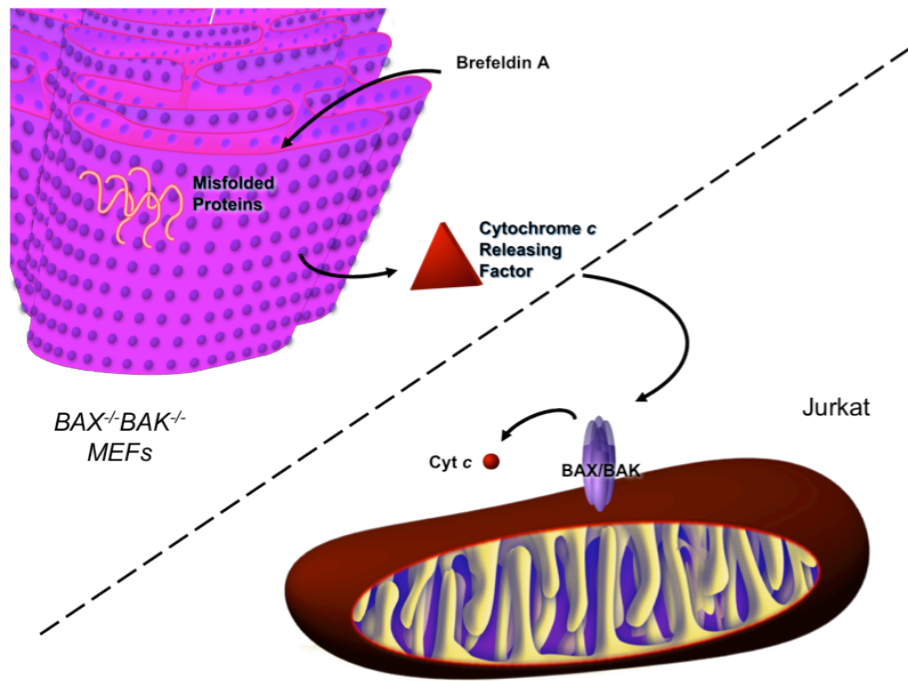


**Fig. 2.1.** Cytochrome c Release Assay. *Bax<sup>-/-</sup>Bak<sup>-/-</sup>* MEFs are treated 24h with 2.5  $\mu$ g/ml Brefeldin A. Cytosolic extract (S100) is isolated by subcellular fractionation. The presence of pro-apoptotic proteins is detected by incubating the S100 with isolated Jurkat mitochondria. Apoptotic activity is measured by cytochrome c release.

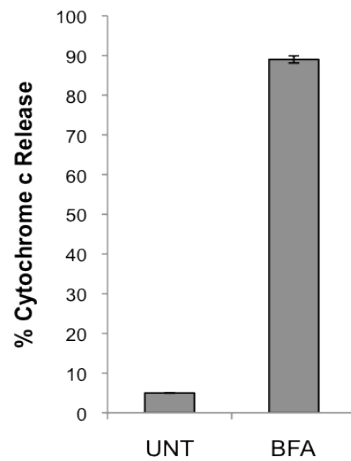


**Fig. 2.2.** Induction of Cytochrome c release from isolated Jurkat mitochondria by cytosolic extracts (S100) from untreated (UNT) and 24h Brefeldin A 2.5 $\mu$ g/ml (BFA) treated *Bax<sup>-/-</sup>Bak<sup>-/-</sup>* MEFs.



The CcRA-containing fractions from the final step (MonoQ gradient) (Fig. 2.3b) of the purification scheme did not contain detectable amounts of any known BH3-only protein by immunoblotting (data not shown), and so were analyzed by MALDI mass spectrometry. Proto-oncogene CT10-regulated kinase (CRK) was the highest confidence protein identified by mass spectrometry in the active fractions, with approximately 25% of the total sequence represented in 6 tryptic peptides (Table 2.1). *C-crkl* encodes two splice isoforms, CRKI (28kD) and CRKII (38kD)(13), which have been previously recognized as adaptor components in multi-protein complexes involved in cell morphology, movement, proliferation, and differentiation(4). CRKI and CRKII share a common Src homology 2 (SH2) domain and SH3 domain, while CRKII contains an additional C-terminal SH3 domain (Fig. 2.3c)(4). As the peptides detected by mass spectrometry are common to both CRKI and CRKII, this information did not differentiate which isoform is present in the analyzed fractions (Table 2.1).

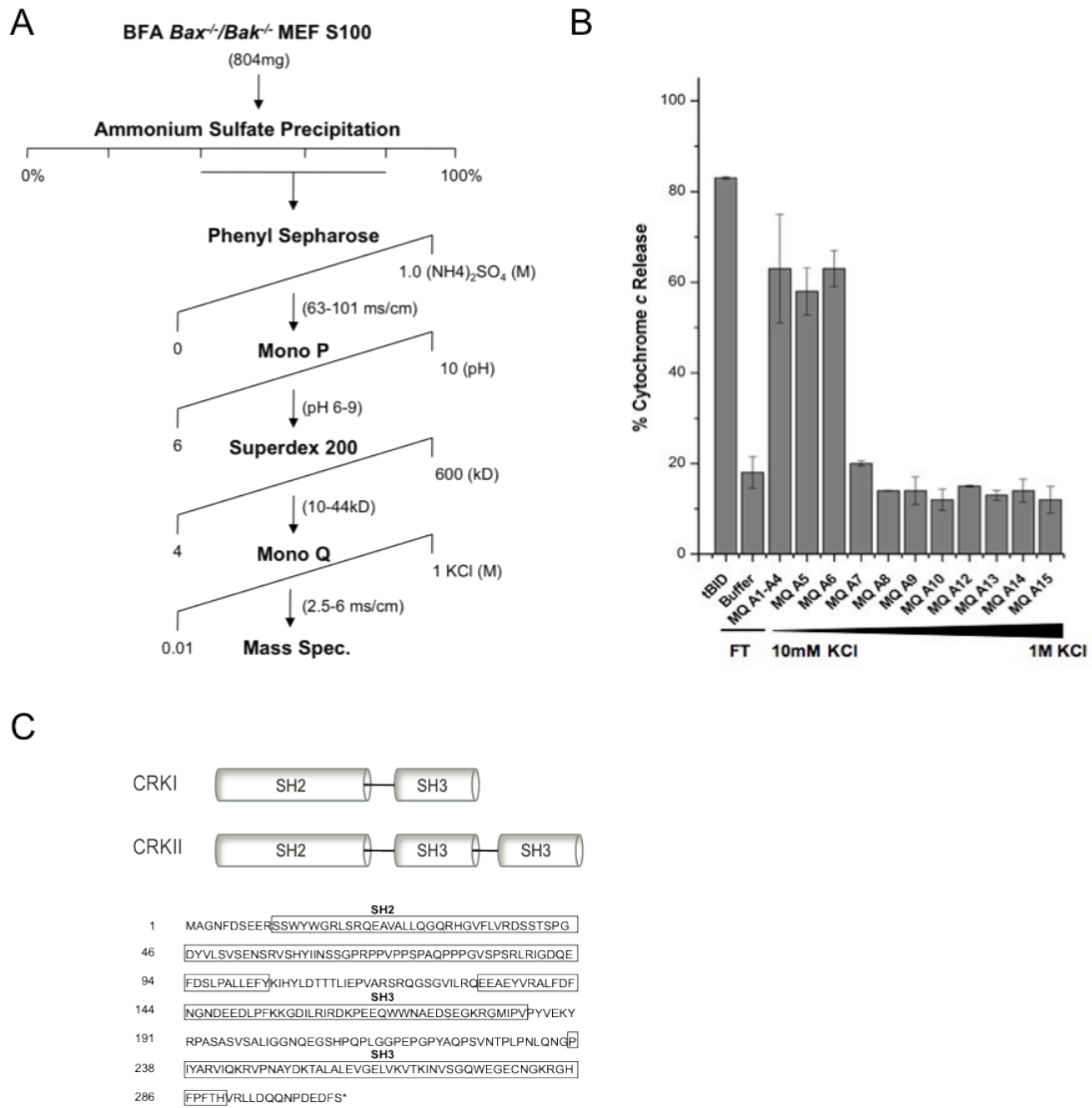


**Fig. 2.3.** (A) FPLC purification scheme of cytochrome *c* releasing activity (CcRA) present in BFA *Bax*<sup>-/-</sup>/*Bak*<sup>-/-</sup> S100. Active fractions from each purification step are indicated. (B) CcRA assay of the fractions from the final step of the purification (MonoQ ion exchange gradient). (C) Diagram of CRK isoforms, domains, and amino acid sequence.

To test if CRK plays a role in ER stress-induced apoptosis in cells, we challenged *crk*<sup>-/-</sup> and wild-type (WT) matched MEFs with BFA or tunicamycin (TUN), an ER stress agent that specifically inhibits *N*-linked glycosylation. As previously reported, these *crk*<sup>-/-</sup> MEFs are derived from genetically engineered embryos that fail to express either CRKI or CRKII (16) (Fig. 2.4c). Notably, *crk*<sup>-/-</sup> MEFs are strikingly resistant to ER stress-induced apoptosis, but as sensitive as WT MEFs to staurosporine (STS), a pan-kinase inhibitor known to activate the mitochondrial apoptotic pathway independently of ER stress (Fig. 2.4a, b). Further confirming that CRK is required for the majority of the ER stress-induced apoptotic signal, S100 from BFA-treated *crk*<sup>-/-</sup> MEFs has significantly decreased CcRA compared to that from BFA-treated WT MEFs (Fig. 2.4d).

Tryptic Peptides Detected by Mass Spectrometry	
1	SSWYWGR
2	HGVFLVR
3	SSTSPGDYVLSVSENSR
4	VSHYIINSSGPRPPVPPSPAQPPPGVSPSR
5	HYLDTTTLIEPVAR
6	GDILRIRD

**Table 2.1** CRK tryptic peptides detected by MALDI MS/MS mass spectrometry analysis.

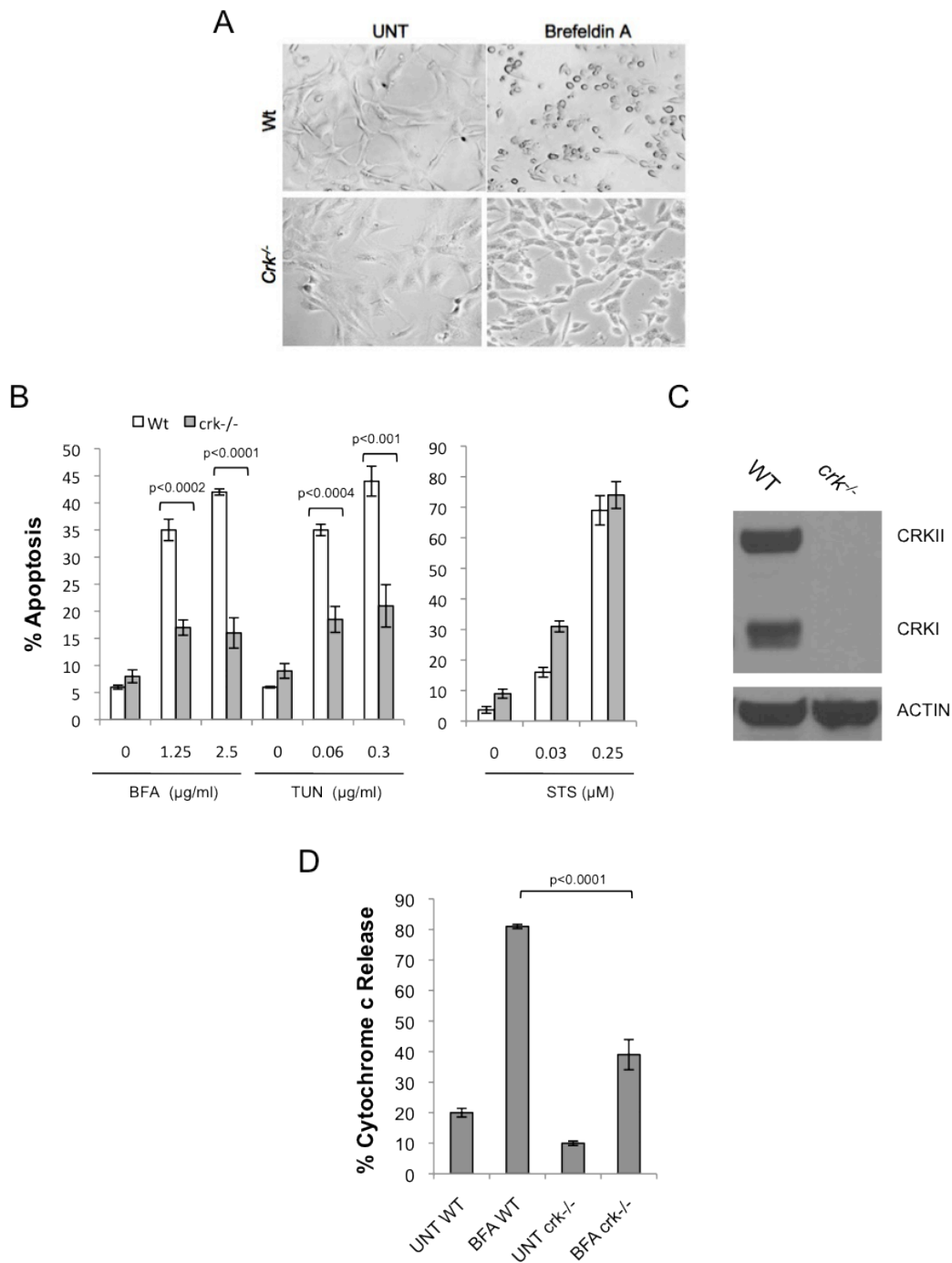


**Fig 2.4.** *Crk*<sup>-/-</sup> MEFs are strikingly resistant to ER stress-induced apoptosis. (A) *Crk*<sup>-/-</sup> MEFs are visually resistant (phase contrast) to ER stress-induced apoptosis (18h BFA 2.5μg/ml). (B, C) *Crk*<sup>-/-</sup> MEFs are strongly resistant to BFA and TUN-induced apoptosis, but equally sensitive to staurosporine (STS), in comparison to wild-type MEFs. (D) 18h BFA (2.5μg/ml)-treated *Crk*<sup>-/-</sup> MEF S100 contains significantly less CcRA in comparison to 18h BFA-treated (2.5μg/ml) wild-type MEF S100.

To investigate which CRK isoform is necessary for ER stress-induced apoptosis, we reconstituted *crk*<sup>-/-</sup> MEFs by transient transfection with expression constructs encoding either *crkl* or *crkll* and evaluated their sensitivity to ER stress-induced apoptosis. Surprisingly, *crkl* and *crkll* are both able to independently rescue the sensitivity of *crk*<sup>-/-</sup> MEFs to ER stress-induced apoptosis, arguing that a sequence common to CRKI and CRKII is required for CRK's apoptotic activity (Fig. 2.5). We next attempted to use retroviral vectors to establish stable cell lines of *crk*<sup>-/-</sup> MEFs expressing either *crkl* or *crkll*. While we had no difficulty recovering cells reconstituted with *crkll*, all attempts to establish stable *crkl* expression in *crk*<sup>-/-</sup> MEFs were unsuccessful, indicating that CRKI may be inherently cytotoxic. Stable reconstitution of *crkll* in *crk*<sup>-/-</sup> MEFs restores sensitivity to ER stress agents, but does not affect the response to STS (Fig. 2.6), recapitulating the transient expression results (Fig. 2.5). Moreover, stable overexpression of *crkll* and transient overexpression of *crkl* further sensitizes WT MEFs to ER stress (Fig. 2.7). Together, these data strongly argue that CRK is a critical component of the ER stress-induced apoptotic pathway.

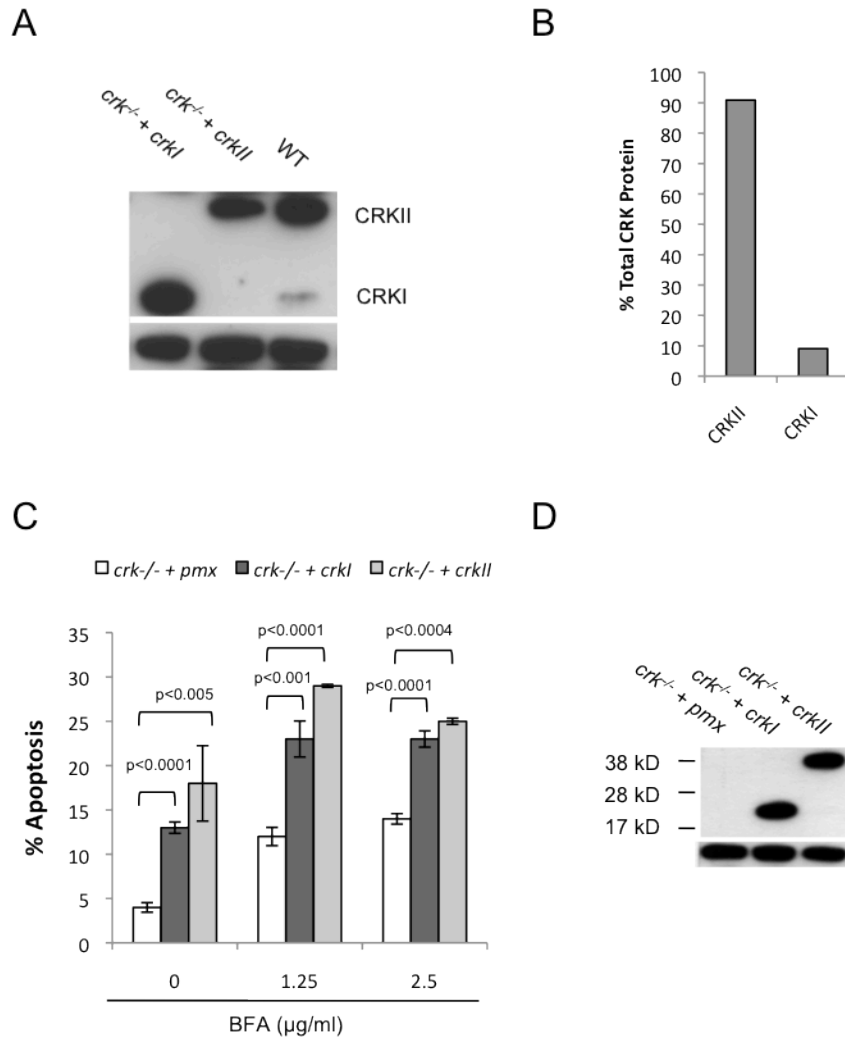


**Fig. 2.5.** CRKI and CRKII restore sensitivity of *crk<sup>-/-</sup>* MEFs to ER stress-induced apoptosis. (A) CRKI and CRKII protein levels in WT MEFs. (B) Densitometric measurement of CRKI and CRKII protein levels in WT MEFs. (C, D) Transient expression of CRKI and/or CRKII sensitizes *crk<sup>-/-</sup>* MEFs to BFA-induced apoptosis.

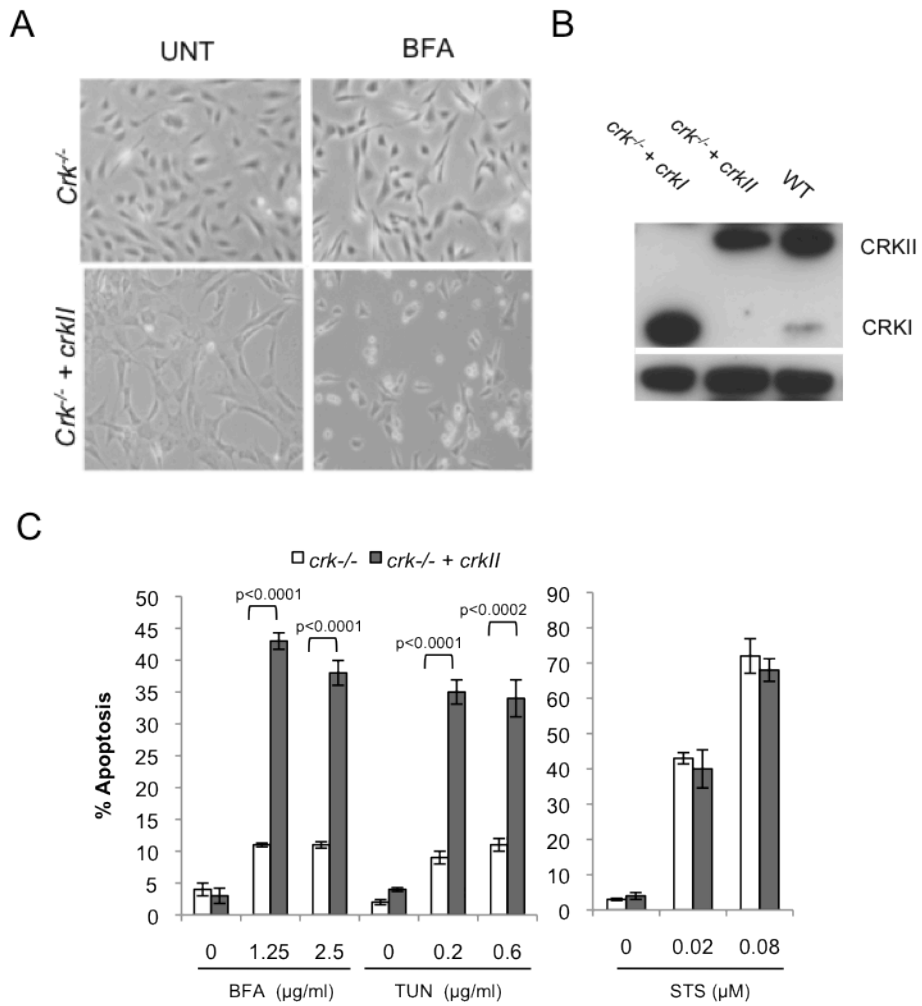


**Fig. 2.6.** Stable CRKII expression restores sensitivity of *crk*<sup>-/-</sup> MEFs to ER stress-induced apoptosis. (A, B, C) Stable CRKII expression in *crk*<sup>-/-</sup> MEFs rescues sensitivity to 24h BFA- and 18h TUN-induced apoptosis, but does not change sensitivity to staurosporine-induced apoptosis

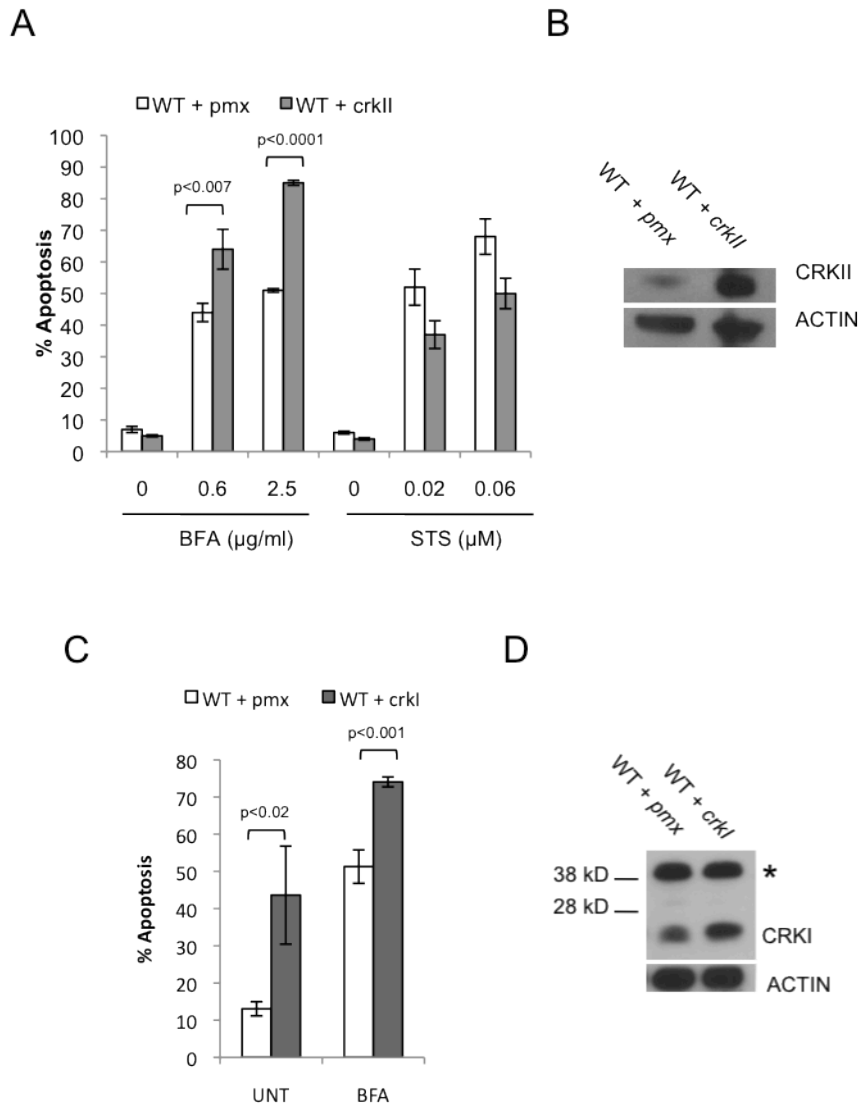


**Fig. 2.7.** Overexpression of CRK1 and/or CRKII sensitizes wild-type MEFs to ER stress-induced apoptosis. (A, B) Stable overexpression of CRKII in wild-type MEFs further increases sensitivity to 18h BFA-induced apoptosis. (C, D) Transient overexpression of CRK1 sensitizes wild-type MEFs to 18h BFA (1.25µg/ml)-induced apoptosis.



As the full sequence of *crkl* is contained within *crkll*, we decided to further study the mechanism of CRK-induced apoptosis by utilizing the *crk*<sup>-/-</sup> MEFs stably expressing *crkll*. However, there is an important regulatory difference between CRKI and CRKII. Phosphorylation of tyrosine 221 (Y221) in CRKII, which is not present in the truncated CRKI isoform (Fig. 2.3c), is reported to facilitate an intramolecular folding of the protein via binding in *cis* with the N-terminal SH2 domain of CRKII. This auto-inhibitory folding event prevents binding of various signaling molecules to the SH2 and SH3 domains of CRKII, effectively inhibiting CRKII-dependent downstream signaling pathways. We tested whether the phosphorylation state of Y221 changes in response to ER stress. Indeed, upon 14h BFA treatment, we found that Y221 is completely dephosphorylated (Fig. 2.8a). To determine if Y221 phosphorylation regulates CRKII's apoptotic activity, we transiently expressed a CRKII mutant (Y221F), in which tyrosine 221 cannot be phosphorylated (Fig. 2.9b). Y221F restores ER stress-induced apoptosis to levels comparable to wild-type *crkll* (Fig. 2.8c, d), indicating that phosphorylation of this tyrosine residue may not be a critical negative regulatory event in the activation of pro-apoptotic CRKII.

PTP1B is the only known phosphatase to dephosphorylate the Y221 site and has been previously implicated in the ER stress-induced apoptotic pathway, as *ptp1b*<sup>-/-</sup> MEFs have been shown to be resistant to ER stress. We generated a stable siRNA knock-down of PTP1B in wild-type MEFs (PTP1B KD) and monitored their response to ER stress-induced apoptosis upon 18h BFA

treatment. In support of our previous data indicating the Y221 dephosphorylation event may not play a role in the apoptotic activity of CRKII (Fig. 2.8c, d), PTP1B KD MEFs show equal sensitivity to BFA-induced cell death in comparison to wild-type MEFs (Fig. 2.9a, b). In addition, CRK is efficiently dephosphorylated and depleted in the absence of PTP1B (Fig. 2.9c). These data further support our conclusion that the dephosphorylation event may not play a significant role in CRK's pro-apoptotic activity and suggest that there is a novel phosphatase responsible for Y221 dephosphorylation upon ER stress.

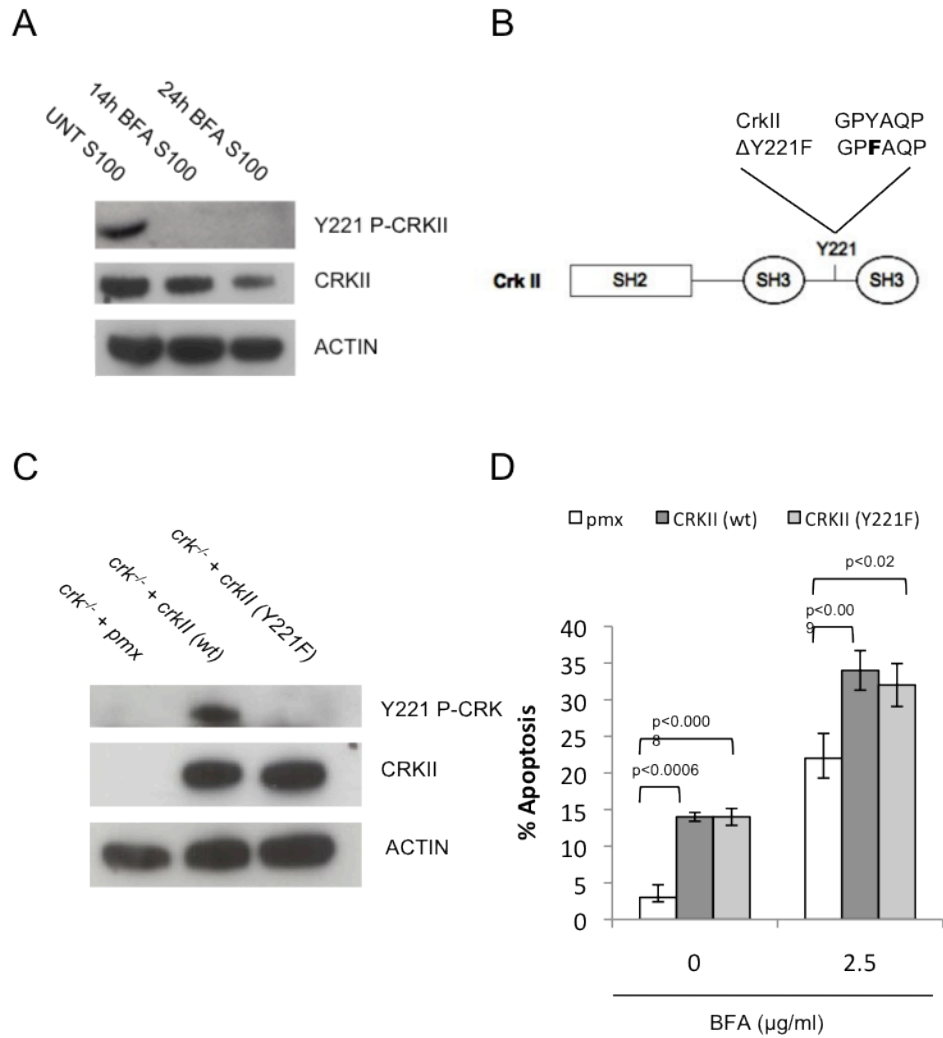


**Fig. 2.8.** CRKII is dephosphorylated upon ER stress. (A) In *Bax*<sup>-/-</sup>*Bak*<sup>-/-</sup> MEFs, CRKII is completely dephosphorylated within 14 hours of BFA (2.5µg/ml) treatment. Dephosphorylation is followed by a depletion of full-length CRKII in the cytosol. (B) Diagram of mutated (Y221F) auto-inhibitory tyrosine phosphorylation site of CRKII. (C, D) Y221F and wild-type CRKII transient expression result in comparable sensitivity of *crk*<sup>-/-</sup> MEFs to ER stress-induced apoptosis (24h BFA treatment).

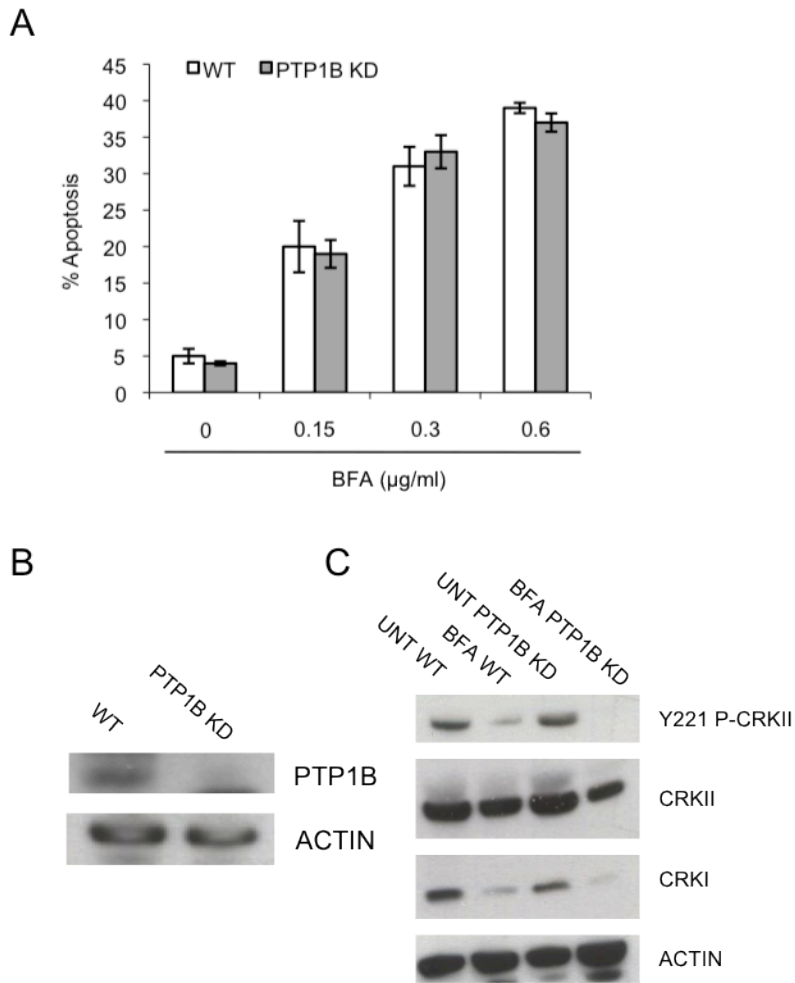


**Fig. 2.9.** PTP1B is not responsible for CRKII Y221 dephosphorylation. (A, B) Stable siRNA knock-down of PTP1B in wild-type MEFs did not confer resistance to ER stress-induced apoptosis. (C) CRKII Y221 is efficiently dephosphorylated following 18h BFA (2.5µg/ml) treatment. CRKI and CRKII are depleted similarly to 18h BFA-treated (2.5µg/ml) wild-type MEFs.

Unexpectedly, we also found that ER stress causes depletion of full-length CRKII (Fig. 2.10a). To determine if CRKII is reduced in a specific subcellular compartment, we probed subcellular fractions from *Bax*<sup>-/-</sup>*Bak*<sup>-/-</sup> MEFs and found that CRKII is partially localized to the ER, mitochondria, and cytosol (Fig. 2.10b). Moreover, upon ER stress, 38kD ER- and cytosol- localized CRKII is reduced, while levels of the mitochondrion-localized full-length CRKII change very little (Fig. 2.10b). Interestingly, we found that upon ER stress, CRKII appears to be sequentially cleaved at least twice, resulting in several distinct fragments (Fig. 2.10b, c). Proteolytic cleavage is a post-translational modification recognized to activate other known pro-apoptotic proteins, such as BID, but had not been described previously for CRK (6, 11, 23, 24).

We tested if CRKI also undergoes cleavage events upon ER stress. Following ER stress, at least one CRKI-specific cleavage product is readily observed (Fig. 2.11a). In addition, we observe depletion of full-length endogenous CRKI and CRKII in both WT and *Bax*<sup>-/-</sup>*Bak*<sup>-/-</sup> MEFs upon BFA treatment (Fig. 2.11b), indicating that their cleavage occurs upstream of the mitochondrial apoptotic pathway.

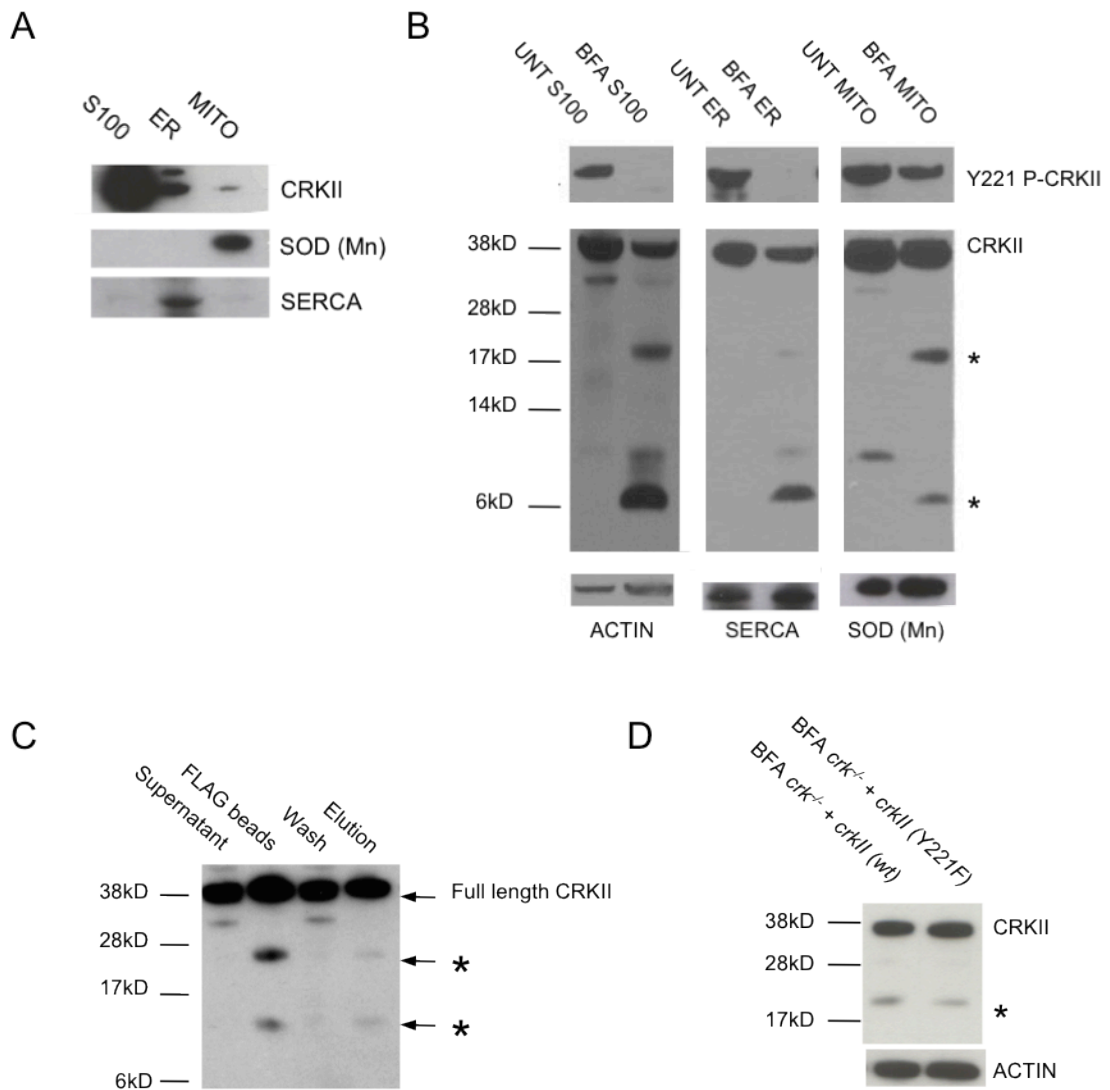


**Fig. 2.10.** CRKII undergoes cleavage upon irremediable ER stress. (A) Subcellular localization of CRKII. CRKII is largely localized to the cytosol and partially to the ER and mitochondrion. (B) Upon 24h BFA (2.5  $\mu\text{g/ml}$ ) treatment of *Bax<sup>-/-</sup>Bak<sup>-/-</sup>* MEFs, cytosolic and ER-localized CRKII is dephosphorylated at Tyrosine221 (Y221). Full-length CRKII (detected by CRKII-specific antibody) is depleted in the cytosol and at the ER. CRKII-specific fragments (\*) appear in the cytosol, ER, and mitochondria. (C) *crk<sup>-/-</sup>* MEFs reconstituted with C terminal FLAG-CRKII were treated for 24 hours with BFA (2.5  $\mu\text{g/ml}$ ). CRKII fragments were isolated using FLAG antibody conjugated beads and then eluted from beads using a 3x FLAG peptide. Asterisks indicate C-terminal specific CRKII fragments that appear upon ER stress induction. (D) Upon 24h BFA (2.5  $\mu\text{g/ml}$ ) treatment, cleavage of Y221F is comparable to wild-type CRKII.

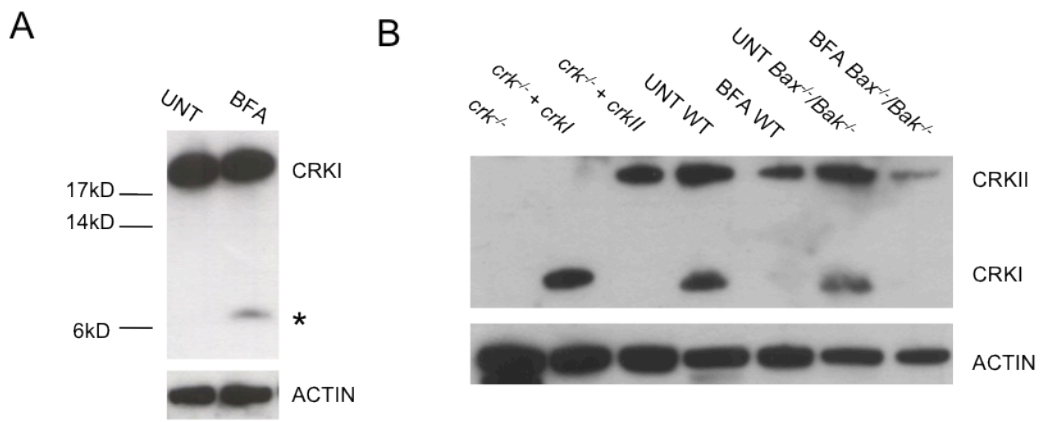


**Fig. 2.11.** (A) Transiently expressed CRKI is also cleaved upon 24h BFA-treatment in *crk*<sup>-/-</sup> MEFs. \* = CRKI-specific fragment. (B) Loss of endogenous CRKI and CRKII observed upon 18h BFA treatment of WT and *Bax*<sup>-/-</sup>/*Bak*<sup>-/-</sup> MEFs.

Furthermore, cells must distinguish between low levels of ER stress that can be resolved through increases in protein folding capacity and irremediable ER stress that is incompatible with survival. Hence, ER damage sensors likely exist to alert the cell when this critical threshold has been crossed so that apoptotic signaling can be initiated. Given that CRK is required for ER stress-induced apoptosis and is partly localized to the ER, we wondered whether its activation threshold for responding to ER stress is set higher than that of cytoprotective signals from the UPR. Notably, while sub-lethal doses of ER stress agents readily lead to UPR homeostatic signaling outputs from IRE1 $\alpha$  (XBP1 splicing), they do not result in CRKII dephosphorylation or cleavage (Fig. 2.12a). In contrast, CRK becomes activated only at levels of ER stress that trigger apoptosis (Fig. 2.12b). These data suggest that CRK may be functioning to both sense extreme ER stress and communicate this information to the mitochondrial apoptotic machinery. To further investigate which signaling branch of the UPR communicates irremediable ER stress to CRK, we analyzed *perk*<sup>-/-</sup>, *atf6* $\alpha$ <sup>-/-</sup>, and *ire1* $\alpha$ <sup>-/-</sup> MEFs for CRKII dephosphorylation and CRK cleavage. Of note, we observed that CRKII dephosphorylation and CRK cleavage is significantly inhibited in the absence ATF6 $\alpha$  (Fig 2.12c). These data indicate that CRK senses and executes an ER stress-induced apoptotic signal downstream of ATF6 $\alpha$ .



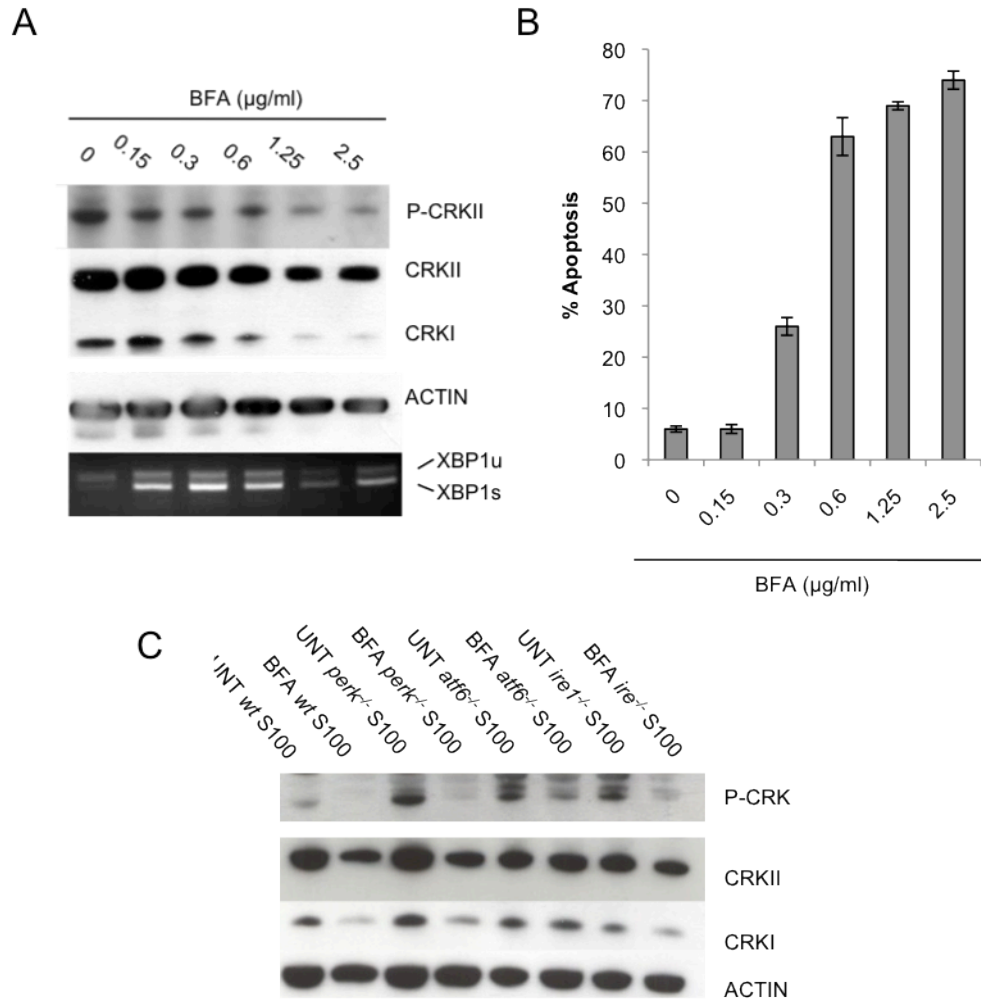


**Fig. 2.12.** CRK senses and executes an apoptotic signal downstream of ATF6. (A) Decreasing doses of BFA (18h) treated WT MEF whole cell lysate immunoblotted for CRK and phosphorylated (Y221) CRKII. XBP1 splicing assay of decreasing doses of BFA treated WT MEFs. (B) WT MEFs treated with decreasing doses of BFA (18h). Apoptosis measured by Annexin-V expression. (C) *Perk*<sup>-/-</sup>, *atf6*<sup>-/-</sup>, *ire1*<sup>-/-</sup> MEFs, the Unfolded Protein Response transmembrane sensors, were treated 14h with BFA (2.5 μg/ml) and analyzed by western blot for CRKII Y221 dephosphorylation and CRK cleavage.

In an attempt to determine the role of CRK cleavage for its apoptotic activity, we tested a small panel of protease inhibitors for their ability to block this event (data not shown). We found that the pan-cysteine protease inhibitor ZVAD-FMK prevents ER stress-induced loss of full-length CRKI and CRKII (Fig.2.13a) and protects *Bax*<sup>-/-</sup>*Bak*<sup>-/-</sup> MEFs from the cytopathic effects of ER stress (Fig. 2.13b). We previously identified caspase-2 as a pre-mitochondrial cysteine protease activated by ER stress<sup>10</sup>. However, caspase-2 is poorly inhibited by ZVAD-FMK and *in vitro* experiments with recombinant caspase-2 do not result in CRK cleavage (data not shown). These data suggest that a novel ER stress-activated cysteine protease is responsible for CRK cleavage.

To determine if the observed ER stress-induced cleavage of CRK is critical for its apoptotic activity, we individually mutated each potential cysteine protease cleavage site (aspartic acid) in the CRK sequence. When stably reconstituted into *crk*<sup>-/-</sup> MEFs, CRKII ΔD110A (*crk*<sup>-/-</sup> +*crkII* (ΔD110A)) was the only aspartic acid mutant unable to be cleaved in response to ER stress (Fig. 2.14a). Furthermore, non-cleavable CRKII ΔD110A is defective in restoring *crk*<sup>-/-</sup> MEF sensitivity to ER stress-induced apoptosis (Fig. 2.14b, c), arguing that this cleavage event is critical for its apoptotic activity.

Cleavage at D110 is predicted to produce one fragment of approximately 25kD, which can be detected by a C-terminal-specific antibody (Fig. 2.14a), and a second N-terminal fragment of ~14kD, which is undetectable using available antibodies. As both CRKI and CRKII restore *crk*<sup>-/-</sup> sensitivity to ER stress, it is likely the shared N-terminal fragment (~14kd) contains the critical domain for its

apoptotic function. To test this prediction, we transiently expressed the N-terminally FLAG-tagged fragment (NF110) in the absence of ER stress (Fig. 2.14d) and measured apoptosis. As predicted, NF110 is able to potently induce cell death independently of ER stress (Fig. 2.14e, f). From these data, we conclude that CRK is cleaved upon ER stress at D110, to produce a novel pro-apoptotic fragment. Further studies will be necessary to identify the upstream protease and its connection to the unfolded protein response pathway.

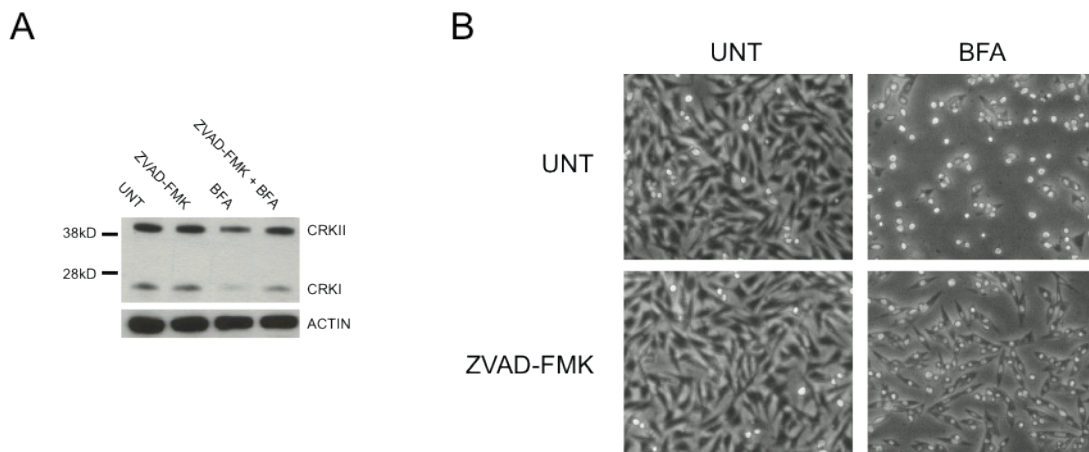


**Fig. 2.13** (A) Cleavage of CRKI and CRKII in *Bax*<sup>-/-</sup>*Bak*<sup>-/-</sup> MEFs treated 24h with 100 $\mu$ M pan-cysteine protease inhibitor (ZVAD-FMK) followed by 18h BFA (1.25  $\mu$ g/ml) is significantly decreased in comparison to *Bax*<sup>-/-</sup>*Bak*<sup>-/-</sup> MEFs treated with BFA alone (B). CRK is cleaved by a cysteine protease upstream of the mitochondria. *Bax*<sup>-/-</sup>*Bak*<sup>-/-</sup> MEFs treated 24h with 100 $\mu$ M pan-cysteine protease inhibitor (ZVAD-FMK) followed by 18h BFA (1.25  $\mu$ g/ml) show visibly decreased cytopathic effects of ER stress-induced apoptosis.

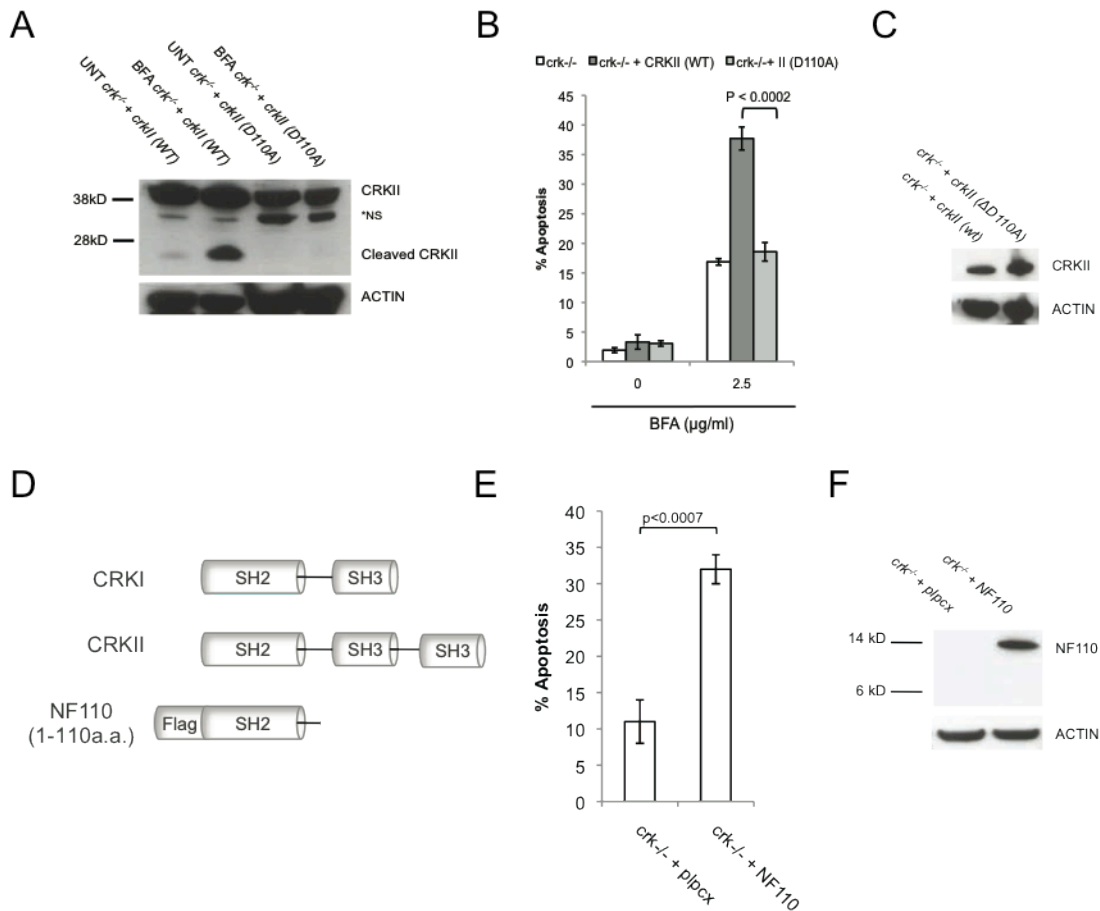


**Fig. 2.14** (A) Upon ER stress, CRK is cleaved at D110. Mutation of this site (D110A) in CRKII prevents cleavage following 24h 2.5 μg/ml BFA treatment in stably reconstituted in *crk*<sup>-/-</sup> MEFs. (B, C) CrkII (D110A) is not able to rescue *crk*<sup>-/-</sup> MEF sensitivity to ER stress-induced apoptosis induced by 24h 2.5 μg/ml BFA, in contrast to *crk*<sup>-/-</sup> MEFs stably expressing wild-type (WT) CRKII. (D) Diagram of CRK (1-110a.a.) cleavage fragment (NF110) produced upon ER stress. (E, F) Transient expression of NF110 induces apoptosis independent of ER stress.

To further investigate the mechanism by which CRK triggers cell death, we tested if CRK-induced apoptosis is a BAX/BAK-dependent process. Transient overexpression of CRKI or CRKII triggers apoptosis in WT MEFs, but not *Bax*<sup>-/-</sup> *Bak*<sup>-/-</sup> MEFs, confirming that both isoforms signal upstream of the BAX/BAK-dependent mitochondrial apoptotic pathway (Fig. 2.15). Pro-apoptotic BH3-only proteins are the only known molecules capable of activating BAX and/or BAK either directly or by inhibiting anti-apoptotic BCL-2 family proteins (10). Through sequence analysis, we identified a putative BH3-like domain within CRK that contains a number of conserved amino acids present in several recognized BH3-only proteins (Fig. 2.16a). This sequence is present in both *crk* splice forms and located within the common N-terminal 110 a.a. pro-apoptotic fragment (Fig. 2.3c, 2.16a). In support of our hypothesis that CRK contains a BH3-like domain, we determined that CRK is capable of binding a prototypical anti-apoptotic BCL-2 family protein (BCL-XL), a common feature of most BH3-only proteins. Following ER stress induction, transiently expressed FLAG-CRKII co-immunoprecipitates with BCL-XL on FLAG-specific agarose beads (Fig. 2.16b).

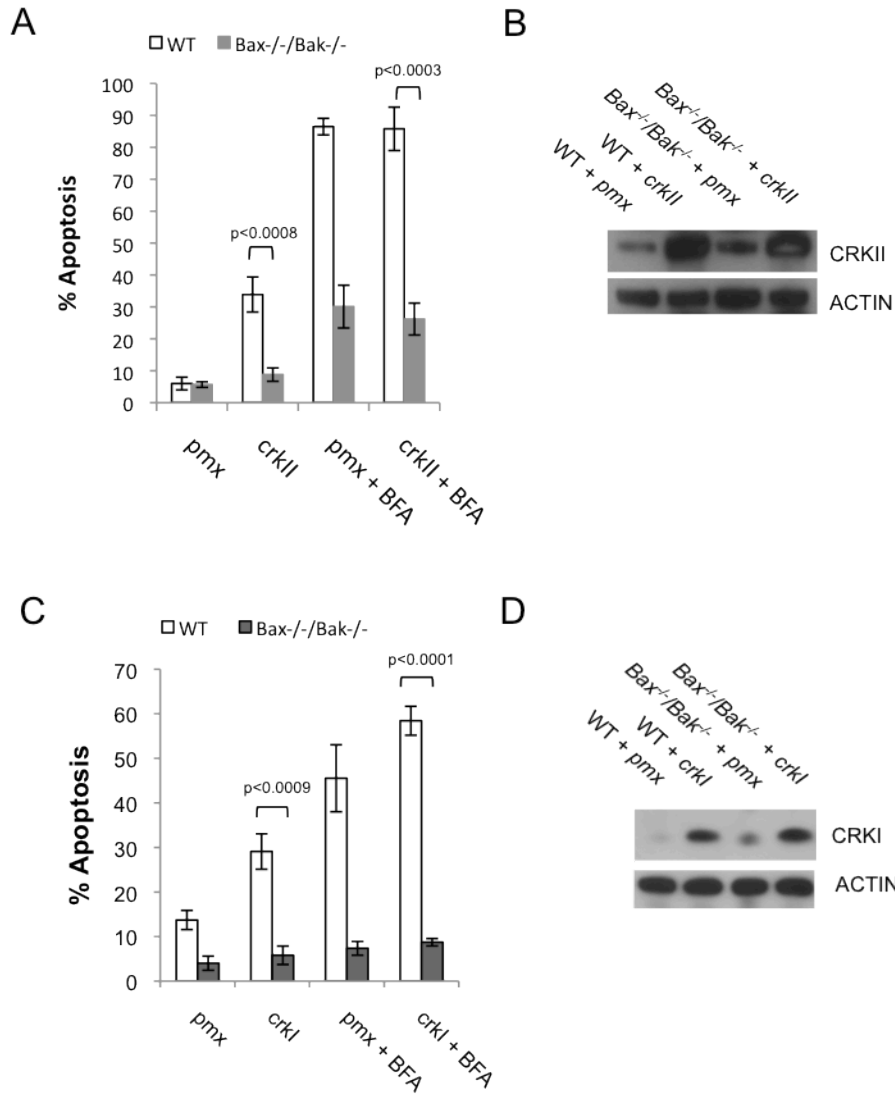


**Fig. 2.15.** CRK triggers BAX/BAK-dependent apoptosis. (A, B) CRKII and empty vector were transiently overexpressed in WT and *Bax<sup>-/-</sup>Bak<sup>-/-</sup>* MEFs using retroviral infection. 24h post retroviral infection cells were treated with BFA (2.5  $\mu$ g/ml) for an additional 24h and analyzed for Annexin-V expression by flow cytometry and protein expression by immunoblotting. (C, D) CRKI and empty vector (pmx) were transiently overexpressed in WT and *Bax<sup>-/-</sup>Bak<sup>-/-</sup>* MEFs. 24h post transfection cells were treated an additional 18h with BFA (2.5  $\mu$ g/ml) and analyzed for Annexin-V expression by flow cytometry and protein expression by immunoblotting.

To determine if this sequence has BH3-like pro-apoptotic activity, we treated isolated Jurkat mitochondria with a synthetic CRK BH3 domain (77-96 a.a.) and measured cytochrome *c* release. There are two classes of BH3-only domains, those that sensitize or activate BAX/BAK-dependent mitochondrial apoptosis(5). BH3 domains that directly “activate” BAX and/or BAK at mitochondria, such as the BH3 domain of BID, are able to cause cytochrome *c* release from isolated mitochondria. In contrast, “sensitizing” BH3 domains, such as the BH3 domains of BAD and BIK, sensitize isolated mitochondria to release cytochrome *c* in the presence of a second “activating” BH3 domain. *In vivo*, sensitizer BH3-only proteins are thought to competitively bind anti-apoptotic proteins, releasing bound “activating” BH3-only proteins to induce mitochondrial permeability. While the CRK BH3 domain is unable to induce cytochrome *c* release alone, it significantly potentiates with low concentrations of truncated BID (tBID) to cause cytochrome *c* release (Fig. 2.16c).

To further examine if this putative BH3 domain is required for CRK’s pro-apoptotic activity in cells, we mutated the highly conserved aspartic acid (*D91A*) in *crkII* and evaluated the ability of this mutant to rescue the *crk*<sup>-/-</sup> MEF phenotype. In comparison to wild-type *crk*, the BH3 mutant *crk (D91A)* has significantly decreased apoptotic activity, arguing that this region is critical for its pro-death signaling (Fig. 2.17a, b).

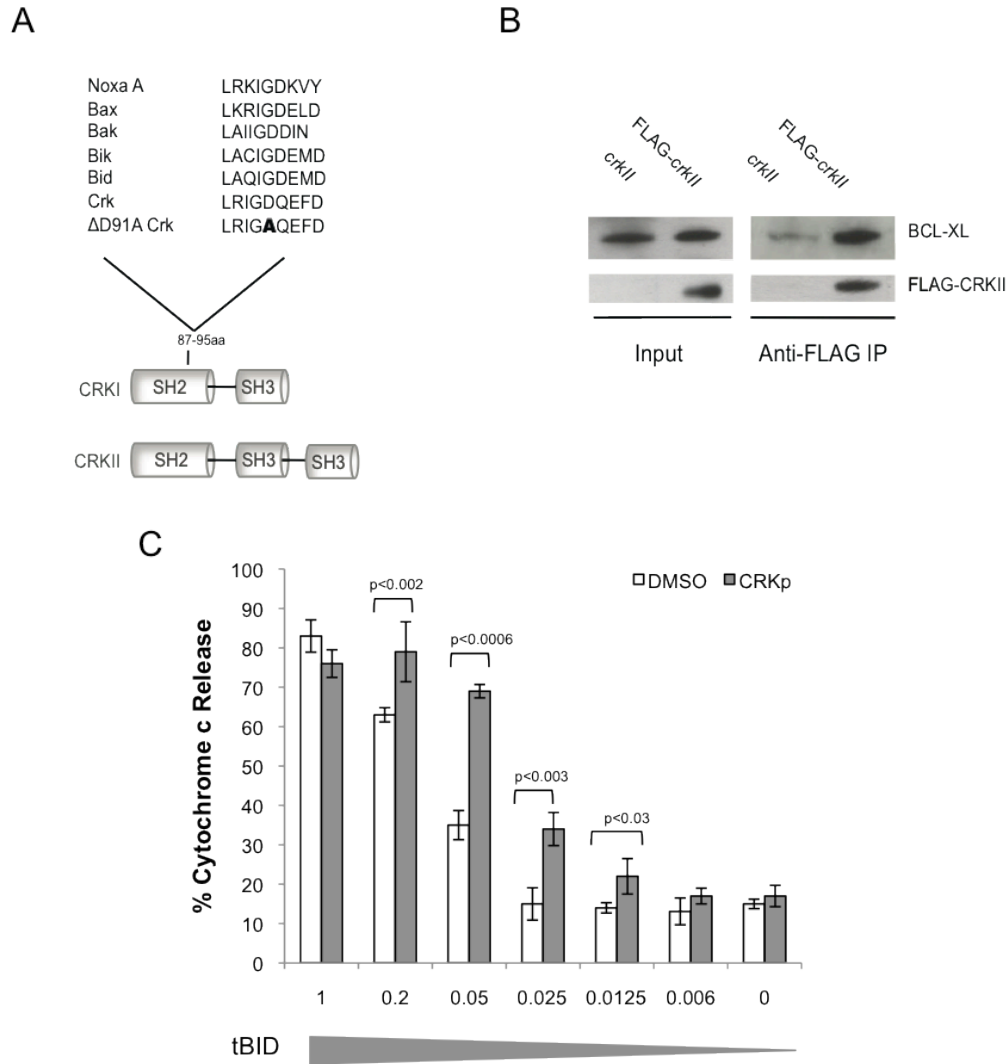


**Fig. 2.16** (A) The sequences of the putative BH3-only domain of CRK and the “BH3 domain” point mutation D91A are aligned against BH3 domains of several known BH3-only proteins. (B) 293 cells were transiently transfected 24h with *Flag-crkl/* or untagged *crkl/*, then treated 14h BFA (1.25 $\mu$ g/ml). Lysates were incubated with FLAG-specific agarose beads. Beads were immunoblotted for endogenous BCL-XL. (C) Cytochrome c release from isolated Jurkat mitochondria incubated with decreasing doses of tBID and CRK BH3 domain peptide.



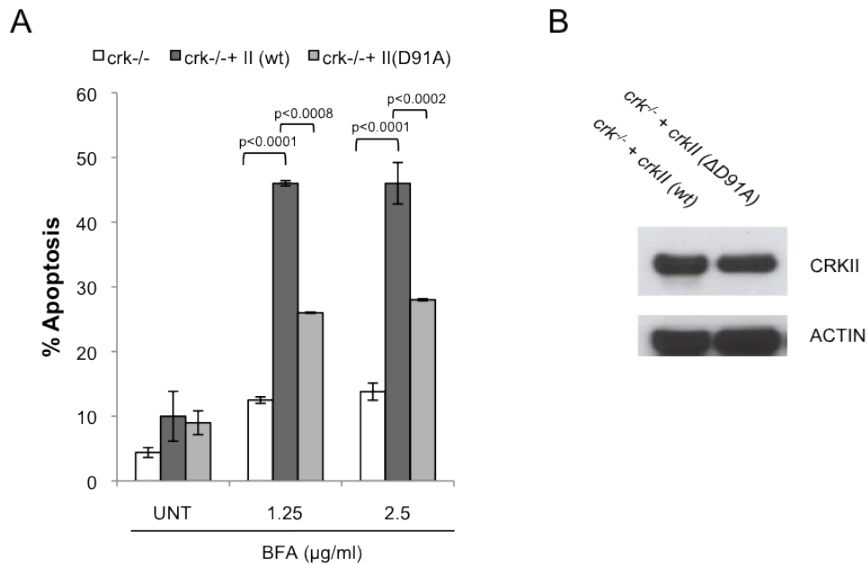


**Fig. 2.17** (A, B) Stable reconstitution of D91A *crkII* into *crk<sup>-/-</sup>* MEFs is significantly less effective at restoring ER stress-induced apoptosis (24h BFA treatment) in comparison to expression of wild-type *crkII*.

## DISCUSSION

Together, these results identify CRK as a major pro-apoptotic signal required for the execution of ER stress-induced cell death. During ER stress, CRKI and CRKII are cleaved by a yet to be identified cysteine protease to generate an N-terminal fragment with potent apoptotic activity. Furthermore, CRK interacts with anti-apoptotic BCL-XL and its apoptotic activity is upstream of the BAX/BAK-dependent mitochondrial pathway. Both CRK isoforms contain a putative BH3 domain, which sensitizes isolated mitochondria to tBID-induced cytochrome *c* release and when mutated diminishes apoptotic activity in cells. These data argue that CRK is a novel BH3-only-like protein, which upon ER stress is proteolytically processed into a pro-death signal. Our findings suggest that CRK may be a valuable therapeutic target in diseases where ER stress-induced cell loss is implicated, including some forms of neurodegeneration and

diabetes (7, 12).

We have identified a previously unknown pro-apoptotic function common to both CRK isoforms. CRK was initially identified through its homology with transforming *v-crk*(13). However, only CRKI has been shown to have transforming activity in some cell culture models, and it is upregulated in a number of human cancers (14). Clues that CRK mediates apoptosis are present in other species. For example, the *C. elegans* Crk-homologue CED-2 regulates apoptotic engulfment (20, 21). Mammalian CRKII has been reported to induce death in some transformed cell types upon overexpression (17) and is required for apoptotic activity that can be detected in *Xenopus* egg extracts (3). Our work is the first to connect CRK to apoptosis, specifically under ER stress, in mammalian cells.

In addition to the shared pro-apoptotic function we have discovered for CRKI and CRKII, there are notable and possibly functionally significant differences between the isoforms. Our inability to establish a cell line stably overexpressing CRKI, in contrast to multiple cell lines stably overexpressing CRKII, suggests that CRKI may be the more cytotoxic isoform. Indeed, the expression of endogenous CRKI is restricted to approximately 10% that of CRKII (Fig. 2.8a, b), perhaps to limit its toxicity. In support of this notion, we observe that CRKI is cleaved more efficiently and at earlier kinetics than CRKII in response to ER stress (Fig. 2.12b, 2.13b). These observations and our discovery that CRKI can be converted into a pro-apoptotic protein in response to ER stress raise the possibility that pharmacologic inducers of ER stress may

have therapeutic efficacy in cancers where *crkl* is upregulated.

## MATERIALS AND METHODS

**Cellular Fractionation and Cytochrome c Release Assay.** MEFS were resuspended in mitochondria isolation buffer (200mM sucrose, 10mM Tris/MOPS (morpholinepropanesulfonic acid) [pH 7.4], 1mM EGTA) plus 1x protease inhibitor cocktail (PIC, Sigma) and manually disrupted by shearing the suspension 10x through a 27-gauge and then 10x through a 30-gauge needle. Mitochondria (heavy membrane) were isolated from the suspension with an initial 700xg 4°C centrifugation to remove nuclei, followed by a 7000xg 4°C centrifugation to isolate heavy membrane (mitochondrial) fraction. The endoplasmic reticulum (light membrane) was isolated from the cytosolic fraction (S100) by a 100,000xg 4°C centrifugation. Mitochondrial and ER fractions were resuspended in RIPA (150mM NaCl, 1% NP40, 0.5% DOC, 0.1% SDS, 50mM Tris [pH 8.0]). S100 was dialyzed for 2 hours into 10% glycerol-containing mitochondria experimental buffer (MEB; 125mM KCl, 10mM Tris/MOPS [pH 7.4], 5mM glutamate, 1.25mM malate, 2 $\mu$ M EGTA, 1 $\mu$ M KPhos). Jurkat mitochondria for the cytochrome c releasing assay were isolated as described above, minus the second shearing through the 30-gauge needle. For the cytochrome c releasing assay reaction, 100-200 $\mu$ g (sample dependent) of S100 extract was incubated with 50 $\mu$ g of isolated Jurkat mitochondria for 45 minutes at room temperature. Following the incubation, the supernatant and pellet were separated by a 4°C 16,000xg centrifugation. The remaining cytochrome c was released from mitochondria by resuspending the pellet in PBS plus 0.05% Triton-

X. The amount of cytochrome *c* present in the supernatant and lysed pellets was quantified using a human cytochrome *c* linked immunosorbent assay (ELISA)(R&D systems) per the manufacturer's instructions. The percentage of cytochrome *c* release was calculated by dividing the amount of cytochrome *c* present in the supernatant by the sum of cytochrome *c* present in both the supernatant and pellet fractions.

**Purification of Cytochrome *c* Releasing Activity.** The ER stress apoptotic factor was purified using the CcRA assay described above. Briefly, 804mg of S100 protein isolated from 24h BFA (2.5  $\mu$ g/ml) treated *Bax*<sup>-/-</sup>*Bak*<sup>-/-</sup> MEFs was initially precipitated with 40-80% saturated ammonium sulfate. This active fraction was then further purified on a Phenyl Sepharose column (GE Healthcare) by loading in 1M Ammonium Sulfate and eluting with a 100mM Na<sub>2</sub>HPO<sub>4</sub> – 100mM Na<sub>2</sub>HPO<sub>4</sub> gradient. The CcRA eluted in the 100.925-62.875ms/cm range and was further purified on a MonoP column (GE Healthcare) gradient pH 6-10. The CcRA eluted between pH 9-6. This fraction was then purified further on the Superdex 200 column (GE Healthcare) and eluted in the 10-44kD range. This CcRA containing-fraction was run over a MonoQ column (GE Healthcare) 10mM KCl-1M KCl gradient. The purified CcRA fraction was analyzed in-gel and in-solution by MS/MS mass spectrometry by the UCSF Biomolecule Core Facility and the Stanford University of Medicine, Protein and Nucleic Acid Facility (PAN).

**Cell culture and biological reagents.** SV40 transformed *Bax*<sup>-/-</sup>*Bak*<sup>-/-</sup> and WT control MEFs were passaged as previously described(25). *Crk*<sup>-/-</sup> and WT control MEFs were 3T3 immortalized. All MEFs were maintained in Iscove's modified Dulbecco's medium supplemented with 10% fetal bovine serum, 100U/ml penicillin, 100ug/ml streptomycin, 2mM glutamine, and nonessential amino acids (UCSF cell culture facility). Human Jurkat cells were maintained in RPMI supplemented with 10% fetal bovine serum, 100U/ml penicillin, 100ug/ml streptomycin, 2mM glutamine, 100mM HEPES, and nonessential amino acids (UCSF cell culture facility). Annexin-V FITC was purchased from BioVision. Protease inhibitor cocktail (PIC), IPTG (isopropyl-4-D-thiogalactopyranoside), thapsigargin (TG), brefeldin A (BFA), staurosporine (STS), tunicamycin (TUN), and ZVAD-FMK were purchased from Sigma.

**Antibodies, immunoprecipitation, and Western Blot analysis.** Antibodies used for Western Blot analysis include anti-CRKII (Sigma), anti-CRK (BD Biosciences), anti-Mn SOD (assay designs), anti-SERCA (affinity bioreagents), anti-BCL-XL (santa cruz technologies) and anti-ACTIN (Sigma). Secondary antibodies were purchased from Jackson ImmunoResearch (anti mouse, anti-rat, and anti-rabbit antibodies) and Bio-Rad (anti-goat antibody). FLAG-CRKII pull down utilized anti-FLAG M2 affinity gel (SIGMA).

**Transient transfection and stable cell line selection.** MEFs were transiently transfected using Lipofectamine 2000 (Invitrogen) per the manufacturer's

instructions. 293 cells were transfected using Fugene6 (Promega) per the manufacturer's instructions. The *crkl* and *crklI* stable cell lines were made by transfecting a retroviral packaging line (293GPG or Phoenix) with *pmx-crkl*, *pmx-crklI*, and *plpcx-crklI* plasmids. Virus was harvested and titered from the supernatants of these packaging cell lines. Following infection with the virus, stable lines were isolated using puromycin selection.

**Plasmid Construction.** *crklI* mutants were generated using Stratagene Quickchange Lightning Site-directed Mutagenesis Kit.

**qPCR.** *Crk* isoform mRNA levels were quantitated using qPCR. Sybrgreen (applied biosystems) was used to measure *crk* isoforms with primers designed to recognize only *crklI*. The amount of *crklI* mRNA was subtracted from total *crk* mRNA (primers specific to both isoforms) in order to quantitate the amount of *crkl* mRNA present.

**Annexin V staining and FACS analysis.** Cells were harvested with 0.25% trypsin, washed once with 1x PBS, and incubated with Annexin V binding buffer (2mM CaCl<sub>2</sub>, 80mM NaCl, 1% HEPES plus 1μg/ml fluorescein isothiocyanate-annexin V) for 5 min. The cells were subsequently passed through a FACSCalibur machine (Becton Dickinson) and detected with CellQuest software (BD Biosciences). Statistical analyses were completed using Student's *t* test.

**CRK synthetic peptide.** The CRK BH3 domain peptide was synthesized by ELIM biopharm. Sequence synthesized: QPPPGVSPSRLRIGAQEFDS.

<b>Plasmid</b>	<b>Source</b>
CRKI/pmx	this work
CRKII/pmx	this work
pmx	this work
Y221FCRKII/pmx	this work
D91ACRKII/pmx	this work
C-FLAG-CRKII/plpcx	this work
N-FLAG CRK 110/plpcx	this work
PTP1BshRNAG6/pGIPZ	Thermo Scientific
Negative shRNA1/pGIPz	Thermo Scientific
Negative shRNA2/pGIPz	Thermo Scientific
PTP1BshRNAE5/pGIPz	Thermo Scientific

**Table 2.2.** Plasmids used in Chapter 2.



## REFERENCES

1. **Chipuk, J. E., and D. R. Green.** 2009. PUMA cooperates with direct activator proteins to promote mitochondrial outer membrane permeabilization and apoptosis. *Cell Cycle* **8**:2692-2696.
2. **Du, C., M. Fang, Y. Li, L. Li, and X. Wang.** 2000. Smac, a mitochondrial protein that promotes cytochrome c-dependent caspase activation by eliminating IAP inhibition. *Cell* **102**:33-42.
3. **Evans, E. K., W. Lu, S. L. Strum, B. J. Mayer, and S. Kornbluth.** 1997. Crk is required for apoptosis in *Xenopus* egg extracts. *EMBO J* **16**:230-241.
4. **Feller, S. M.** 2001. Crk family adaptors-signalling complex formation and biological roles. *Oncogene* **20**:6348-6371.
5. **Letai, A., M. C. Bassik, L. D. Walensky, M. D. Sorcinelli, S. Weiler, and S. J. Korsmeyer.** 2002. Distinct BH3 domains either sensitize or activate mitochondrial apoptosis, serving as prototype cancer therapeutics. *Cancer Cell* **2**:183-192.
6. **Li, H., H. Zhu, C. J. Xu, and J. Yuan.** 1998. Cleavage of BID by caspase 8 mediates the mitochondrial damage in the Fas pathway of apoptosis. *Cell* **94**:491-501.
7. **Lin, J. H., P. Walter, and T. S. Yen.** 2008. Endoplasmic reticulum stress in disease pathogenesis. *Annu Rev Pathol* **3**:399-425.
8. **Lindsten, T., A. J. Ross, A. King, W. X. Zong, J. C. Rathmell, H. A. Shiels, E. Ulrich, K. G. Waymire, P. Mahar, K. Frauwirth, Y. Chen, M. Wei, V. M. Eng, D. M. Adelman, M. C. Simon, A. Ma, J. A. Golden, G. Evan, S. J. Korsmeyer, G. R. MacGregor, and C. B. Thompson.** 2000. The combined functions of proapoptotic Bcl-2 family members bak and bax are essential for normal development of multiple tissues. *Mol Cell* **6**:1389-1399.
9. **Liu, X., C. N. Kim, J. Yang, R. Jemmerson, and X. Wang.** 1996. Induction of apoptotic program in cell-free extracts: requirement for dATP and cytochrome c. *Cell* **86**:147-157.
10. **Lomonosova, E., and G. Chinnadurai.** 2008. BH3-only proteins in apoptosis and beyond: an overview. *Oncogene* **27 Suppl 1**:S2-19.
11. **Luo, X., I. Budihardjo, H. Zou, C. Slaughter, and X. Wang.** 1998. Bid, a Bcl2 interacting protein, mediates cytochrome c release from mitochondria in response to activation of cell surface death receptors. *Cell* **94**:481-490.
12. **Marciniak, S. J., and D. Ron.** 2006. Endoplasmic reticulum stress signaling in disease. *Physiol Rev* **86**:1133-1149.
13. **Matsuda, M., S. Tanaka, S. Nagata, A. Kojima, T. Kurata, and M. Shibuya.** 1992. Two species of human CRK cDNA encode proteins with distinct biological activities. *Mol Cell Biol* **12**:3482-3489.
14. **Miller, C. T., G. Chen, T. G. Gharib, H. Wang, D. G. Thomas, D. E. Misek, T. J. Giordano, J. Yee, M. B. Orringer, S. M. Hanash, and D. G. Beer.** 2003.

- Increased C-CRK proto-oncogene expression is associated with an aggressive phenotype in lung adenocarcinomas. *Oncogene* **22**:7950-7957.
15. **Oakes, S. A., S. S. Lin, and M. C. Bassik.** 2006. The control of endoplasmic reticulum-initiated apoptosis by the BCL-2 family of proteins. *Curr Mol Med* **6**:99-109.
  16. **Park, T. J., K. Boyd, and T. Curran.** 2006. Cardiovascular and craniofacial defects in Crk-null mice. *Mol Cell Biol* **26**:6272-6282.
  17. **Parrizas, M., V. A. Blakesley, D. Beitner-Johnson, and D. Le Roith.** 1997. The proto-oncogene Crk-II enhances apoptosis by a Ras-dependent, Raf-1/MAP kinase-independent pathway. *Biochem Biophys Res Commun* **234**:616-620.
  18. **Strasser, A.** 2005. The role of BH3-only proteins in the immune system. *Nat Rev Immunol* **5**:189-200.
  19. **Susin, S. A., H. K. Lorenzo, N. Zamzami, I. Marzo, B. E. Snow, G. M. Brothers, J. Mangion, E. Jacotot, P. Costantini, M. Loeffler, N. Larochette, D. R. Goodlett, R. Aebersold, D. P. Siderovski, J. M. Penninger, and G. Kroemer.** 1999. Molecular characterization of mitochondrial apoptosis-inducing factor. *Nature* **397**:441-446.
  20. **Tosello-Trampont, A. C., E. Brugnera, and K. S. Ravichandran.** 2001. Evidence for a conserved role for CRKII and Rac in engulfment of apoptotic cells. *J Biol Chem* **276**:13797-13802.
  21. **Tosello-Trampont, A. C., J. M. Kinchen, E. Brugnera, L. B. Haney, M. O. Hengartner, and K. S. Ravichandran.** 2007. Identification of two signaling submodules within the CrkII/ELMO/Dock180 pathway regulating engulfment of apoptotic cells. *Cell Death Differ* **14**:963-972.
  22. **Upton, J.-P., K. Austgen, M. Nishino, K. M. Coakley, A. Hagan, D. Han, F. R. Papa, and S. A. Oakes.** 2008. Caspase 2 Cleavage of BID is a critical apoptotic signal downstream of Endoplasmic Reticulum Stress. *Molecular and Cellular Biology* **28**:3943-3951.
  23. **Wang, K., X. M. Yin, D. T. Chao, C. L. Milliman, and S. J. Korsmeyer.** 1996. BID: a novel BH3 domain-only death agonist. *Genes Dev* **10**:2859-2869.
  24. **Wei, M. C., T. Lindsten, V. K. Mootha, S. Weiler, A. Gross, M. Ashiya, C. B. Thompson, and S. J. Korsmeyer.** 2000. tBID, a membrane-targeted death ligand, oligomerizes BAK to release cytochrome c. *Genes Dev* **14**:2060-2071.
  25. **Wei, M. C., W. X. Zong, E. H. Cheng, T. Lindsten, V. Panoutsakopoulou, A. J. Ross, K. A. Roth, G. R. MacGregor, C. B. Thompson, and S. J. Korsmeyer.** 2001. Proapoptotic BAX and BAK: a requisite gateway to mitochondrial dysfunction and death. *Science* **292**:727-730.

## **Identification of the cysteine protease responsible for CRK cleavage upon irremediable ER stress**

### **Background**

The ER stress-induced apoptotic pathway is poorly understood, but is therapeutically relevant to multiple diseases. There is a great need for expansion of available knowledge about the signaling components of this pathway. The previous chapter described the discovery of a novel pro-apoptotic protein, CRK, and its role in transducing the pro-death signal from the ER to the mitochondrion. These new data not only offer further understanding of this pathway, but also provide a tool with which to identify upstream proteins in this important pathway.

The cleavage of CRK at aspartic residue 110 converts the adaptor molecule into a pro-apoptotic BH3-only protein. This cleavage event is required for activity, and in addition, expression of the produced fragment (~14kD) alone is sufficient to induce cell death independently of ER stress (Fig. 3.1). During the identification of the cleavage site, it was discovered that CRK is cleaved by a cysteine protease and that inhibiting this cleavage correlates with a decrease in the cytopathic effects caused by ER stress-induced apoptosis (Fig. 3.2).

Identification of the cysteine protease responsible for CRK cleavage will further connect this pathway and provide a novel therapeutic target.

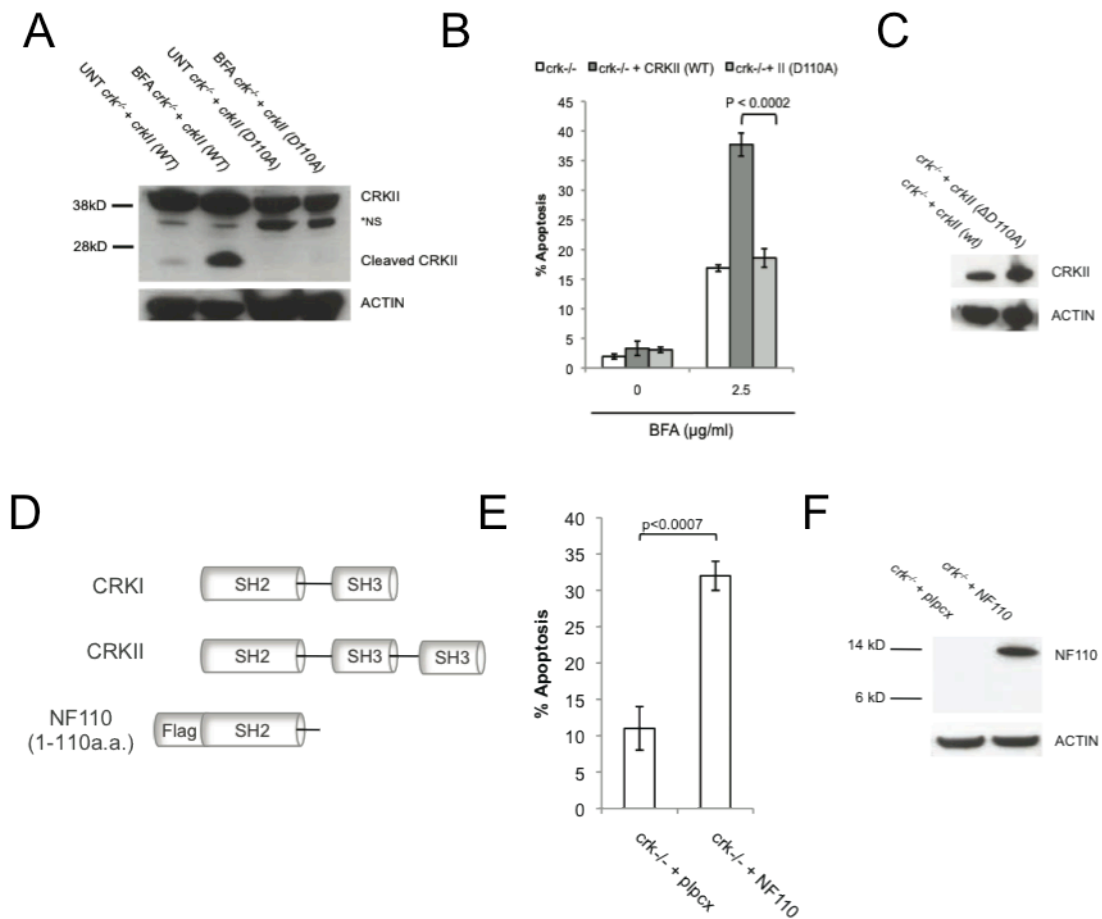


**Fig. 3.1** (A) Upon ER stress, CRK is cleaved at D110. Mutation of this site (D110A) in CRKII prevents cleavage following 24h 2.5 μg/ml BFA treatment in stably reconstituted in *crk*<sup>-/-</sup> MEFs. (B,C) CrkII (D110A) is not able to rescue *crk*<sup>-/-</sup> MEF sensitivity to ER stress-induced apoptosis induced by 24h 2.5 μg/ml BFA, in contrast to *crk*<sup>-/-</sup> MEFs stably expressing wild-type (WT) CRKII. (D) Diagram of CRK (1-110a.a.) cleavage fragment (NF110) produced upon ER stress. (E, F) Transient expression of NF110 induces apoptosis independent of ER stress.

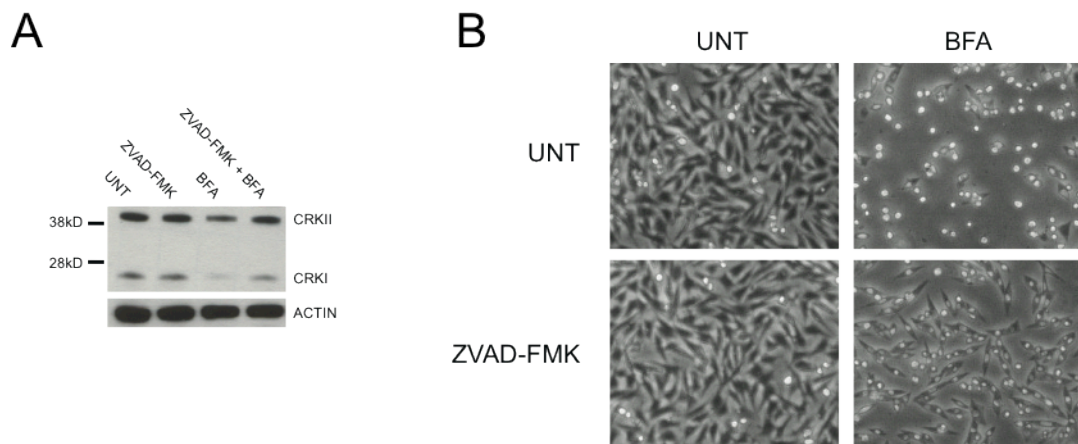


**Fig. 3.2** (A) Cleavage of CRKI and CRKII in *Bax*<sup>-/-</sup>*Bak*<sup>-/-</sup> MEFs treated 24h with 100μM pan-cysteine protease inhibitor (ZVAD-FMK) followed by 18h BFA (1.25 μg/ml) is significantly decreased in comparison to *Bax*<sup>-/-</sup>*Bak*<sup>-/-</sup> MEFs treated with BFA alone (B) . CRK is cleaved by a cysteine protease upstream of the mitochondria. *Bax*<sup>-/-</sup>*Bak*<sup>-/-</sup> MEFs treated 24h with 100μM pan-cysteine protease inhibitor (ZVAD-FMK) followed by 18h BFA (1.25 μg/ml) show visibly decreased cytopathic effects of ER stress-induced apoptosis.

Protease inhibitors constitute one of the largest potential drug target enzyme families. The catalytic efficiency of a small amount of these enzymes suggests their inhibition will have significant effects, therefore, making them appealing targets. However, the disparate nature of the physiological roles of proteases, the commonality of activating sites, and the diversity of their substrates has made them challenging to target and achieve a specific outcome. In spite of these challenges, the huge therapeutic potential of these enzymes remains. Identification of a novel cysteine protease involved in the ER stress-induced apoptotic pathway could lead to the development of a potent therapy for many diseases; including neurodegeneration, Type II diabetes, and some types of cancer and viral infections (2, 7, 12-14).

Cysteine proteases are grouped into two superfamilies: the family of enzymes related to interleukin 1 $\beta$  converting enzyme (ICE), and the papain superfamily. While both superfamilies share the active site cysteine characteristic, members of the papain family are distinct in their specificity for aspartate as the S1 amino acid, an uncommon cleavage site among proteases. Within the papain family there are four subgroups; calpains, bleomycin hydrolases, caspases, and cathepsins (4).

The cysteine protease inhibitor, **N-Benzylloxycarbonyl-Val-Ala-Asp(O-Me) fluoromethyl ketone** (C<sub>22</sub>H<sub>30</sub>FN<sub>3</sub>O<sub>7</sub>)(ZVAD-FMK), was utilized to determine that a cysteine protease is responsible for CRK cleavage. ZVAD-FMK is commonly and misleadingly portrayed in the literature as a caspase inhibitor. However, it inhibits members of both the ICE and papain families to varying

degrees (18). While the caspase family is widely acknowledged to be the main subfamily of cysteine proteases involved in apoptosis and targeted by ZVAD-FMK, our data indicate that any member of this superfamily could be responsible for CRK cleavage. Here we investigate which ER stress-induced cysteine protease is responsible for CRK cleavage and the mechanism of its activation.

## Results and Discussion

We discovered in a previous purification that BID is cleaved and activated upon irremediable ER stress and that this proteolysis is executed by caspase 2 (Fig. 3.3A). However, we clearly show that ZVAD-FMK does not efficiently inhibit caspase 2 *in vitro* (Fig. 3.3B). This argues that CRK is not cleaved by caspase 2, but by an as yet unidentified cysteine protease (22).

Interestingly, the mass spectrometry data from the biochemical purification contained a seemingly aberrant candidate. Fractions containing the pro-apoptotic activity contained a lysosomal cysteine protease, cathepsin L (Fig 3.4). This is surprising since the starting material for the purification was cytosolic extract. In healthy cells, cathepsins are mostly localized in the lysosome and the confinement of lysosomal content is tightly controlled. The presence of a lysosomal cysteine protease in the cytosol at levels high enough to be detected by mass spectrometry is of note.

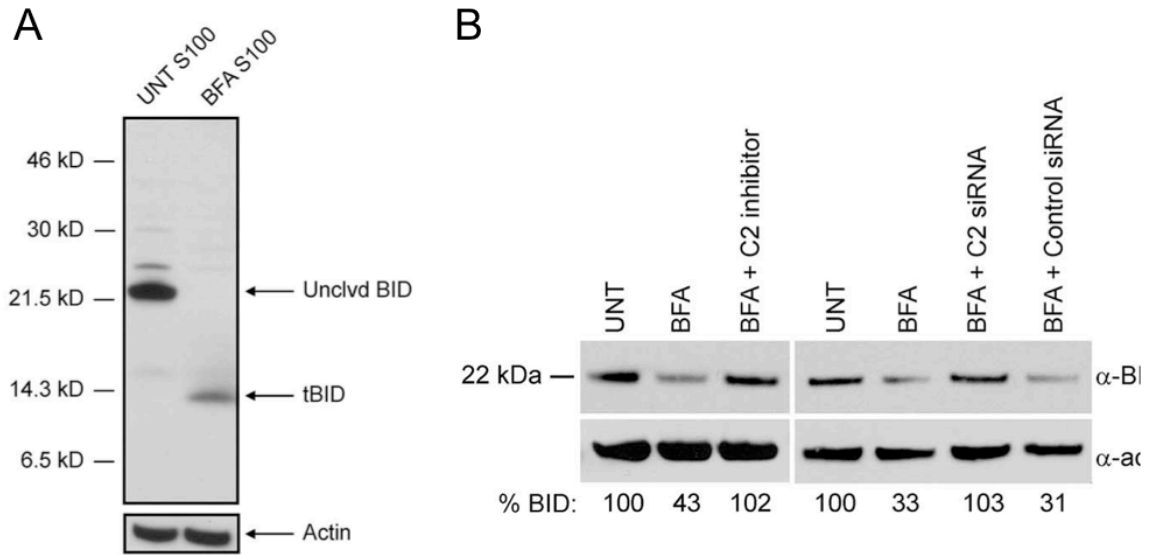


**Fig. 3.3.** (A) S100 extracts from untreated DKO MEFs and DKO MEFs treated with 2.5  $\mu\text{g/ml}$  BFA were immunoblotted for BID and actin. Only tBID was detected in the BFA S100 extract. Unclvd, uncleaved. (B) DKO MEFs were left untreated or were pretreated with 50  $\mu\text{M}$  z-VDVAD-fmk (C2 inhibitor), control siRNA, or caspase-2 siRNA (C2 siRNA), followed by treatment with 2.5  $\mu\text{g/ml}$  of BFA for 24 h. Immunoblotting for BID and subsequent quantification by densitometry showed that inhibiting or knocking down caspase-2 protected against BFA-induced cleavage of endogenous full-length BID. ", anti. *Upton and Austgen et. al. Mol and Cell. Biol. 2008.*

Peptide Information									
Calc. Mass	Obsrv. Mass	$\pm$ da	$\pm$ ppm	Start Seq.	End Sequence Seq.	Ion Score	C. I.	%	Modification
919.4631	919.4229	-0.0402	-44	117	123 SVDWREK	7		0	
919.4631	919.4229	-0.0402	-44	117	123 SVDWREK				
1047.5404	1047.4985	-0.0419	-40	50	57 AIWEKNMR				
1047.5404	1047.4985	-0.0419	-40	50	57 AIWEKNMR	17		0	
1063.5353	1063.5009	-0.0344	-32	50	57 AIWEKNMR				Oxidation (M)[7]
1063.5353	1063.5009	-0.0344	-32	50	57 AIWEKNMR				Oxidation (M)[7]
1347.7452	1347.6747	-0.0705	-52	103	113 GRLFQEPLMLK				Oxidation (M)[9]
1452.6866	1452.6273	-0.0593	-41	39	49 LYGTNEEEWRR				
1452.6866	1452.6273	-0.0593	-41	39	49 LYGTNEEEWRR	36	97.999		
1472.8545	1472.7759	-0.0786	-53	105	116 LFQEPLMLKIPK				Oxidation (M)[7]
1472.8545	1472.7759	-0.0786	-53	105	116 LFQEPLMLKIPK				Oxidation (M)[7]
1902.8762	1902.7883	-0.0879	-46	317	334 DRDNHCGLATAASYPPV N				

**Fig. 3.4.** Mass spectrometry hit from CcRA containing fractions from MonoQ in biochemical purification.



Cathepsins could be called the caspases of the lysosome, given the many parallels between the two types of cysteine protease. Caspases can be activated autocatalytically (endopeptidases) or by other caspases (exopeptidases). Cathepsins also contain these two subtypes. Furthermore, caspase activity can be directly inhibited by inhibitors of apoptosis (IAPs)(24). Similarly, cathepsins are directly inhibited by cystatins (1, 20, 21). The main difference between caspases and cathepsins is the subcellular localization. Caspases are located in the cytosol and cathepsins are largely confined to and function in the low pH (5.0) of the lysosome (19). This subcellular localization likely limits cathepsin access to potential substrates located outside of the lysosome. However, the presence of a cathepsin in the cytosolic extract raises the possibility that ER stress could induce cathepsin relocalization.

To test this possibility and determine if cathepsins are responsible for CRK cleavage, we utilized the lysosomal cysteine protease inhibitor, E64. The trans-epoxysuccinyl group (active moiety) of E-64 irreversibly binds to an active thiol group in many cysteine proteases, such as papain, actinidase, and cathepsins B, H, and L to form a thioether linkage (10). *Bax<sup>-/-</sup>Bak<sup>-/-</sup>* (DKO) MEFs were treated with E64, for two hours followed by 18h treatment with Brefeldin A (BFA), a chemical inducer of ER stress. CRK cleavage was significantly inhibited following BFA treatment in the presence of E64 (Fig. 3.5A). Furthermore, E64 reduces WT MEF sensitivity to ER stress-induced apoptosis (Fig. 3.5B). These data indicate that a cysteine protease inhibited by E64 is responsible for CRK

cleavage. Given these findings and the presence of cathepsins in the cytosol, we hypothesize a cathepsin is responsible for CRK cleavage.

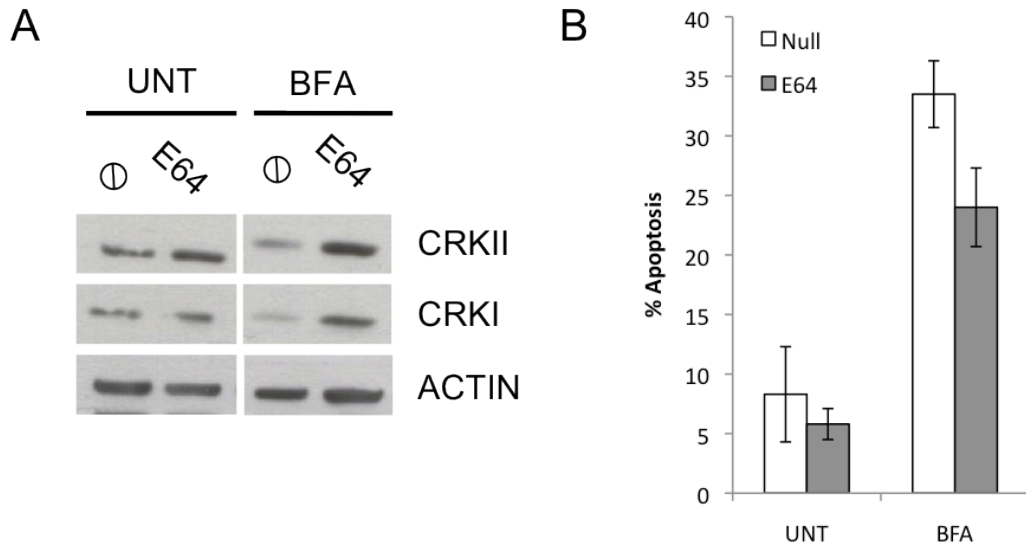


**Fig. 3.5.** (A) WT MEFS pretreated 2 hours with 1 $\mu$ M E64 followed by 18h BFA treatment. Whole cell lysate probed for loss of full-length CRKI and CRKII with anti-CRK antibody. (B) Annexin V staining of E64 pretreated cells followed by BFA treatment.

Cathepsins were discovered in the early 20<sup>th</sup> century. However, their complex role in cell biology has only recently come to light. Initially they were described as scavengers, non-specifically degrading proteins within the lysosome. There are eleven known human cysteine protease cathepsins (Table 3.1) (11). These enzymes are active as monomers of ~30kD and are either endo- or exopeptidases. Similarly to most other proteases, cathepsins are synthesized as inactive precursors (oligomers) and are activated by proteolytic removal of the N-terminal propeptide. The propeptide blocks the active site and prevents substrate binding. The propeptide can be autocatalytically removed

(endopeptidase) or removed by another protease (exo-peptidase). Activation of endopeptidases can be facilitated by a drop in pH and/or by glycosaminoglycans (15-17). However, it has been demonstrated that certain cathepsins also retain activity at neutral pH (3).

Name	Type
Cathepsin B	Endo-, exopeptidase
Cathepsin C	exopeptidase
Cathepsin F	exopeptidase
Cathepsin H	Endo-, exopeptidase
Cathepsin K	Exopeptidase
Cathepsin L	Endo-, exopeptidase
Cathepsin O	Exopeptidase
Cathepsin S	Endo-, exopeptidase
Cathepsin V	exopeptidase
Cathepsin W	exopeptidase
Cathepsin X	exopeptidase

**Table 3.1.** Cysteine protease cathepsins and their peptidase activities.

Cathepsins have been shown to play a poorly understood role in cell death. Cathepsin B is the best studied in the context of apoptosis. Cathepsin B has been shown to cleave BID and degrade a number of anti-apoptotic proteins: Bcl-2, Bcl-xL, Mcl-1 (5, 6). Cathepsin B is also necessary for TNF $\alpha$ -mediated hepatocyte apoptosis (9). However the mechanisms behind these observations are not well documented or understood.

To differentiate which E64 target is responsible for the observed activity we tested if recombinant cathepsin B or L could cleave endogenous CRKII *in vitro*. One active unit of Cathepsin B or L was incubated with cytosolic extract from untreated *crk*<sup>-/-</sup> MEFs reconstituted with full-length CRKII. Cathepsin B efficiently cleaved full-length CRKII when incubated and produced a ~20kD fragment, mirroring the ER stress-induced cleavage event (Fig. 3.6A). In contrast, when cytosolic extract from untreated *crk*<sup>-/-</sup> MEFs reconstituted with full-length CRKII was incubated with Cathepsin L, little to no depletion of full-length CRKII is observed. However, a seemingly specific ~10kD fragment is inefficiently produced (Fig. 3.6B), though the size of the fragment does not appear to correlate with any previously observed ER stress-induced cleavage products (Fig. 3.6C). From these data we can conclude that cathepsin B efficiently cleaves CRKII at a site close to the proven activating cleavage site. It is unclear from these experiments, if cathepsin L is also playing a role in CRK cleavage. It may be working coordinately with cathepsin B, subsequently cleaving the cathepsin B-produced ~20kD fragment. More studies are needed to determine the role of cathepsin L in ER stress-induced CRK cleavage.

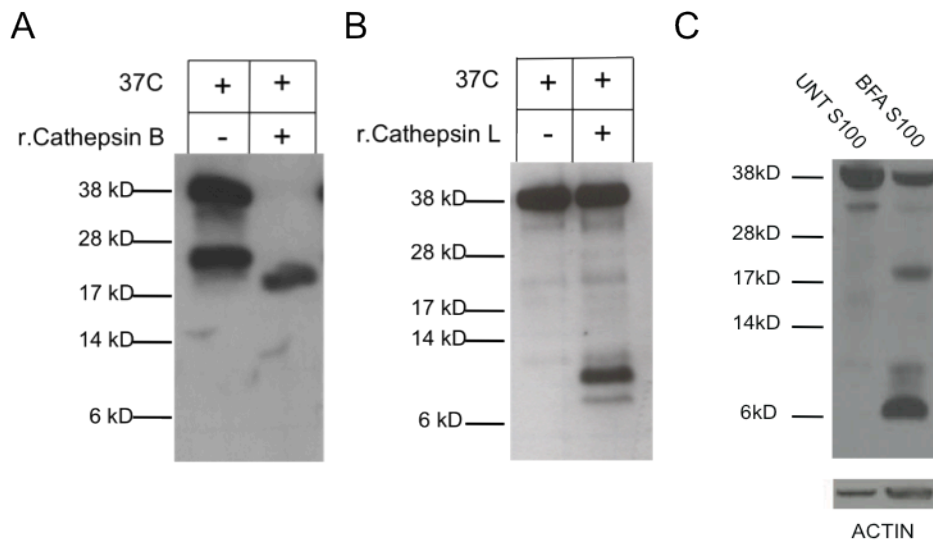


**Fig. 3.6.** (A) r.Cathepsin B incubated 1 hour, 37C with UNT *crk*<sup>-/-</sup> + CRKII S100. Probed with anti-CRK antibody. (B) r.Cathepsin L incubated 1 hour, 37C with UNT *crk*<sup>-/-</sup> + CRKII S100. Probed with anti-CRK antibody. (C) ER stress-induced (BFA) CRKII cleavage events in DKO MEFs.

As previously mentioned, cathepsins are normally localized to the lysosome post modification within the ER. Co-translational translocation of cathepsin B into the ER results in the formation of a preproenzyme with the subsequent removal of the signal peptide. Procathepsin B is produced upon removal of the signal peptide, is then N-glycosylated, and shuttled to the Golgi apparatus. Within the Golgi, further modification of the oligosaccharides to unique high-mannose carbohydrates occurs. Phosphorylation of the mannose residues directs the enzyme to the endosomal/lysosomal compartment via the mannose-6-phosphate receptor pathway (19). However, the ability of cathepsin B to specifically cleave CRKII in a pattern mirroring that produced by ER stress suggests that under conditions of stress, the protease may somehow get access to CRKII outside of the lysosome. This could occur during the post-translational modification process, the translocation to the lysosome, or via selective permeabilization of the lysosome. The selective release of cathepsins from the lysosome to the cytosol has been observed previously. Hepatocytes exposed to TNF release of cathepsin B from acidic vesicles into the cytoplasm, which results in the subsequent release of cytochrome c from mitochondria and execution of the caspase cascade (8).

To determine if cathepsin B translocates from the lysosome upon ER stress, we probed subcellular fractions from untreated and BFA-treated DKO MEFs. We observe a strong depletion of active cathepsin B from the lysosomal fraction and what appears to be the accumulation of cathepsin B in the ER (Fig.

3.7). However, the accumulation of cathepsin B at the ER upon BFA treatment must be repeated with another inducer of ER stress, as BFA prevents ER to Golgi transport. The observed accumulation may be artificially due to the chemical inhibition of transport of newly post-translationally modified pro-cathepsin B and not a result of translocation from the lysosome. Further studies are needed to differentiate between these possibilities and determine where the lysosomal cathepsin B is relocating.

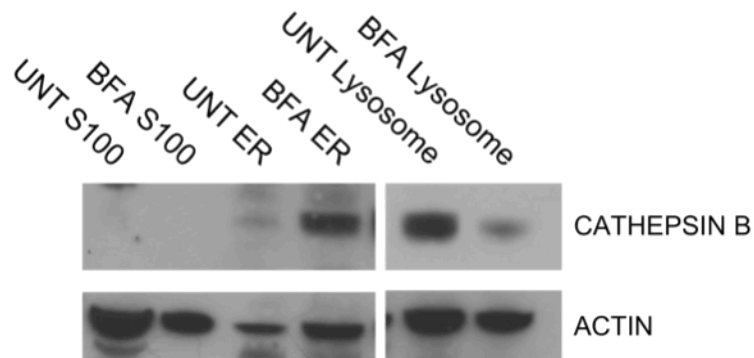


**Fig. 3.7.** Subcellular localization of cathepsin B following 24h 2.5 $\mu$ g/ml BFA treatment. Fractions probed with antibody to active cathepsin B.



If the cathepsin B knockout MEFs are resistant to irremediable ER stress, this would confirm that cathepsin B is the cysteine protease responsible for CRK cleavage. Preliminary studies with the cathepsin B-specific inhibitor, CA-074-Me, were unsuccessful due to the toxicity of the inhibitor at concentrations used. Of note, the cathepsin B knockout mice are viable. However, cathepsin B and L double knockout mice are embryonic lethal. This indicates that cathepsin B and L are redundant in processes vital to development and survival, such as their role in general lysosomal degradation. Confirmation that the lack of cathepsin B confers resistance to ER stress-induced apoptosis will solidify that CRK is cleaved by cathepsin B upon irremediable ER stress. We have discovered that a novel cysteine protease plays a critical role in the ER stress-induced apoptotic pathway and provide a short list of promising candidates for its identification.

## Materials and Methods

**Cell Culture and Reagents.** SV40 transformed *Bax*<sup>-/-</sup>*Bak*<sup>-/-</sup> and WT control MEFs were passaged as previously described (23). *Crk*<sup>-/-</sup> and WT control MEFs were 3T3 immortalized. All MEFs were maintained in Iscove's modified Dulbecco's medium supplemented with 10% fetal bovine serum, 100U/ml penicillin, 100ug/ml streptomycin, 2mM glutamine, and nonessential amino acids (UCSF cell culture facility). Annexin-V FITC was purchased from BioVision. Protease inhibitor cocktail (PIC), Brefeldin A, E64, and ZVAD-FMK were purchased from Sigma. CA-074-Me was purchased from (EMD chemicals).

**Cellular Fractionation.** . MEFs were resuspended in mitochondria isolation buffer (200mM sucrose, 10mM Tris/MOPS (morpholinepropanesulfonic acid) [pH 7.4], 1mM EGTA) plus 1x protease inhibitor cocktail (PIC, Sigma) and manually disrupted by shearing the suspension 10x through a 27-gauge and then 10x through a 30-gauge needle. Mitochondria (heavy membrane) were isolated from the suspension with an initial 700xg 4°C centrifugation to remove nuclei, followed by a 7000xg 4°C centrifugation to isolate heavy membrane (mitochondrial) fraction. The endoplasmic reticulum (light membrane) was isolated from the cytosolic fraction (S100) by a 100,000xg 4°C centrifugation. Mitochondrial and ER fractions were resuspended in RIPA (150mM NaCl, 1% NP40, 0.5% DOC, 0.1% SDS, 50mM Tris [pH 8.0]). S100 was dialyzed for 2 hours into 10% glycerol-containing mitochondria experimental buffer (MEB; 125mM KCl, 10mM Tris/MOPS [pH 7.4], 5mM glutamate, 1.25mM malate, 2μM EGTA, 1μM KPhos).

**Transient transfection and stable cell line selection.** MEFs were transiently transfected using Lipofectamine 2000 (Invitrogen) per the manufacturer's instructions. 293 cells were transfected using Fugene6 (Promega) per the manufacturer's instructions. Stable cell lines were made by selecting 48 hours post-transfection with 1.25  $\mu\text{g/ml}$  puromycin (Sigma Aldrich).

**Antibodies and Western Blot analysis.** Antibodies used for Western Blot analysis include anti-CRKII (Sigma), anti-CRK (BD Biosciences), anti-Cathepsin L (Abcam), anti-cathepsin B (Abcam), and anti-ACTIN (Sigma). Secondary antibodies were purchased from Jackson ImmunoResearch (anti mouse, anti-rat, and anti-rabbit antibodies) and Bio-Rad (anti-goat antibody).

## References

1. **Barrett, A. J., H. Fritz, A. Grubb, S. Isemura, M. Jarvinen, N. Katunuma, W. Machleidt, W. Muller-Esterl, M. Sasaki, and V. Turk.** 1986. Nomenclature and classification of the proteins homologous with the cysteine-proteinase inhibitor chicken cystatin. *Biochem J* **236**:312.
2. **Bi, M., C. Naczki, M. Koritzinsky, D. Fels, J. Blais, N. Hu, H. Harding, I. Novoa, M. Varia, J. Raleigh, D. Scheuner, R. J. Kaufman, J. Bell, D. Ron, B. G. Wouters, and C. Koumenis.** 2005. ER stress-regulated translation increases tolerance to extreme hypoxia and promotes tumor growth. *EMBO J* **24**:3470-3481.
3. **Buck, M. R., D. G. Karustis, N. A. Day, K. V. Honn, and B. F. Sloane.** 1992. Degradation of extracellular-matrix proteins by human cathepsin B from normal and tumour tissues. *Biochem J* **282 ( Pt 1)**:273-278.
4. **Chapman, H. A., R. J. Riese, and G. P. Shi.** 1997. Emerging roles for cysteine proteases in human biology. *Annu Rev Physiol* **59**:63-88.
5. **Cirman, T., K. Oresic, G. D. Mazovec, V. Turk, J. C. Reed, R. M. Myers, G. S. Salvesen, and B. Turk.** 2004. Selective disruption of lysosomes in HeLa cells triggers apoptosis mediated by cleavage of Bid by multiple papain-like lysosomal cathepsins. *J Biol Chem* **279**:3578-3587.
6. **Droga-Mazovec, G., L. Bojic, A. Petelin, S. Ivanova, R. Romih, U. Repnik, G. S. Salvesen, V. Stoka, V. Turk, and B. Turk.** 2008. Cysteine cathepsins trigger caspase-dependent cell death through cleavage of bid and antiapoptotic Bcl-2 homologues. *J Biol Chem* **283**:19140-19150.
7. **Feldman, D. E., V. Chauhan, and A. C. Koong.** 2005. The unfolded protein response: a novel component of the hypoxic stress response in tumors. *Mol Cancer Res* **3**:597-605.
8. **Guicciardi, M. E., J. Deussing, H. Miyoshi, S. F. Bronk, P. A. Svingen, C. Peters, S. H. Kaufmann, and G. J. Gores.** 2000. Cathepsin B contributes to TNF-alpha-mediated hepatocyte apoptosis by promoting mitochondrial release of cytochrome c. *J Clin Invest* **106**:1127-1137.
9. **Guicciardi, M. E., H. Miyoshi, S. F. Bronk, and G. J. Gores.** 2001. Cathepsin B knockout mice are resistant to tumor necrosis factor-alpha-mediated hepatocyte apoptosis and liver injury: implications for therapeutic applications. *Am J Pathol* **159**:2045-2054.
10. **Hang, H. C., J. Loureiro, E. Spooner, A. W. van der Velden, Y. M. Kim, A. M. Pollington, R. Maehr, M. N. Starnbach, and H. L. Ploegh.** 2006. Mechanism-based probe for the analysis of cathepsin cysteine proteases in living cells. *ACS Chem Biol* **1**:713-723.
11. **Kuester, D., H. Lippert, A. Roessner, and S. Krueger.** 2008. The cathepsin family and their role in colorectal cancer. *Pathol Res Pract* **204**:491-500.
12. **Lee, D. Y., J. Lee, and B. Sugden.** 2009. The unfolded protein response and autophagy: herpesviruses rule! *J Virol* **83**:1168-1172.
13. **Lin, J. H., P. Walter, and T. S. Yen.** 2008. Endoplasmic reticulum stress in disease pathogenesis. *Annu Rev Pathol* **3**:399-425.

14. **Marciniak, S. J., and D. Ron.** 2006. Endoplasmic reticulum stress signaling in disease. *Physiol Rev* **86**:1133-1149.
15. **Menard, R., E. Carmona, S. Takebe, E. Dufour, C. Plouffe, P. Mason, and J. S. Mort.** 1998. Autocatalytic processing of recombinant human procathepsin L. Contribution of both intermolecular and unimolecular events in the processing of procathepsin L in vitro. *J Biol Chem* **273**:4478-4484.
16. **Podobnik, M., R. Kuhelj, V. Turk, and D. Turk.** 1997. Crystal structure of the wild-type human procathepsin B at 2.5 Å resolution reveals the native active site of a papain-like cysteine protease zymogen. *J Mol Biol* **271**:774-788.
17. **Rozman, J., J. Stojan, R. Kuhelj, V. Turk, and B. Turk.** 1999. Autocatalytic processing of recombinant human procathepsin B is a bimolecular process. *FEBS Lett* **459**:358-362.
18. **Schotte, P., W. Declercq, S. Van Huffel, P. Vandenabeele, and R. Beyaert.** 1999. Non-specific effects of methyl ketone peptide inhibitors of caspases. *FEBS Lett* **442**:117-121.
19. **Takahashi, T., P. G. Schmidt, and J. Tang.** 1984. Novel carbohydrate structures of cathepsin B from porcine spleen. *J Biol Chem* **259**:6059-6062.
20. **Turk, B., J. G. Bieth, I. Bjork, I. Dolenc, D. Turk, N. Cimerman, J. Kos, A. Colic, V. Stoka, and V. Turk.** 1995. Regulation of the activity of lysosomal cysteine proteinases by pH-induced inactivation and/or endogenous protein inhibitors, cystatins. *Biol Chem Hoppe Seyler* **376**:225-230.
21. **Turk, V., and W. Bode.** 1991. The cystatins: protein inhibitors of cysteine proteinases. *FEBS Lett* **285**:213-219.
22. **Upton, J. P., K. Austgen, M. Nishino, K. M. Coakley, A. Hagen, D. Han, F. R. Papa, and S. A. Oakes.** 2008. Caspase-2 cleavage of BID is a critical apoptotic signal downstream of endoplasmic reticulum stress. *Mol Cell Biol* **28**:3943-3951.
23. **Wei, M. C., W. X. Zong, E. H. Cheng, T. Lindsten, V. Panoutsakopoulou, A. J. Ross, K. A. Roth, G. R. MacGregor, C. B. Thompson, and S. J. Korsmeyer.** 2001. Proapoptotic BAX and BAK: a requisite gateway to mitochondrial dysfunction and death. *Science* **292**:727-730.
24. **Yang, Y. L., and X. M. Li.** 2000. The IAP family: endogenous caspase inhibitors with multiple biological activities. *Cell Res* **10**:169-177.

## **Lytically replicating Kaposi's Sarcoma Herpes Virus induces XBP1-independent ER expansion.**

### **Background**

The Endoplasmic Reticulum (ER) is the main site within the cell where the folding and maturation of transmembrane and secreted proteins occurs. The protein folding demands on the ER fluctuate throughout the lifecycle of a cell and can be acutely specific to cellular function. For example, pancreatic beta cells face significantly fluctuating insulin folding demands in response to circulating glucose levels. Similarly, the ER is the largest organelle in a plasma cell, as it requires an enormous folding capacity to accommodate antibody production. Mammalian cells have evolved a specialized pathway, the Unfolded Protein Response Pathway (UPR), in order to adapt to these constantly fluctuating and cell-type specific protein folding demands.

Properly folded and modified proteins exit the ER, but misfolded proteins are detected by the three branches of the UPR. This detection initially triggers the cytoprotective signaling pathways of the UPR to re-establish folding homeostasis within the ER. However, if the UPR cannot re-establish ER homeostasis the UPR activates its cytotoxic potential. IRE1 $\alpha$  is one branch of the UPR that has both cytoprotective and cytotoxic outputs. Upon detection of

misfolded proteins, Ire1 $\alpha$  homo-oligomerizes, which induces a conformational change that results in autophosphorylation. This autophosphorylation activates the endoribonuclease activity, which unconventionally splices and removes an intron from XBP1 mRNA (Fig.4.1)(2). The spliced XBP1 message is translated into an active transcription factor that increases the protein folding capacity of the ER by upregulating genes encoding ER chaperones, ER biogenesis enzymes (6, 7), and ER-associated protein degradation (ERAD) components (7). Ectopic XBP-1s expression induces secretory pathway and chaperone genes (Fig. 4.2), increases cell size, and expands the ER (Fig. 4.3)(7, 14-16). Of note, XBP-1s is required for ER biogenesis. Furthermore, XBP-1<sup>-/-</sup> mice are embryonic lethal due to liver apoptosis due to improper ER development (Fig. 4.4)(12). Reconstitution of XBP-1 in these mice results in proper ER development, increased chaperone protein expression, and a proper ER stress response (6). In contrast to the cytoprotective role of XBP1s, upon irremediable ER stress, IRE1 $\alpha$  initiates ER stress-induced apoptosis via a mechanism mediated by the same RNase domain responsible for XBP-1 splicing (4, 9).

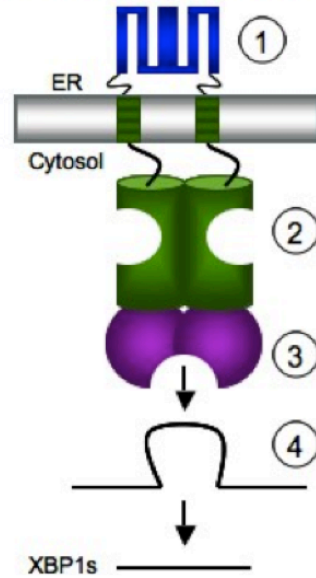


**Fig. 4.1.** The IRE1/XBP1 pathway is comprised of 1) the IRE luminal domain, 2) the IRE1 kinase domain, 3) the IRE1 endoribonuclease domain, and 4) XBP1u mRNA

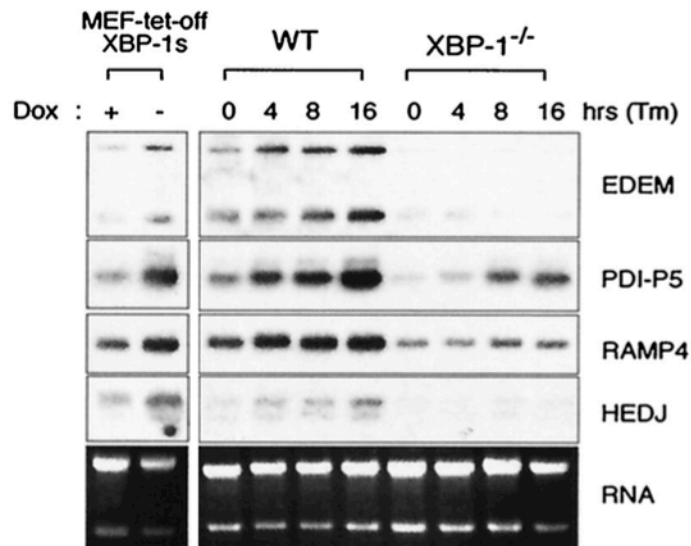


**Fig. 4.2.** XBP-1s exogenous overexpression results in upregulation of chaperones, proteins required for ER-associated degradation  
Adapted from Lee *et. al. Mol Cell Biol.* 2003



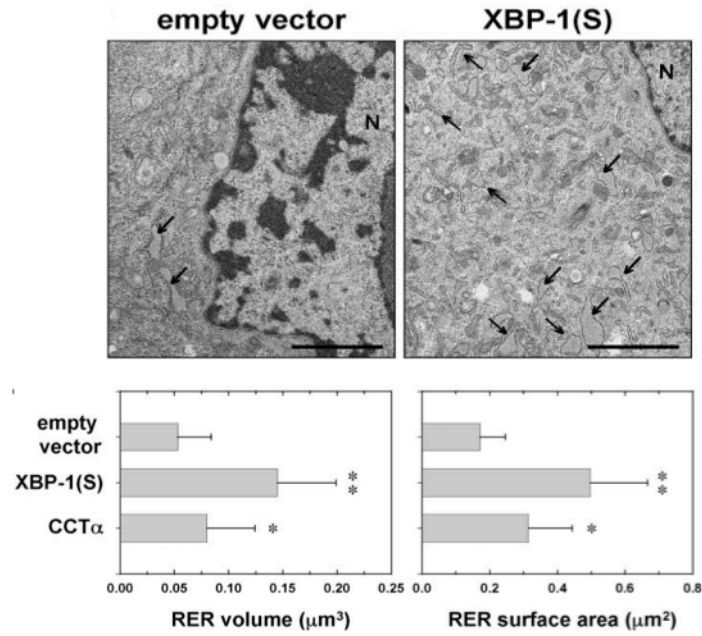


**Fig. 4.3.** XBP-overexpression induces ER expansion measured by electron microscopy. Adapted from Sriburi *et. al. J. Biol. Chem.* 2007

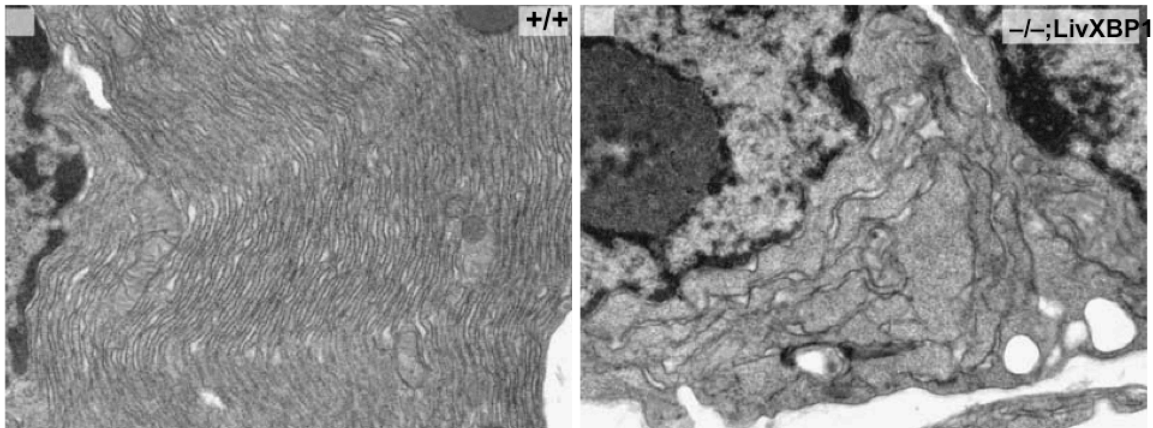


**Fig. 4.4.** Electron micrographs of the basolateral portion of acinar cells from WT and XBP-1<sup>-/-</sup> mice. Scale, 500nm. Adapted from Lee *et. al. EMBO.* 2005

It is well documented that viral replication and persistence of lytic and enveloped viruses are dependent on utilizing the host cell's ER. The replication of multiple viruses has been shown to induce ER expansion and manipulate other aspects of the UPR to the virus' advantage (5, 8, 10, 17, 18, 21). We questioned whether the replication of the large, lytic DNA virus, KSHV, would also result in viral manipulation of the UPR. In addition, to the many protein components of the virion capsid, KSHV encodes multiple glycoproteins involved in immune modulation and viral entry, which require extensive post-translational processing in the ER (21). The massive influx of viral proteins into the ER during this process would be predicted to overwhelm the folding capacity of the ER and lead to ER stress-induced apoptosis. In order to successfully complete the assembly of its viral progeny, we predict that KSHV must manipulate the cytoprotective aspects of the UPR, induce ER biogenesis and increase chaperone levels, while coordinately shifting the UPR-dependent apoptotic threshold to permit successful assembly of infectious virions. If true, it may be possible to exploit these viral targets to further understanding of the UPR's cytoprotective/cytotoxic threshold and identify potential therapeutic targets.

## **Results and Discussion**

Since IRE1 $\alpha$  is the most highly conserved branch of the UPR and contains both cytoprotective and cytotoxic functions, we first assessed its activation state during KSHV replication. Surprisingly, despite lytic reactivation and consequent

massive production and processing of viral proteins, there is no splicing of XBP1 mRNA during KSHV replication (Fig. 4.5). As previously explained, this result may seem counterintuitive because XBP1s is required for expansion of the ER and upregulation of chaperones, both cytoprotective events. However, given the dual function of IRE1, both cytotoxic and cytoprotective, it is plausible that activation of the IRE1/XBP1 pathway has a detrimental effect on the virus, suggesting that its cytotoxic effects outweigh the cytoprotective effects in this context. Since viral content is highly selective, inhibition of the IRE1/XBP1 pathway must somehow benefit KSHV. However, the consequential lack of XBP1s is predicted to result in an impaired ability to expand the ER in response to viral protein folding demand and limit virion production.

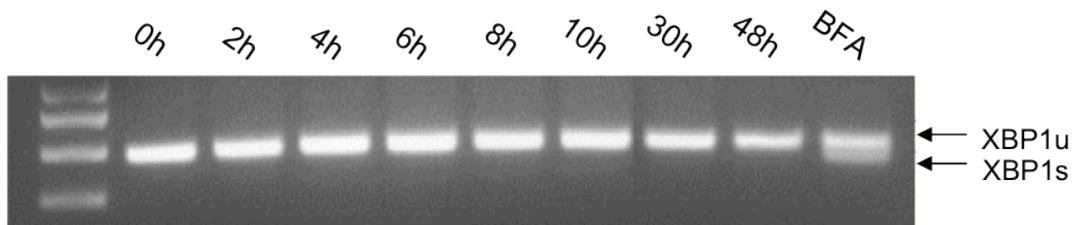


**Fig. 4.5.** rtTA-RTA SLKs were reactivated with 1 $\mu$ g/ml doxycycline and the XBP-1 splicing kinetics were measured throughout lytic reactivation.

It is unknown, however, if the ER is expanded during the lytic cycle of KSHV. We utilized electron microscopy to determine if, as predicted, KSHV replication induces ER expansion. A human SLK cell line was engineered in which 100% of KSHV-infected cells could be lytically reactivated by doxycycline-

inducible expression of RTA (rtTA-RTA)(11). This cell line was infected with recombinant KSHV (r.KSHV.219)(rtTA-RTA.SLK.219) and then treated 48 hours with doxycycline to induce the lytic cycle. ER expansion was visualized by electron microscopy. Surprisingly, despite the lack of XBP1 splicing, we observed extensive ER expansion in lytically reactivated cells. These cells were identified by the presence of packaged virion capsids (Fig. 4.6). No ER expansion was observed in either latently infected or uninfected rtTA-RTA.SLK.

These cells are in different stages of replication and therefore, epigenetic patterns. This may be why we did not see equal ER expansion in every cell observed. To obtain an unbiased quantitation of the amount of overall ER expansion observed, we developed a program using MATLAB with which we could accurately measure the expansion of ER organelles in each cell. We quantified every ER organelle in individual cells (n=100) for both induced and uninduced (Fig. 4.6). Using this method of quantification, we observe ~30% ER expansion in the lytically-induced cell population in comparison to latently infected cells.

This finding is supported by BODIPY-BFA staining, a direct quantifiable readout of ER expansion, of lytically reactivated KSHV-infected SLKs (fig. 4.7) r.KSHV.219-infected SLKs were treated 48 hours with 1.2mM valproic acid (V.A.), a histone deacetylase (HDAC) inhibitor (3). We utilized the RFP encoded downstream of a RTA-responsive promoter (PAN) to gate on lytically reactivated cells. This gate helps to provide an accurate depiction of ER expansion in the

subset of lytic cells in the mixed culture by preventing the inclusion of unreactivated cells in our quantitation (19).

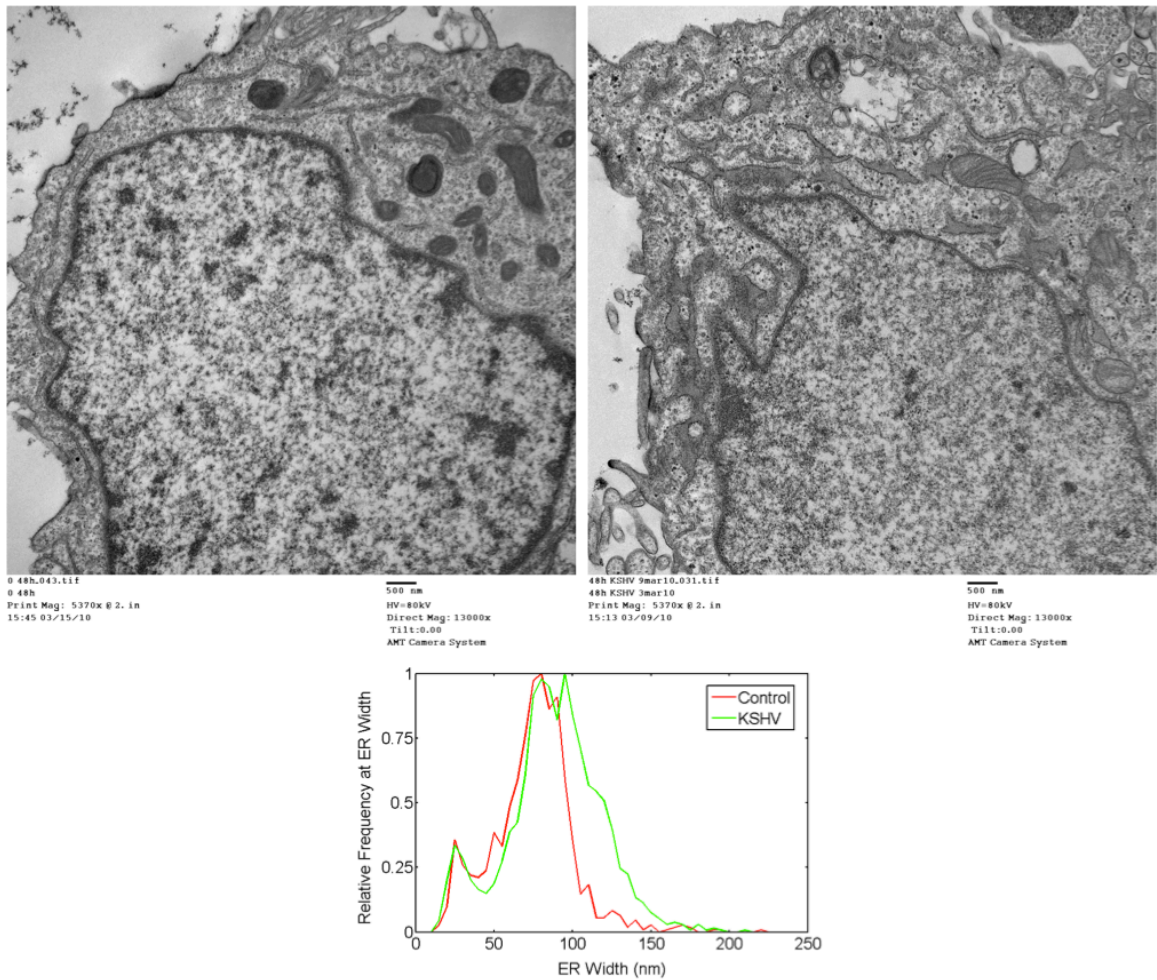


**Fig. 4.6.** Electron micrograph of latently infected rTA-RTA SLK and lytic rTA-RTA SLK (48h 1 $\mu$ g/ml doxycycline). Newly packaged virion capsids are visible in the nucleus of lytic rTA-RTA SLK. ER width is quantitated using custom MATLAB program.

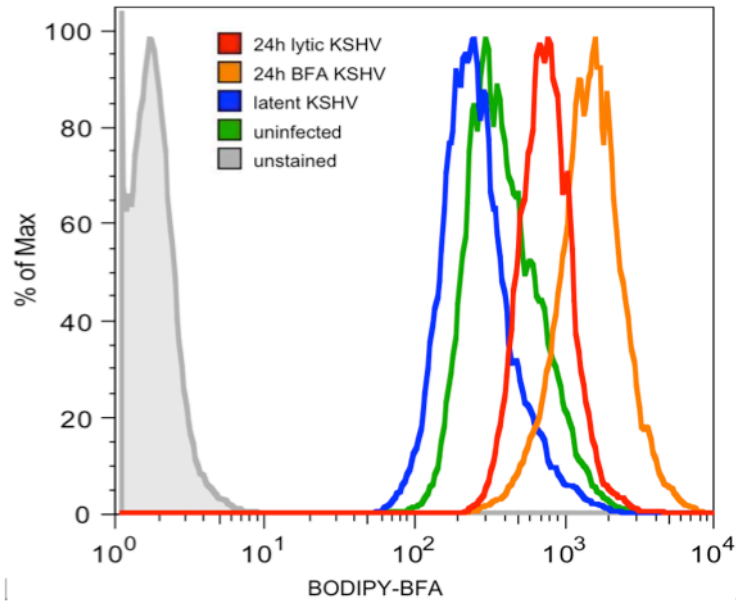


**Fig. 4.7.** BODIPY-BFA ER incorporation in lytically reactivated SLK r.KSHV. Treated 24h with 1.2mM valproic acid. SLK r.KSHV treated 24h with 1.25  $\mu$ g/ml Brefeldin A.

ER expansion during lytic replication in the absence of XBP1 splicing suggests that the UPR is activated and manipulated by KSHV. These data suggest that KSHV may actively inhibit XBP1 splicing. To determine if lytically replicating KSHV actively inhibits the IRE1/XBP-1 pathway, we treated uninfected rtTA-RTA.SLK, latently infected or lytically reactivated rtTA-RTA.SLK.219 with increasing doses of Tunicamycin (TUN), a chemical inducer of ER stress and monitored XBP1 splicing. There is a decreased sensitivity to TUN-induced XBP1 splicing in lytically reactivated rtTA-RTA.SLK.219 in comparison to both latently infected rtTA-RTA.SLK.219 and uninfected rtTA-RTA.SLK (Fig. 4.8). This result indicates that KSHV actively inhibits XBP1 splicing during the lytic cycle and has evolved a mechanism of XBP-1-independent ER expansion.

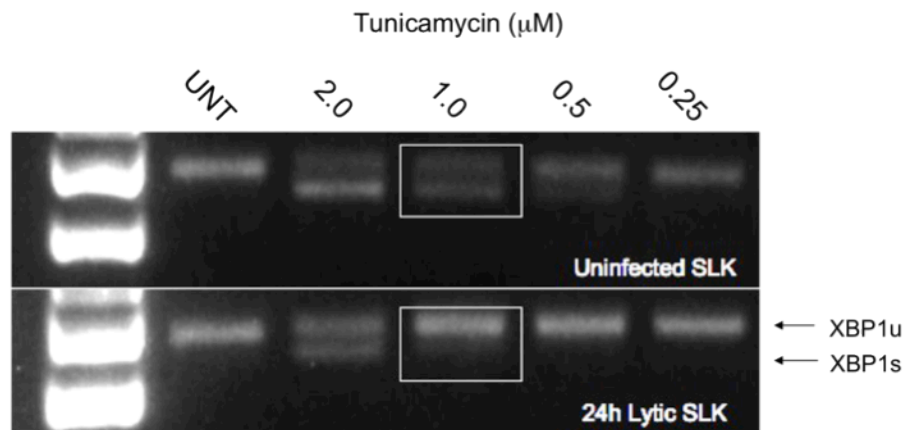


**Fig. 4.8.** XBP1 splicing assay of uninfected rtTA-RTA.SLK treated with decreasing doses of Tunicamycin ( $\mu\text{M}$ ) following 24 hours lytic reactivation using  $1\mu\text{g/ml}$  doxycycline.

Further investigation into the mechanism by which KSHV accomplishes XBP1-independent ER biogenesis may reveal a novel way to increase the folding capacity of Beta or neuronal cells. There are multiple possible mechanisms by which KSHV may be expanding the ER independently of XBP1s. KSHV may encode a novel factor that is able to target the genes required for ER expansion or the virus may utilize other known or unknown cellular factors to substitute for the transcriptional function of XBP1s.

To investigate the possibility that KSHV may encode a “replacement” transcription factor, I screened the KSHV coding sequence for genes that induce ER expansion by transiently expressing the genes individually in an uninfected SLK cell line and measuring ER expansion by flow cytometry analysis of BODIPY-BFA ER incorporation. Unfortunately, the method used to transiently express the plasmids encoding the KSHV open reading frames (ORFs) results in

cellular stress. This stress causes nonspecific fluctuations of ER biogenesis and BODIPY-BFA incorporation (Fig. 4.9 and 4.10). While this preliminary method of screening the KSHV ORFs was unsuccessful due to technical difficulties, the phenotype remains and will be pursued in the future via alternative methods.

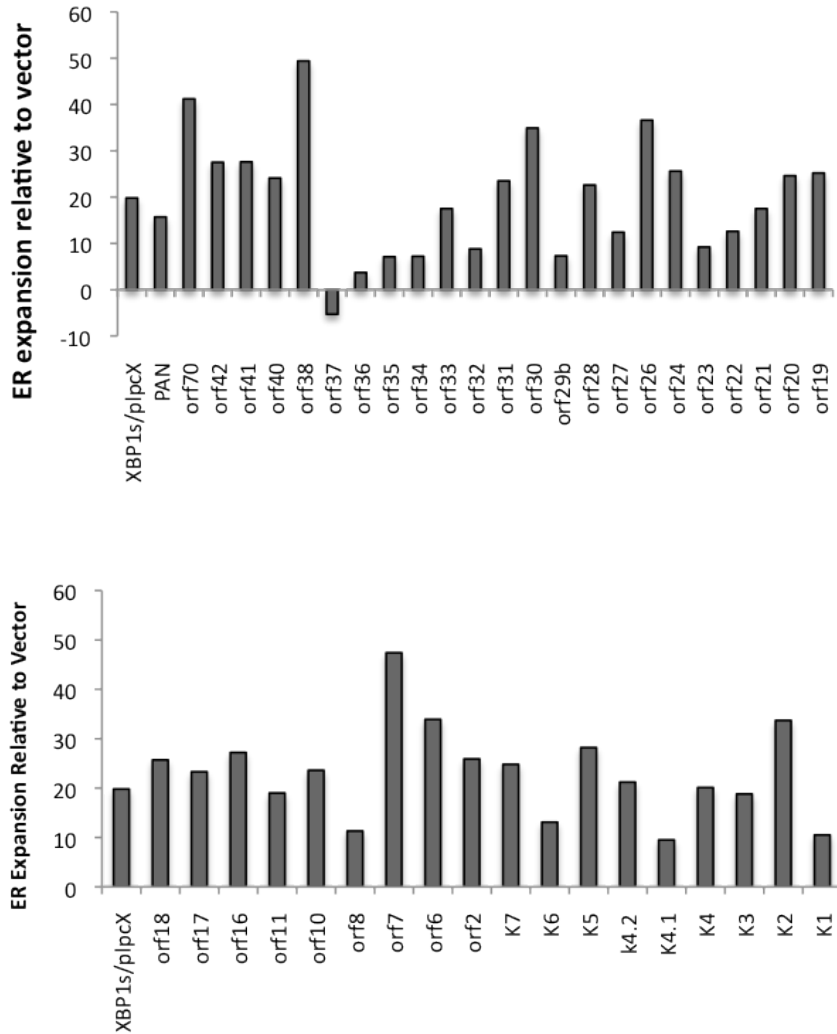


**Fig. 4.9.** Part 1 screen of KSHV ORFs for XBP1s-independent ER expansion factor. ORFs transiently expressed individually in 293. ER size measured by BODIPY-BFA incorporation.



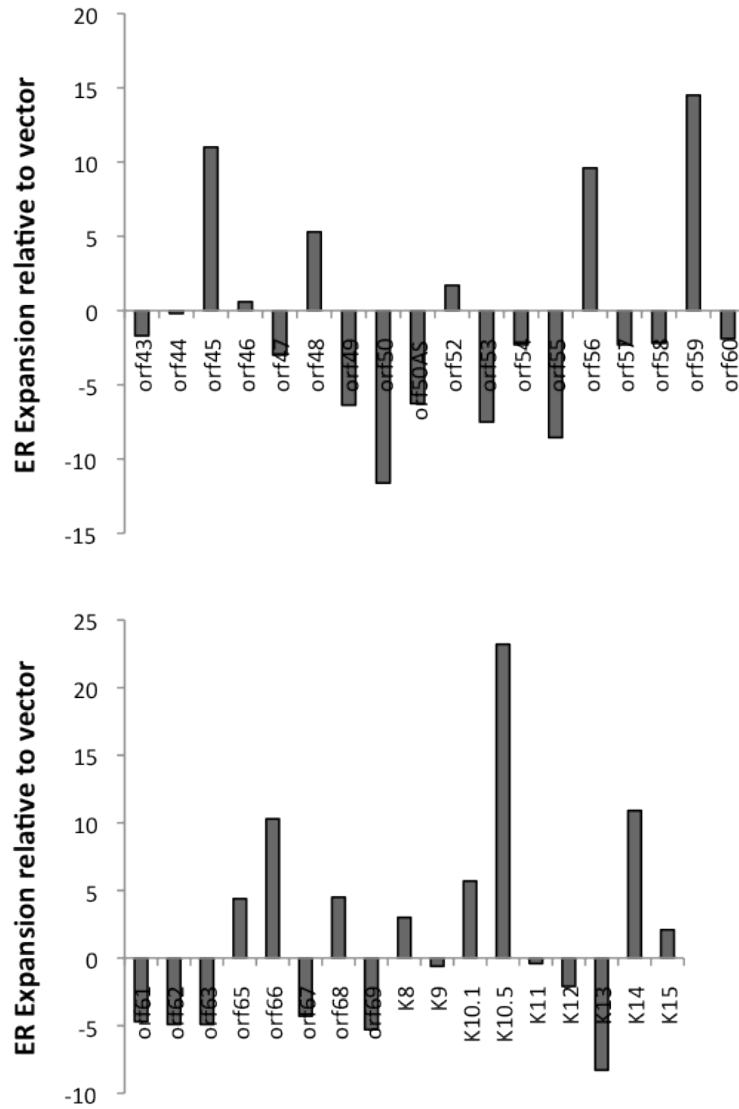


**Fig. 4.10.** Part 2 screen of KSHV ORFs for XBP1s-independent ER expansion factor. ORFs transiently expressed individually in 293. ER size measured by BODIPY-BFA incorporation.

It is also possible that KSHV manipulates, as of yet, unknown or poorly understood alternative pathways of ER biogenesis. For example, a previous study has shown that cleaved ATF6, a transcription factor also activated by ER stress, can induce ER biogenesis in an *in vitro* model (1). The extent of ER biogenesis initiated by ATF6 is significantly less than that induced by XBP1s. This observation is supported by both the *in vitro* data and the less severe phenotype of the *atf6*<sup>-/-</sup> mouse. While the *xbp1*<sup>-/-</sup> phenotype is lethal, *atf6*<sup>-/-</sup> mice are viable and fertile. They have no overt phenotype. However, they are impaired for survival when challenged with ER stress (13, 20). These data present a possible alternative mechanism for KSHV-induced ER biogenesis. Interestingly, while the IRE1 branch of the UPR is inhibited during KSHV lytic infection, ATF6 is cleaved upon lytic reactivation. Further experiments will need to be completed to determine if loss of ATF6 prevents KSHV-induced ER expansion and more interestingly, if this inhibition prevents viral replication. If true, this would suggest that targeting the UPR during viral infection is a possible therapeutic strategy.

The active inhibition of XBP1 splicing by KSHV indicates that the cytotoxic consequences of the IRE1 pathway outweigh the benefit of the cytoprotective outputs. Identification of the mechanism by which KSHV actively inhibits this branch of the UPR could lead to the discovery of a way to manipulate this mechanism to push the cytotoxic/cytoprotective threshold of the IRE1 pathway toward cytotoxicity specifically in cells infected with KSHV. Further studies are necessary to follow up on this promising observation.

## Materials and Methods

**Electron Microscopy.** Latently infected rtTA-RTA.SLK.219, rtTA-RTA.SLK.219 pretreated 24 hours with 1 $\mu$ g/ml doxycycline, or uninfected rtTA-RTA.SLK were fixed according to the UCSF Renal Pathology and Electron Microscopy (EM) Service. EM samples were prepared according to their protocol.

**XBP1 Splicing Assay.** XBP1 splicing was measured by specific primers flanking the splicing site yielding PCR product sizes of 164 and 138bp XBP1u and XBP1s, respectively. Products were resolved on 2.5% agarose gels.

**BODIPY-BFA staining.** For measurement of ER expansion in SLK.219: SLK.219 were treated 24 hours with 1.2mM valproate. BODIPY-BFA (Invitrogen) was incubated with cells 37C, 15 min. Cells fixed in 2% paraformaldehyde and ER expansion was measured by flow cytometry (BD FACS calibur). For ER expansion screen: 293 cells were transfected 24h with plasmids encoding KSHV encoding reading frames using Fugene (Promega). BODIPY-BFA (Invitrogen) was incubated with cells 37C, 15 min. Cells fixed in 2% paraformaldehyde and ER expansion was measured by flow cytometry (BD FACS calibur).

**KSHV ORF ER expansion screen.** 293 cells were transiently transfected 24h with 1 $\mu$ g DNA using Fugene (Promega). The cells were the stained with BODIPY-BFA as specified above and harvested with 0.25% trypsin, washed

once with 1x PBS. The cells were subsequently passed through a FACSCalibur machine (Becton Dickinson) and detected with CellQuest software (BD Biosciences).

## **Acknowledgements**

We thank the UCSF Pathology and Laboratory Medicine Departments, specifically Jean Olson, M.D., for their help with the electron microscopy sample preparation and imaging. We also thank Pete Beemiller, Ph.D. from the Krummel lab, for assistance designing the MATLAB program for ER expansion quantification.

## References

1. **Bommiasamy, H., S. H. Back, P. Fagone, K. Lee, S. Meshinchi, E. Vink, R. Sriburi, M. Frank, S. Jackowski, R. J. Kaufman, and J. W. Brewer.** 2009. ATF6alpha induces XBP1-independent expansion of the endoplasmic reticulum. *J Cell Sci* **122**:1626-1636.
2. **Credle, J. J., J. S. Finer-Moore, F. R. Papa, R. M. Stroud, and P. Walter.** 2005. On the mechanism of sensing unfolded protein in the endoplasmic reticulum. *Proc Natl Acad Sci U S A* **102**:18773-18784.
3. **Gottlicher, M., S. Minucci, P. Zhu, O. H. Kramer, A. Schimpf, S. Giavara, J. P. Sleeman, F. Lo Coco, C. Nervi, P. G. Pelicci, and T. Heinzel.** 2001. Valproic acid defines a novel class of HDAC inhibitors inducing differentiation of transformed cells. *EMBO J* **20**:6969-6978.
4. **Han, D., A. G. Lerner, L. Vande Walle, J. P. Upton, W. Xu, A. Hagen, B. J. Backes, S. A. Oakes, and F. R. Papa.** 2009. IRE1alpha kinase activation modes control alternate endoribonuclease outputs to determine divergent cell fates. *Cell* **138**:562-575.
5. **Isler, J. A., A. H. Skalet, and J. C. Alwine.** 2005. Human cytomegalovirus infection activates and regulates the unfolded protein response. *J Virol* **79**:6890-6899.
6. **Lee, A. H., G. C. Chu, N. N. Iwakoshi, and L. H. Glimcher.** 2005. XBP-1 is required for biogenesis of cellular secretory machinery of exocrine glands. *EMBO J* **24**:4368-4380.
7. **Lee, A. H., N. N. Iwakoshi, and L. H. Glimcher.** 2003. XBP-1 regulates a subset of endoplasmic reticulum resident chaperone genes in the unfolded protein response. *Mol Cell Biol* **23**:7448-7459.
8. **Lee, D. Y., and B. Sugden.** 2008. The LMP1 oncogene of EBV activates PERK and the unfolded protein response to drive its own synthesis. *Blood* **111**:2280-2289.
9. **Lin, J. H., H. Li, D. Yasumura, H. R. Cohen, C. Zhang, B. Panning, K. M. Shokat, M. M. Lavail, and P. Walter.** 2007. IRE1 signaling affects cell fate during the unfolded protein response. *Science* **318**:944-949.
10. **Mulvey, M., C. Arias, and I. Mohr.** 2007. Maintenance of endoplasmic reticulum (ER) homeostasis in herpes simplex virus type 1-infected cells through the association of a viral glycoprotein with PERK, a cellular ER stress sensor. *J Virol* **81**:3377-3390.
11. **Myoung, J., and D. Ganem.** 2011. Generation of a doxycycline-inducible KSHV producer cell line of endothelial origin: Maintenance of tight latency with efficient reactivation upon induction. *J Virol Methods*.
12. **Reimold, A. M., A. Etkin, I. Clauss, A. Perkins, D. S. Friend, J. Zhang, H. F. Horton, A. Scott, S. H. Orkin, M. C. Byrne, M. J. Grusby, and L. H. Glimcher.** 2000. An essential role in liver development for transcription factor XBP-1. *Genes Dev* **14**:152-157.

13. **Rutkowski, D. T., J. Wu, S. H. Back, M. U. Callaghan, S. P. Ferris, J. Iqbal, R. Clark, H. Miao, J. R. Hassler, J. Fornek, M. G. Katze, M. M. Hussain, B. Song, J. Swathirajan, J. Wang, G. D. Yau, and R. J. Kaufman.** 2008. UPR pathways combine to prevent hepatic steatosis caused by ER stress-mediated suppression of transcriptional master regulators. *Dev Cell* **15**:829-840.
14. **Shaffer, A. L., M. Shapiro-Shelef, N. N. Iwakoshi, A. H. Lee, S. B. Qian, H. Zhao, X. Yu, L. Yang, B. K. Tan, A. Rosenwald, E. M. Hurt, E. Petroulakis, N. Sonenberg, J. W. Yewdell, K. Calame, L. H. Glimcher, and L. M. Staudt.** 2004. XBP1, downstream of Blimp-1, expands the secretory apparatus and other organelles, and increases protein synthesis in plasma cell differentiation. *Immunity* **21**:81-93.
15. **Sriburi, R., H. Bommasamy, G. L. Buldak, G. R. Robbins, M. Frank, S. Jackowski, and J. W. Brewer.** 2007. Coordinate regulation of phospholipid biosynthesis and secretory pathway gene expression in XBP-1(S)-induced endoplasmic reticulum biogenesis. *J Biol Chem* **282**:7024-7034.
16. **Sriburi, R., S. Jackowski, K. Mori, and J. W. Brewer.** 2004. XBP1: a link between the unfolded protein response, lipid biosynthesis, and biogenesis of the endoplasmic reticulum. *J Cell Biol* **167**:35-41.
17. **Tardif, K. D., K. Mori, R. J. Kaufman, and A. Siddiqui.** 2004. Hepatitis C virus suppresses the IRE1-XBP1 pathway of the unfolded protein response. *J Biol Chem* **279**:17158-17164.
18. **Umareddy, I., O. Pluquet, Q. Y. Wang, S. G. Vasudevan, E. Chevet, and F. Gu.** 2007. Dengue virus serotype infection specifies the activation of the unfolded protein response. *Virology* **4**:91.
19. **Vieira, J., and P. M. O'Hearn.** 2004. Use of the red fluorescent protein as a marker of Kaposi's sarcoma-associated herpesvirus lytic gene expression. *Virology* **325**:225-240.
20. **Wu, J., D. T. Rutkowski, M. Dubois, J. Swathirajan, T. Saunders, J. Wang, B. Song, G. D. Yau, and R. J. Kaufman.** 2007. ATF6alpha optimizes long-term endoplasmic reticulum function to protect cells from chronic stress. *Dev Cell* **13**:351-364.
21. **Yu, C. Y., Y. W. Hsu, C. L. Liao, and Y. L. Lin.** 2006. Flavivirus infection activates the XBP1 pathway of the unfolded protein response to cope with endoplasmic reticulum stress. *J Virol* **80**:11868-11880.

**Multiple Defects, including premature apoptosis,  
prevent KSHV replication in murine cells.**

**Background**

Kaposi's sarcoma-associated herpesvirus (KSHV; HHV-8) is a lymphotropic herpesvirus linked to several clinical disorders, including Kaposi's sarcoma (KS), primary effusion lymphoma (PEL), and multicentric Castleman's disease (MCD) (3, 5, 8, 11, 12). The development of biological systems with which to study KSHV infection *in vivo* would provide much needed knowledge about viral transmission and disease pathogenesis. However, animal models of KSHV infection have eluded the field for a number of reasons. The host range of KSHV is narrow, with natural infection limited to humans. Moreover, only a few human cell lines have been shown capable of supporting the full KSHV infectious cycle to date (1, 2, 24). Experimental transmission to other animal species, including mice, has generally failed, with common marmosets being the only known exception (7). In SCID/hu mice exposed to KSHV, no murine tissue displayed signs of infection (9). Recently, Mutlu *et al.* engineered a KSHV-dependent mouse model of KS, which required genetic manipulation of the KSHV genome in combination with a bacterial artificial chromosome system (15).

Although a proliferative lesion was generated, even here no evidence of productive KSHV replication was found (20).

## Results and Discussion

True herpesviral infection is characterized by the following: (i) establishment of latency, (ii) entry into the lytic cycle, (iii) viral DNA replication, and (iv) proper assembly and release of infectious virions. We evaluated these criteria of KSHV infection in murine cells to begin to define at which stage the block occurs. In this study, we use r.KSHV.219, which constitutively expresses GFP (green fluorescent protein) from the E1 $\alpha$  promoter. This fluorescent readout of infectivity greatly improves the ability to sensitively quantify infection by flow cytometry. In addition, r.KSHV.219 encodes RFP (red fluorescent protein) downstream of a RTA (replication and transcription activator)-responsive promoter (PAN), resulting in a quantitative assay to detect expression of the lytic switch protein RTA and entry into the lytic cycle (27). Using the increased sensitivity of the r.KSHV.219 system, we determined the steps at which KSHV infection of murine cells is blocked and investigated the possibility of overcoming this inhibition.

Earlier studies showed that mouse cells can support viral entry, genome circularization and expression of LANA-1 (as judged by immunofluorescence)(1, 16, 24). In Fig 5.1, we confirmed that entry of r.KSHV.219 in a murine cell line (mouse embryonic fibroblasts, MEFs) occurs - here assayed by GFP expression, as detected by flow cytometry. Fig 5.1 also shows that such entry



occurs with efficiency comparable to permissive human cell lines (e.g. 293, SLK, and HFF). When such infected cells are examined for viral transcripts by hybridization of their extracted RNA to a custom KSHV genomic tiling array (6), a highly restricted pattern of gene expression is observed (Fig. 5.6A, Lane “Latent”). The principal transcripts detected in this array correspond to the major latency locus encoding LANA, v-cyclin and v-FLIP (see arrow in Fig. 5.6A). For a full enumeration of the latent genes expressed in murine cells, and quantitation of their expression levels relative to those in KSHV-infected SLK cells, see Fig. 5.2.

Next, we evaluated the ability of r.KSHV.219 stably-infected cell lines (MEF r.KSHV and SLK r.KSHV) to be lytically induced from latency. First, the cells were infected with an adenovirus expressing the lytic switch protein RTA; 48 hours later, cells were examined microscopically and by flow cytometry for RFP expression. Interestingly, under conditions in which ~30% of SLK cells expressed RFP, only sporadic MEF r.KSHV cells (~2% of the culture) were RFP-positive (Fig 5.3, left panel). Western blotting of the two cultures for RTA (Fig 5.3, right panel) confirmed that both lines were comparably infected with adenovirus and expressed equivalent amounts of RTA. Since RFP in r.KSHV.219 is directly controlled by RTA, this suggests that RTA functions inefficiently in a murine environment. Consistent with this, quantitative RT-PCR for numerous key delayed-early and late lytic transcripts was negative in Ad-RTA infected MEF r.KSHV cells, despite strong expression of these RNAs in SLK r.KSHV cells (Fig. 5.4). Furthermore, supernatant from MEF r.KSHV cells infected with AdRTA for 5 days did not contain detectable infectious virions (data not shown).

Since ectopic RTA expression in mouse cells has earlier been shown to function in the activation of transfected reporter genes (14, 15, 25), we wondered if the defects observed above might have to do with the nature of the chromatinized DNA template. Accordingly, we asked if lytic reactivation would be more efficient if induction was triggered by exposure to histone deacetylase (HDAC) inhibitors like valproic acid or sodium butyrate (N-butyrate). Consistent with this, we found that, in the presence of either HDAC inhibitor, induction of RTA-dependent RFP expression proceeded nearly as efficiently in KSHV-positive MEFs as in SLK cells (Fig 5.5, left panel). However, despite this fact, we observed that the supernatants of MEFs induced by prolonged valproate exposure still displayed barely detectable infectious virus (Fig 5.5, right panel).

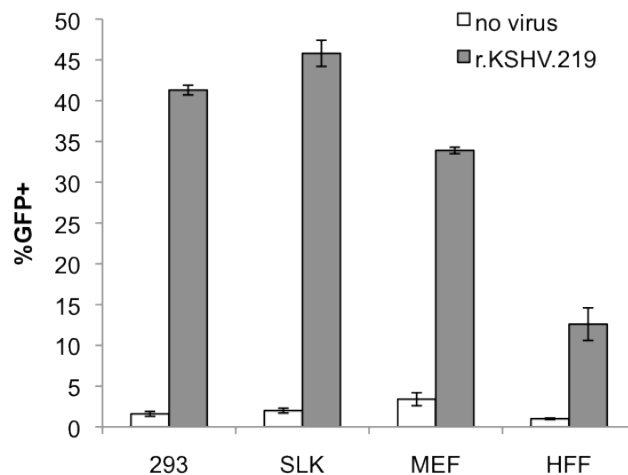


**Fig. 5.1.** Mouse embryonic fibroblasts (MEF), SLK, 293, and human foreskin fibroblasts (HFF) were infected with  $5 \times 10^4$  GFP focus-forming units/ml of r.KSHV.219. Infection efficiency was measured by quantifying GFP-expressing cells.

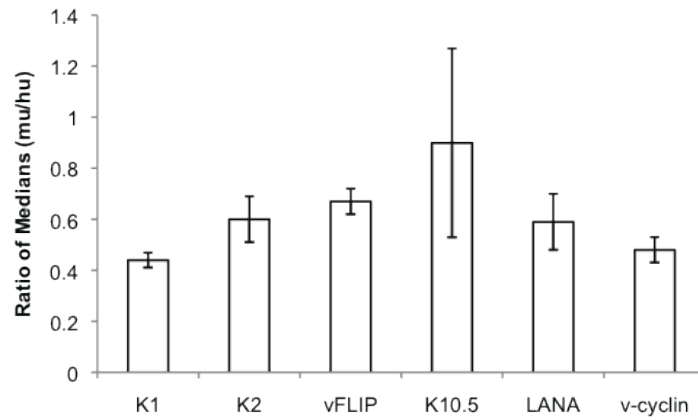


**Fig. 5.2** MEF:SLK ratio of KSHV latent gene transcripts during latency. Measured by averaging microarray data for five probes specific to each transcript, then calculating the ratio of medians of biological replicates.

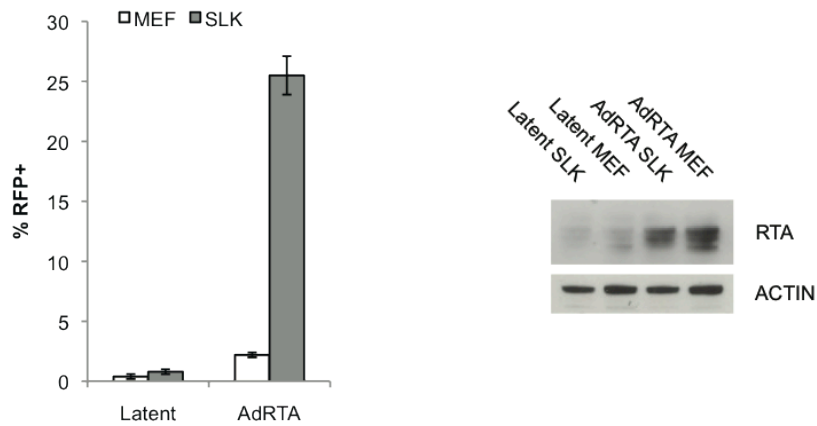


**Fig. 5.3.** (A) r.KSHV.219 stably-infected MEFs and SLKs were treated for 48 hrs with AdRTA and 1.2mM valproate. Lytic reactivation measured by RFP+ quantification by flow cytometry. (B) Immunoblot of RTA expression in 48h AdRTA treated MEF r.KSHV and SLK r.KSHV.

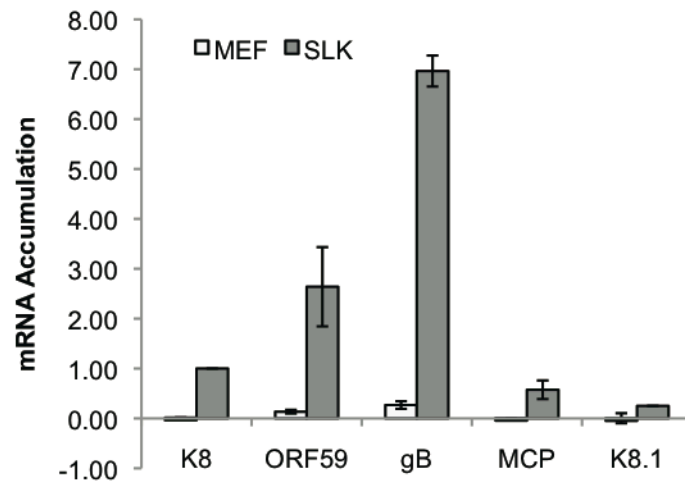


**Fig. 5.4** Expression, measured by qRT-PCR, of lytic genes in MEF r.KSHV and SLK r.KSHV following 48h AdRTA infection, normalized relative to mRNA levels of K8 transcript, which was set to 1.0 units.

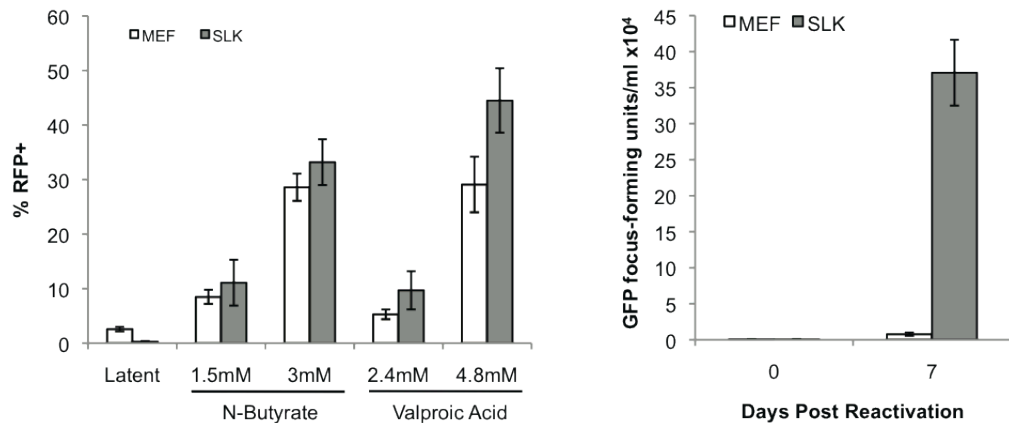


**Fig. 5.5.** (A) r.KSHV.219 stably-infected MEFs and SLKs were treated for 48 hrs with N-butyrate and valproic acid at indicated doses. Reactivation efficiency was measured by flow cytometric quantification of RFP-expressing cells (RFP is downstream of the PAN promoter). (B) r.KSHV.219 stably-infected MEFs and SLKs were treated 0 and 7 days with 4.8mM valproic acid. MEF and SLK supernatant were incubated with 293 cells and virus production was quantified 24 hrs post supernatant transfer by flow cytometric analysis of GFP-expressing 293 cells

To determine at what stage this block to virus production occurs, we analyzed viral transcript accumulation in valproate- reactivated MEF r.KSHV by expression profiling on the KSHV genomic array (6)(Fig 5.6A). This revealed the accumulation of RNAs homologous to large segments of the viral genome, including late genes such as those encoding capsid and envelope proteins. The array data were confirmed by qPCR analysis of a subset of specific viral transcripts (Fig. 5.6B). However, although inhibition of histone deacetylase rescued extensive lytic transcription, several lines of evidence suggested that this transcriptional program was not correctly executed. First, several transcripts strongly expressed in MEF r.KSHV cells upon lytic entry are absent in human cell line infection (denoted by asterisks in Fig. 5.6A), suggesting they are aberrant. Second, despite extensive delayed-early transcription, viral DNA synthesis did not occur in induced MEF r.KSHV cells. This is shown in Fig 5.6C, in which levels of total viral DNA prior to and 72 hours post valproic acid treatment were quantitated by qPCR. This fact suggests that the delayed early transcription program is defective, indicating that the observed extensive transcription of the viral genome does not faithfully reflect correct lytic gene expression. This inference is also sustained by the observation (Figs 5.6A-B) that abundant expression of RNAs for late genes is observed despite the absence of lytic DNA replication. This aberrant lytic RNA profile could be due to defects in epigenetic modifications in viral chromatin, primary abnormalities in transcription, and/or abnormalities in viral RNA turnover; further studies will be necessary to distinguish among these possibilities.

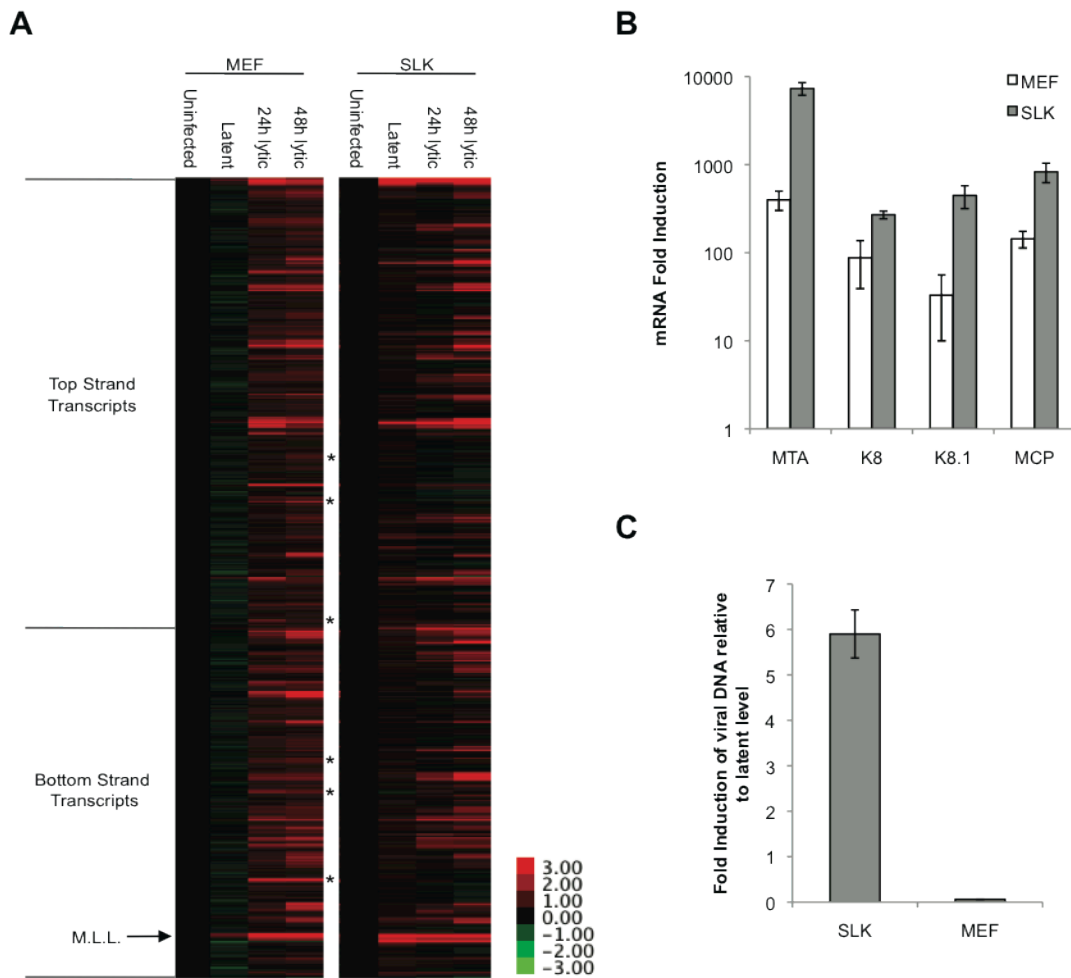


**Fig. 5.6** (A) Microarray analysis of KSHV mRNA transcription in r.KSHV. 219 stably infected MEFs and SLKs induced 0, 24, and 48 hrs with 4.8mM valproic acid. Using Agilent technology, 13,746 60-mer KSHV-specific oligonucleotide probes specific to KSHV genome sequence (GenBank accession no. U75698.1) were printed in duplicate. Each probe overlapped a neighboring probe by 40 nucleotides (nt), resulting in a tiling design with probes offset by 20 nucleotides. Arrow indicates the major latency locus (M.L.L.). Asterisks (\*) indicate transcripts upregulated in MEFs that are absent in SLKs. (B) Fold induction of lytic mRNA in MEFs and SLKs upon 24 hr treatment with 4.8mM valproic acid. (C) KSHV DNA replication in MEFs and SLKs following 72h 4.8mM valproic acid treatment. Viral DNA replication measured by qPCR of LANA DNA.

Interestingly, by 72 hours following valproic acid treatment, MEF r.KSHV display extensive cytopathic effects (CPE)(Fig. 5.7A). This is in stark contrast to SLK r.KSHV, which display no visible CPE until approximately 6 days post lytic reactivation. This observation led us to measure the kinetics of apoptosis following lytic reactivation in MEF and SLK cells, as judged by flow cytometry for Annexin V. This revealed that approximately 50% of MEF r.KSHV are apoptotic by 72 hours post lytic reactivation (4.8mM valproic acid), while uninfected MEFs, SLKs, or SLK r.KSHV remain viable in response to similar treatment with valproic acid at this timepoint (Fig. 5.7B). SLK r.KSHV and MEF r.KSHV both efficiently enter the lytic cycle (as judged by RFP expression) under these conditions (Fig. 5.7C). These observations suggest that although valproate-induced murine cells express many KSHV transcripts, apoptosis is initiated prematurely in these cells, which could account for many of the subsequent defects in viral replication (see below). Furthermore, according to array data, transcripts encoding KSHV anti-apoptotic factors, including v-Cyclin, v-Bcl-2, K7, and K1, are expressed upon lytic cycle entry (Figure 5.6A). However, quantitative RT-PCR revealed that these transcripts are expressed at somewhat lower levels in MEFs in comparison to SLKs (Fig. 5.8). It is possible these lower expression levels of anti-apoptotic transcripts are not sufficient to prevent premature apoptosis in MEFs.

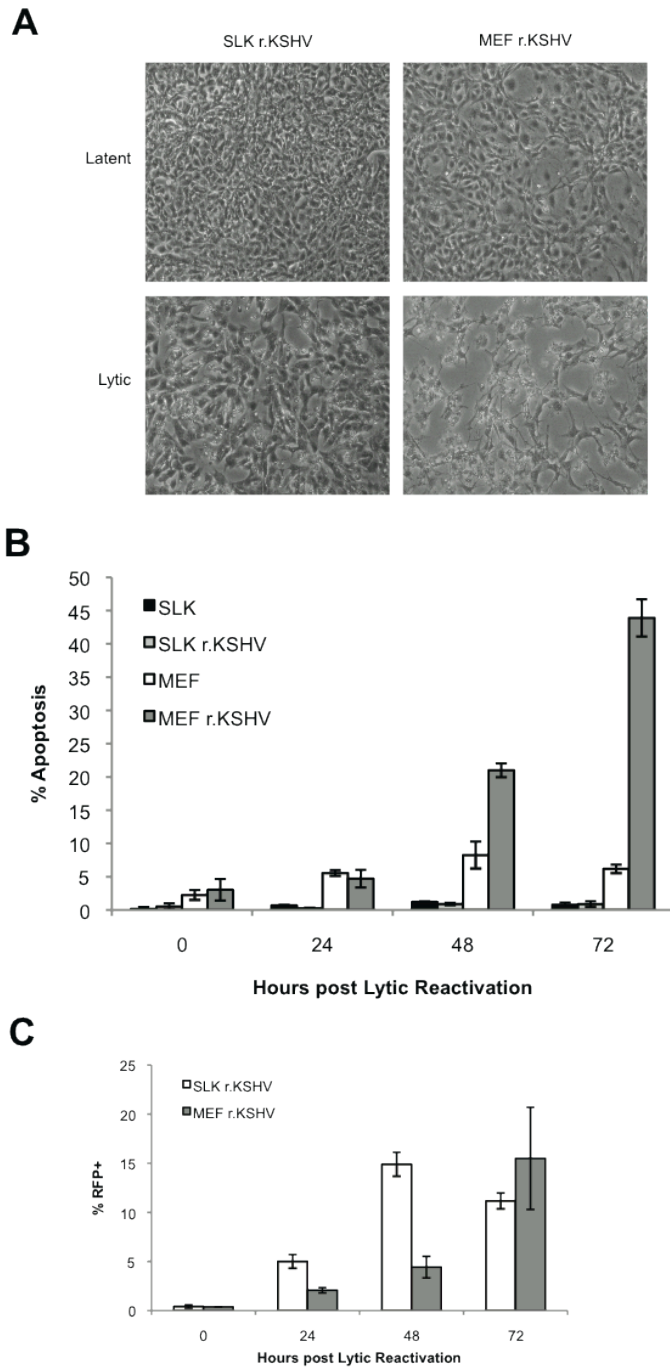


**Fig. 5.7** (A) Cytopathic effects observed in MEF r.KSHV.219 following 72h 4.8mM valproic acid treatment. (B) Apoptotic kinetics were measured by Annexin V staining following lytic reactivation (4.8mM valproic acid) of r.KSHV.219 stably infected MEFs and SLKs. (C) Quantification of RFP+ cells as a measurement of lytic reactivation upon 4.8mM valproic acid treatment.



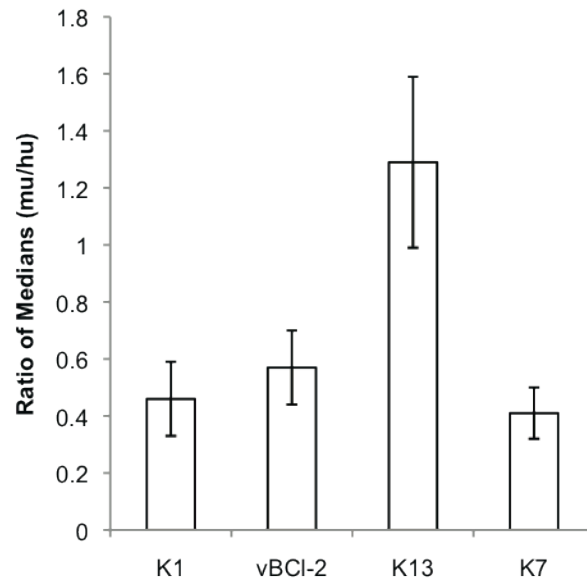


**Fig. 5.8.** MEF:SLK ratio of KSHV anti-apoptotic gene transcript levels 48h post HDAC treatment. Measured by averaging microarray data for five probes specific to each transcript, then calculating the ratio of medians of biological replicates.

Intrinsic cell damage culminates in activation of the mitochondrial apoptotic pathway, which requires the pro-apoptotic BCL-2 family proteins BAX and BAK (22). Homo-oligomerization of BAX and/or BAK consequently results in mitochondrial permeability, release of pro-apoptotic factors (e.g., cytochrome c), and activation of effector caspases and cell death (10, 19, 26). Therefore, cells doubly deficient in *bax* and *bak* are significantly resistant to multiple forms of intrinsic cell death (18, 28). To determine if early apoptosis is the primary block to viral replication in murine cells, we established a r.KSHV.219 stably-infected *bax*<sup>-/-</sup>*bak*<sup>-/-</sup> MEF line (DKO r.KSHV). We hypothesized that inhibition of intrinsic apoptosis could delay apoptosis long enough in the murine cells to permit proper viral DNA replication and virion assembly. As predicted, apoptosis is substantially delayed in DKO r.KSHV in comparison to MEF r.KSHV, but still occurs earlier than in SLK r.KSHV (Fig. 5.9A). As judged by RTA-dependent RFP expression, DKO r.KSHV reactivate at least as efficiently as MEF r.KSHV, likely due to the delay in cell death-initiated degradation of viral transcripts and proteins (Fig. 5.9B). Importantly, delaying the apoptotic kinetics permits viral DNA replication in DKO r.KSHV, albeit to a lower level than in comparison to human SLK r.KSHV (Fig. 5.9C). However, despite these changes, no infectious virions are produced by DKO r.KSHV (Fig. 5.9D).

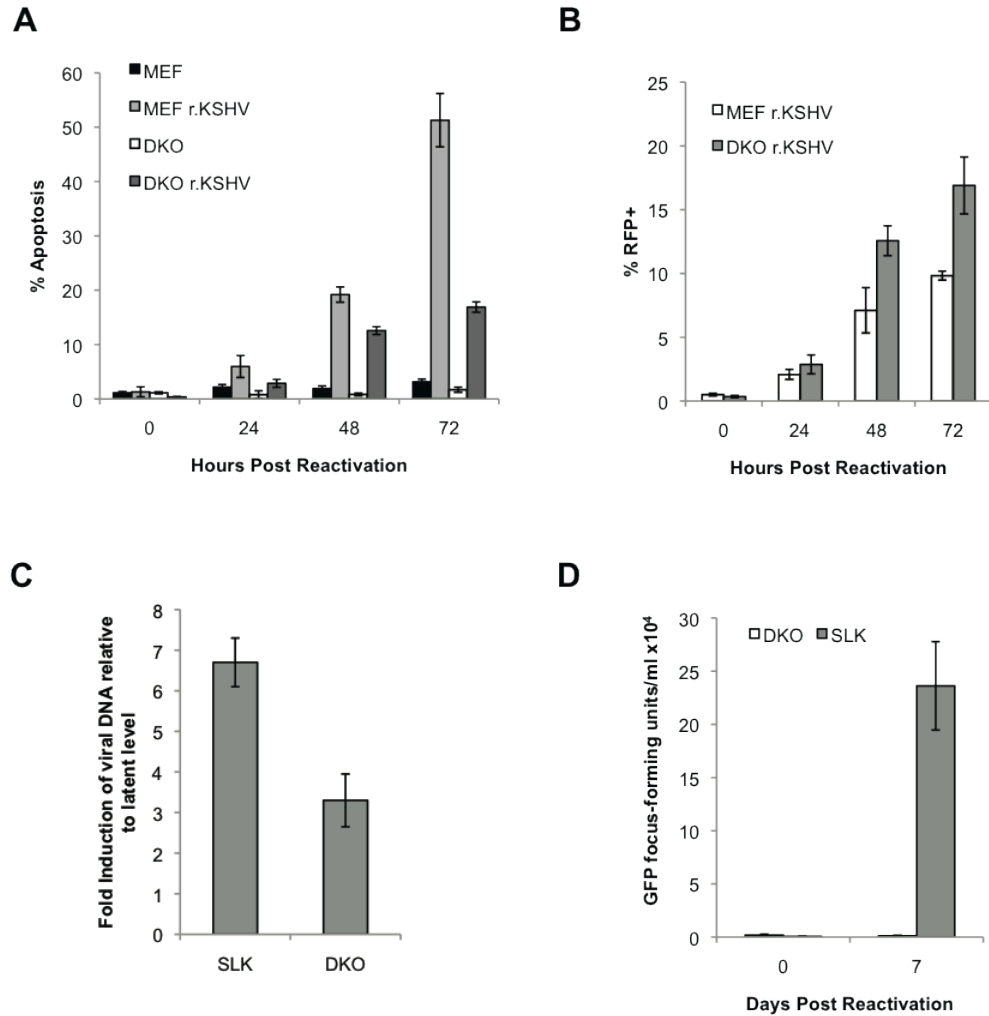


**Fig. 5.9** (A) Apoptosis was measured by Annexin V staining following lytic reactivation (4.8mM valproic acid) of r.KSHV.219 stably infected DKO, MEFs, and SLKs. (B) Quantification of RFP+ cells as a measurement of lytic reactivation upon 4.8mM valproic acid treatment. (C) DNA replication in DKO and SLKs following 72hr 4.8mM valproic acid treatment. DNA replication measured by qPCR of LANA gene copies. (D) Virus production (GFP expressing cells) measured by infecting 293 cells with supernatant from DKO r.KSHV and SLK r.KSHV cells treated 0 and 7 days with 4.8mM valproic acid.

We speculate that the induction of premature cell death may be due to the dysregulation of immediate early and delayed early genes, many of which can be pro-apoptotic when overexpressed (4, 23). Aberrant expression of late genes could also contribute to this phenotype. By inhibiting the intrinsic apoptotic pathway with DKO MEFs we can delay cell death long enough to permit viral DNA replication (Fig. 5.9C). However, despite this apoptotic delay, few virions are produced. This suggests that other defects in late gene expression, virion assembly or egress are also present in infected murine cells. Alternatively (or additionally), the premature engagement of other forms of cell death, such as extrinsic apoptosis or necrosis, may be responsible. Consistent with this, induced DKO r.KSHV cells display morphological signs of cell injury a full 48 hours before such changes are evident in infected human SLK cells (data not shown).

We note that our results differ slightly from earlier experiments published by Liang and Ganem (2004). They observed very low level virus production following super-infection with high titers of Ad-RTA of a single, spontaneously immortalized line of mouse fibroblasts transiently infected with wild-type (unmarked) KSHV at very high multiplicities (estimated at 5000-10,000 viruses per cell)(17). The high MOI used, the transient nature of the infection prior to reactivation, and the fact that they employed a single, multiply passaged mouse line are important differences between that study and the present one, and likely account for this disparity. While those results suggest that there are conditions *in vitro* under which limited KSHV growth can occur in murine cells, our present

results, in accord with all earlier *in vitro* animal experiments, suggest that this situation is a laboratory phenomenon unlikely to be encountered *in vivo*.

Taken together, our data indicate that multiple post-entry blocks to KSHV lytic replication exist. Viral episomes in stably infected latent mouse cells respond incorrectly to exogenous RTA expression, with extremely attenuated lytic gene expression. When these defects are (partially) bypassed via HDAc inhibition, the resulting lytic program remains aberrant; this dysregulation does not allow viral DNA replication, and is associated with premature apoptosis. When the latter is blocked experimentally, DNA replication can proceed but additional blocks continue to prevent infectious virion production. Thus, murine cells block lytic KSHV replication at multiple stages in the cycle, rendering it unlikely that any single genetic manipulation of transgenic mice can bypass these obstacles.

## Materials and Methods

**Tissue culture, virus preparation, and infection.** SLK, wild-type MEF, and *bax*<sup>-/-</sup>*bak*<sup>-/-</sup> MEF cells were cultured in DMEM with 10% FBS. Stable SLK r.KSHV, MEF r.KSHV, DKO r.KSHV cells were constructed by infecting each cell type with rKSHV.219 produced from rtTA-RTA-SLK cells (21) harboring the recombinant virus (courtesy of J. Vieira). Cells were induced to enter lytic replication with valproic acid (VA), AdRTA (adenovirus harboring the ORF50 cDNA), or sodium butyrate (N-Butyrate.). To determine if infectious virions were produced from these stable cell lines, the cells were lytically induced as indicated in the text, cultured for 5 days following induction, the virus was isolated as previously described (13). In brief, supernatants were cleared of cells by centrifugation (2000 RPM for 10 min) with subsequent filtration through a 0.45 µm filter, and the virions were pelleted at 27,000 °—g for 2 h. Viral pellets were resuspended in 1/125 of the original volume. Infectious units (IUs) of virus stocks were determined on 293 cells. Briefly, virus stock was serially diluted and infected 293 cells for 6 h in a 24-well plate. After fresh media was added, cells were further cultured for 48 h before the percentage of GFP+ cells was determined by FACS Calibur. IUs were calculated by multiplying the percentage of GFP+ cells by the total number of 293 cells in a well at the time of flow cytometric analysis.

### **KSHV tiling microarray construction, sample labeling, and microarray**

**hybridization.** The KSHV genome sequence used for the microarray design was obtained from GenBank accession number U75698.1. Thirteen thousand seven hundred forty-six 60-mer KSHV-specific oligonucleotide probes were printed in duplicate using Agilent technology. Each probe overlapped a neighboring probe by 40 nucleotides (nt), resulting in a tiling design with probes offset by 20 nucleotides. Probes were designed from sequences of both strands of the genome. The custom tiling microarray also contained control probes (approximately 1,500) and probes detecting host transcripts (approximately 16,311). This custom KSHV tiling microarray can be obtained from Agilent using the custom design identification number 017577. Total RNA from the experimental samples was purified as indicated above. The reference RNA was a mixture of RNAs of both infected and uninfected human and mouse cells, including TIME, HUVEC, BJAB, BCBL-1, MEF, and SLK cells. The integrity of the RNAs was analyzed using a model 2100 Bioanalyzer (Agilent), or the RNAs were analyzed using conventional formaldehyde-agarose gel electrophoresis and staining. RNAs were quantified using an ND1000 spectrophotometer (Nanodrop). A Quick Amp labeling kit (Agilent) was used according to the manufacturer's protocol to generate labeled cRNA from 450ng of total RNA. Experimental samples were labeled with Cy5, and reference samples were labeled with Cy3 and then competitively hybridized to the custom KSHV tiling microarray according to the manufacturer's protocol for the whole human genome oligonucleotide microarrays (Agilent). Hybridized microarrays were washed according to the manufacturer's protocol (Agilent) and scanned with a GenePix

4000B scanner (Axon Instruments) and all feature intensities collected using GenePix Pro 6.0 software. TIFF images of scanned slides were analyzed using Feature Extraction Software, version 9.5.3 (Agilent), using a custom grid file. All reported raw microarray data are MIAME (minimum information about a microarray experiment) compliant and are stored in NCBI's Gene Expression Omnibus (GEO), ([http://www.ncbi.nlm.nih.gov/geo/query/acc.cgi?acc\\_GSE20443](http://www.ncbi.nlm.nih.gov/geo/query/acc.cgi?acc_GSE20443)). A graphical presentation of processed data (heat map) was generated by Java Treeview.

**Flow cytometry.** SLK, wild-type MEF, and *bax*<sup>-/-</sup>*bak*<sup>-/-</sup> MEF cells were subjected to flow cytometric analysis to detect expression of green fluorescent protein (GFP) and red fluorescent protein (RFP). Cells were analyzed using a FACSCalibur (BD Biosciences), and the resulting data were analyzed using FlowJo. Cells were prepared for flow cytometric analysis by trypsinization to harvest the cells, followed by a 10 minute fixation period with 2% paraformaldehyde with or without annexin V-APC (BD biosciences) staining.

**RNA preparation.** HFF and SLK cell samples were harvested in RLT buffer, and RNA was isolated using an RNeasy minikit according to the manufacturer's protocol (Qiagen).



## References

1. **Bechtel, J. T., Y. Liang, J. Hvidding, and D. Ganem.** 2003. Host range of Kaposi's sarcoma-associated herpesvirus in cultured cells. *J Virol* **77**:6474-6481.
2. **Blackbourn, D. J., E. Lennette, B. Klencke, A. Moses, B. Chandran, M. Weinstein, R. G. Glogau, M. H. Witte, D. L. Way, T. Kutzkey, B. Herndier, and J. A. Levy.** 2000. The restricted cellular host range of human herpesvirus 8. *AIDS* **14**:1123-1133.
3. **Boshoff, C., and R. A. Weiss.** 1998. Kaposi's sarcoma-associated herpesvirus. *Adv Cancer Res* **75**:57-86.
4. **Cannon, M. L., and E. Cesarman.** 2004. The KSHV G protein-coupled receptor signals via multiple pathways to induce transcription factor activation in primary effusion lymphoma cells. *Oncogene* **23**:514-523.
5. **Cesarman, E., Y. Chang, P. S. Moore, J. W. Said, and D. M. Knowles.** 1995. Kaposi's sarcoma-associated herpesvirus-like DNA sequences in AIDS-related body-cavity-based lymphomas. *N Engl J Med* **332**:1186-1191.
6. **Chandriani, S., and D. Ganem.** 2010. Array-based transcript profiling and limiting-dilution reverse transcription-PCR analysis identify additional latent genes in Kaposi's sarcoma-associated herpesvirus. *J Virol* **84**:5565-5573.
7. **Chang, H., L. M. Wachtman, C. B. Pearson, J. S. Lee, H. R. Lee, S. H. Lee, J. Vieira, K. G. Mansfield, and J. U. Jung.** 2009. Non-human primate model of Kaposi's sarcoma-associated herpesvirus infection. *PLoS Pathog* **5**:e1000606.
8. **Chang, Y., E. Cesarman, M. S. Pessin, F. Lee, J. Culpepper, D. M. Knowles, and P. S. Moore.** 1994. Identification of herpesvirus-like DNA sequences in AIDS-associated Kaposi's sarcoma. *Science* **266**:1865-1869.
9. **Dittmer, D., C. Stoddart, R. Renne, V. Linnquist-Stepps, M. E. Moreno, C. Bare, J. M. McCune, and D. Ganem.** 1999. Experimental transmission of Kaposi's sarcoma-associated herpesvirus (KSHV/HHV-8) to SCID-hu Thy/Liv mice. *J Exp Med* **190**:1857-1868.
10. **Du, C., M. Fang, Y. Li, L. Li, and X. Wang.** 2000. Smac, a mitochondrial protein that promotes cytochrome c-dependent caspase activation by eliminating IAP inhibition. *Cell* **102**:33-42.
11. **Dupin, N., C. Fisher, P. Kellam, S. Ariad, M. Tulliez, N. Franck, E. van Marck, D. Salmon, I. Gorin, J. P. Escande, R. A. Weiss, K. Alitalo, and C. Boshoff.** 1999. Distribution of human herpesvirus-8 latently infected cells in Kaposi's sarcoma, multicentric Castleman's disease, and primary effusion lymphoma. *Proc Natl Acad Sci U S A* **96**:4546-4551.
12. **Ganem, D.** 2006. KSHV infection and the pathogenesis of Kaposi's sarcoma. *Annu Rev Pathol* **1**:273-296.
13. **Grossmann, C., and D. Ganem.** 2008. Effects of NFkappaB activation on KSHV latency and lytic reactivation are complex and context-dependent. *Virology* **375**:94-102.
14. **Lan, K., D. A. Kuppers, S. C. Verma, N. Sharma, M. Murakami, and E. S. Robertson.** 2005. Induction of Kaposi's sarcoma-associated herpesvirus latency-

- associated nuclear antigen by the lytic transactivator RTA: a novel mechanism for establishment of latency. *J Virol* **79**:7453-7465.
15. **Liang, Y., J. Chang, S. J. Lynch, D. M. Lukac, and D. Ganem.** 2002. The lytic switch protein of KSHV activates gene expression via functional interaction with RBP-Jkappa (CSL), the target of the Notch signaling pathway. *Genes Dev* **16**:1977-1989.
  16. **Liang, Y., and D. Ganem.** 2003. Lytic but not latent infection by Kaposi's sarcoma-associated herpesvirus requires host CSL protein, the mediator of Notch signaling. *Proc Natl Acad Sci U S A* **100**:8490-8495.
  17. **Liang, Y., and D. Ganem.** 2004. RBP-J (CSL) is essential for activation of the K14/vGPCR promoter of Kaposi's sarcoma-associated herpesvirus by the lytic switch protein RTA. *J Virol* **78**:6818-6826.
  18. **Lindsten, T., A. J. Ross, A. King, W. X. Zong, J. C. Rathmell, H. A. Shiels, E. Ulrich, K. G. Waymire, P. Mahar, K. Frauwirth, Y. Chen, M. Wei, V. M. Eng, D. M. Adelman, M. C. Simon, A. Ma, J. A. Golden, G. Evan, S. J. Korsmeyer, G. R. MacGregor, and C. B. Thompson.** 2000. The combined functions of proapoptotic Bcl-2 family members bak and bax are essential for normal development of multiple tissues. *Mol Cell* **6**:1389-1399.
  19. **Liu, X., C. N. Kim, J. Yang, R. Jemmerson, and X. Wang.** 1996. Induction of apoptotic program in cell-free extracts: requirement for dATP and cytochrome c. *Cell* **86**:147-157.
  20. **Mutlu, A. D., L. E. Cavallin, L. Vincent, C. Chiozzini, P. Eroles, E. M. Duran, Z. Asgari, A. T. Hooper, K. M. La Perle, C. Hilsher, S. J. Gao, D. P. Dittmer, S. Raffi, and E. A. Mesri.** 2007. In vivo-restricted and reversible malignancy induced by human herpesvirus-8 KSHV: a cell and animal model of virally induced Kaposi's sarcoma. *Cancer Cell* **11**:245-258.
  21. **Myoung, J., and D. Ganem.** 2011. Generation of a doxycycline-inducible KSHV producer cell line of endothelial origin: maintenance of tight latency with efficient reactivation upon induction. *J Virol Methods* **174**:12-21.
  22. **Oakes, S. A., S. S. Lin, and M. C. Bassik.** 2006. The control of endoplasmic reticulum-initiated apoptosis by the BCL-2 family of proteins. *Curr Mol Med* **6**:99-109.
  23. **Ojala, P. M., M. Tiainen, P. Salven, T. Veikkola, E. Castanos-Velez, R. Sarid, P. Biberfeld, and T. P. Makela.** 1999. Kaposi's sarcoma-associated herpesvirus-encoded v-cyclin triggers apoptosis in cells with high levels of cyclin-dependent kinase 6. *Cancer Res* **59**:4984-4989.
  24. **Renne, R., D. Blackbourn, D. Whitby, J. Levy, and D. Ganem.** 1998. Limited transmission of Kaposi's sarcoma-associated herpesvirus in cultured cells. *J Virol* **72**:5182-5188.
  25. **Spadavecchia, S., O. Gonzalez-Lopez, K. D. Carroll, D. Palmeri, and D. M. Lukac.** 2010. Convergence of Kaposi's sarcoma-associated herpesvirus reactivation with Epstein-Barr virus latency and cellular growth mediated by the notch signaling pathway in coinfecting cells. *J Virol* **84**:10488-10500.
  26. **Susin, S. A., H. K. Lorenzo, N. Zamzami, I. Marzo, B. E. Snow, G. M. Brothers, J. Mangion, E. Jacotot, P. Costantini, M. Loeffler, N. Larochette, D. R. Goodlett, R. Aebersold, D. P. Siderovski, J. M. Penninger, and G.**

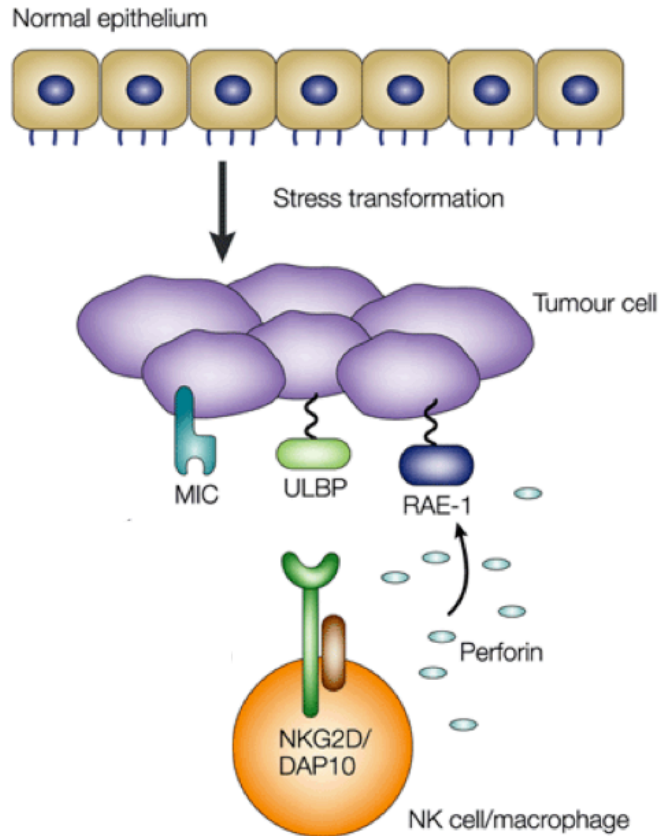
- Kroemer.** 1999. Molecular characterization of mitochondrial apoptosis-inducing factor. *Nature* **397**:441-446.
27. **Vieira, J., and P. M. O'Hearn.** 2004. Use of the red fluorescent protein as a marker of Kaposi's sarcoma-associated herpesvirus lytic gene expression. *Virology* **325**:225-240.
28. **Wei, M. C., W. X. Zong, E. H. Cheng, T. Lindsten, V. Panoutsakopoulou, A. J. Ross, K. A. Roth, G. R. MacGregor, C. B. Thompson, and S. J. Korsmeyer.** 2001. Proapoptotic BAX and BAK: a requisite gateway to mitochondrial dysfunction and death. *Science* **292**:727-730.

## **Purification and Identification of Glioblastoma secreted factor responsible for NK cell ligand upregulation on primary monocytes**

### **Background**

Glioblastoma multiforme (GBM) is the most common and aggressive form of primary brain tumor in humans. Given its aggressive nature, it has one of the worst prognoses of any CNS malignancy, with a median survival time of approximately 14 months (17). This type of brain cancer originates from a particular kind of glial cell, star-shaped brain cells in the cerebrum called astrocytes. Treatment options for this aggressive tumor type are limited. Surgical removal remains the mainstay of treatment, provided that unacceptable neurologic injury can be avoided. The extremely infiltrative nature of this tumor makes complete surgical removal impossible. Although radiotherapy rarely cures glioblastoma, studies show that it doubles the median survival of patients, compared to supportive care alone. Long-term survival (at least five years) falls well under 3% (2). Novel, less invasive detection and treatment options are greatly needed for this deadly cancer.

A very promising treatment option for GBM is immunotherapy; however its effectiveness is dependent on immune effector cells, such as natural killer (NK) cells. NK cells are a lymphocytic component of innate immunity against pathogens and tumors. These cells were originally discovered due to their ability to kill tumor cells *in vitro* and loss of these cells *in vivo* results in increased tumor proliferation and progression (15). NK cells respond to both activating and inhibitory signals on target cells. Unlike T and B cells, NK cells use a number of receptors (e.g. NKG2D, NKp44, NKG2C) that bind various ligands to enable targeting of a broad range of cells (13, 14). Upon activation, these receptors initiate a signaling cascade that results in the release of perforin, a cytolytic protein found in the secretory vesicles or granules of NK and cytotoxic T cells. Upon degranulation, perforin inserts itself into the cell membrane of target cell, creating a pore and initiating apoptosis (Fig. 6.1)(9).



Nature Reviews | Immunology

**Fig. 6.1.** Model of tumor cell recognition and killing by natural killer (NK) cells. Tumor cells express stress-induced ligands for NK cell receptors, such as NKG2D. These ligand-bearing cells are recognized and eliminated by NK cells via the secretion of Perforin. Adapted from Cerwenka, et al. Nature Reviews Immunology (2001).

Specifically, NKG2D recognizes several MHC-class I-like ligands. MHC-class-I-chain related A and B antigens consist of 3 alpha domains and are present in low levels in adult tissue. These are expressed to varying degrees on healthy cells as well as virally infected and tumor cells (Table 6.1)(3, 4). However, it is generally accepted that the levels of NKG2D ligands on healthy cells is below the detection threshold necessary to initiate an immune response.

Tumor cells have evolved a number of strategies to evade this host defense. Despite the expression of MIC and ULBP family member ligands on tumor cells, these cells are not efficiently cleared by NK cells *in vivo* (5, 7). GBM cells may avoid detection by NK cells by secreting immunosuppressive molecules (e.g. IL-10 or TGF $\beta$ ) and downregulating activating receptors on NK cells, inhibiting their ability to detect the activating ligands, MICA/B and ULBP1/2, expressed on their cell surface (Fig 6.2)(7). Interestingly, despite the downregulation of activating receptors and the presence of secreted inhibitory molecules, NK cells efficiently target and kill tumor-localized monocytes, but not tumor cells. This indicates that the previously mentioned mechanisms are not sufficient to completely inactivate NK cell cytotoxic activity and that there is an additional mechanism by which the tumor cells are able to “redirect” NK cell killing.

	<b>MIC</b>	<b>ULBP</b>
Structure	MHC-class-I-like, $\alpha$ 1-, $\alpha$ 2-, $\alpha$ 3-loops, no $\beta$ 2m, no peptide	MHC-class-I-like, $\alpha$ 1-, $\alpha$ 2-loops, GPI-anchored, no $\beta$ 2m, no peptide
Expression	Gut epithelium, tumour cell lines, spontaneous tumors	Tumour cell lines
Inducibility	Heat shock, HCMV infection, transformation	Transformation
Subtypes	A, B	1-6

**Table 6.1.** Comparison of Human NKG2D-ligands. B2m,  $\beta$ 2-microglobulin; GPI, glycosylphosphatidylinositol; HCMV, human cytomegalovirus; MHC, major histocompatibility complex; MIC, MHC-class-I-chain related molecules; ULBP, UL16-binding protein. *Modified from Cerwenka A, Lanier LL. Nat Rev Immunol. 2001 Oct;1(1):41-9.*

The regulation of NKG2D ligands plays a complex and important role in both viral infection and tumor progression and development, therefore further understanding of their manipulation in these conditions is vital to the efficacy of immunotherapy. NKG2D ligand expression is regulated transcriptionally, post-transcriptionally, and post-translationally. NKG2D transcription can be induced by DNA damage, TLR stimulation, and cytokine exposure(5). The DNA damage response is critical for maintaining genome integrity. Upon double-strand DNA breaks, DNA replication is stalled, cell cycle arrest occurs, and if extensive apoptosis induced. Following treatment with DNA damage agents, NKG2D



ligands are upregulated and this upregulation is dependent on DNA damage pathway machinery. In addition, as expected of an immune regulator, NKG2D ligands are upregulated upon TLR (Toll-like receptor) signaling. TLRs detect foreign peptides that initiate both the innate and adaptive immune responses. Lastly, cytokines also affect NKG2D ligand expression. Individual interferons are able to alternatively upregulate or downregulate specific ligands. Also, heat shock proteins are able to regulate these ligands as heat shock response elements are contained within the promoters of MICA and MICB (5).

Surprisingly, glioma cells secrete an unknown factor that upregulates MICA/B and ULBP1 on primary monocytes in the absence of cellular stresses. This suggests a novel mechanism through which glioma cells evade NK cell killing. Glioma cells secrete a factor that preferentially upregulates NK-activating ligands on monocytes. This mechanism cripples the innate immune response to GBM twofold. First, NK cells initiate monocyte apoptosis, removing the pro-inflammatory protective effects of the monocytes themselves. Secondly, the release of perforin directed at monocytes exhausts the NK cells, preventing them from also targeting the MICA/B- and ULBP1-expressing glioma cells (Fig 6.3). Identification of the unknown secreted factor will help to more completely understand the evasion tactics of this aggressive tumor and also possibly reveal an efficacious therapeutic target.

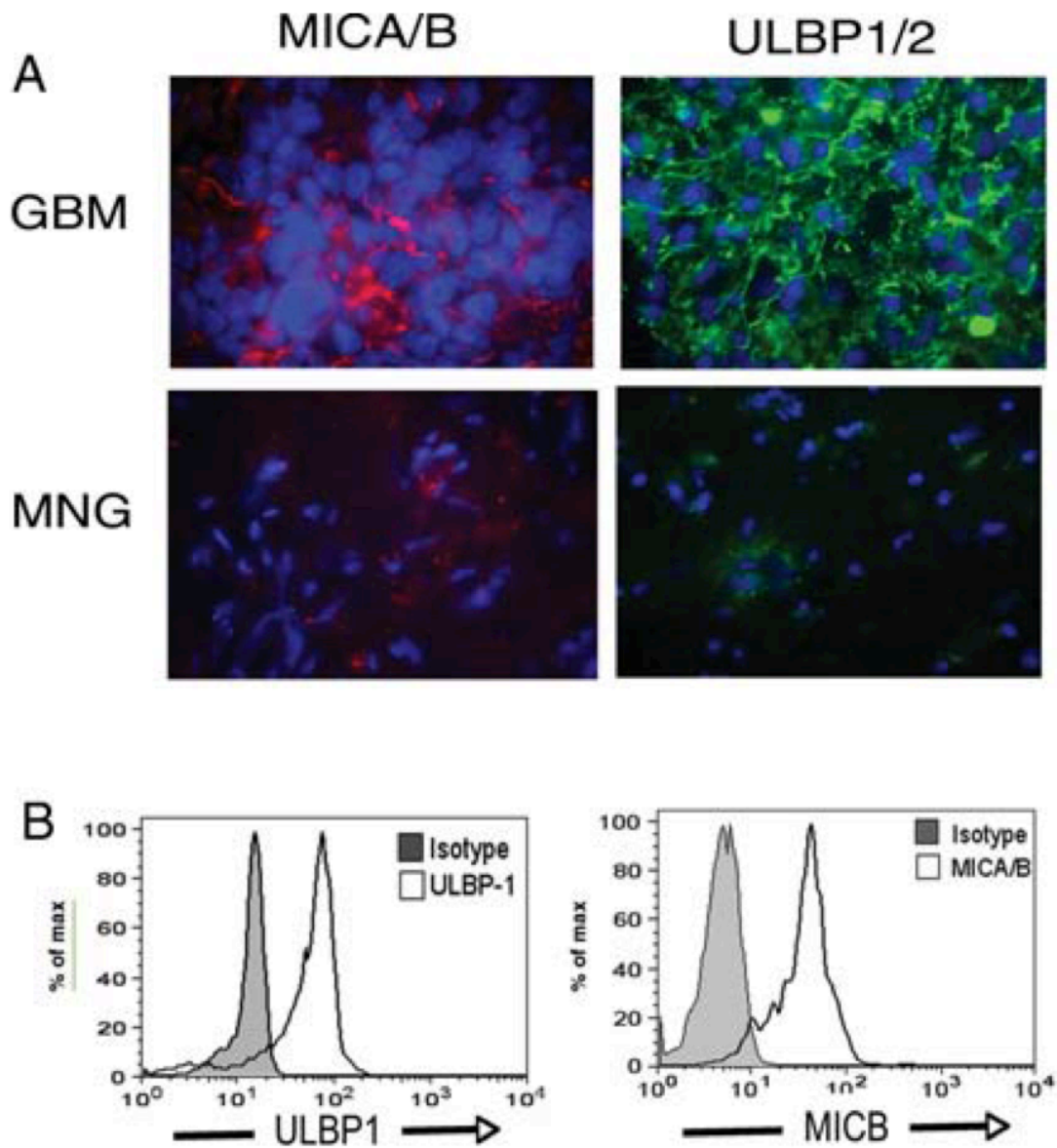


**Fig. 6.2.** GBM tumor cells express NKG2D ligands on the surface. (A) Immunofluorescence staining of 10-mm frozen tissue sections with monoclonal antibody cocktails with either anti-MICA (clone M673) and anti-MICB (clone M362) (left panels, red) or anti-ULBP1 (clone M295) and anti-ULBP-2 (M310) (right panels, green) in GBM or MNG tumor sections. Nuclei were stained with DAPI (blue). Images are representative of 11 GBM samples analyzed. Crane *et al.* Neuro-Oncology 12(1):7–13, 2010

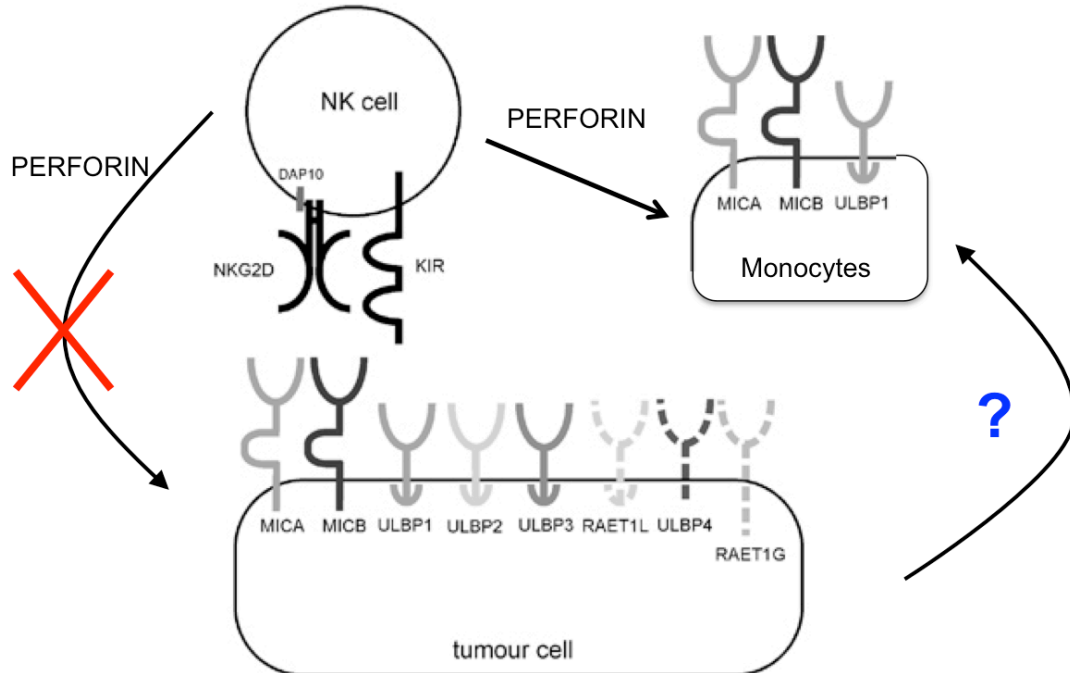


**Fig. 6.3.** Model of Glioma cell NK cell evasion. Glioma cells secrete an unknown factor that upregulates NK cell ligands, MICA, MICB, and ULBP1, on primary monocytes. Monocytes are then targeted by NK cells, exhausting their ability to kill the tumor cells. Adapted from Waldhauer and Steinle *Oncogene* (2008) **27**, 5932–5943

## Results and Discussion

Cultured glioblastoma cells (U-87) secrete an unknown factor(s) responsible for upregulation of NK activating ligands (MICB and ULBP1) on primary monocytes. We have developed an *in vitro* system and biochemical purification scheme to identify this factor(s) (Fig 6.4).

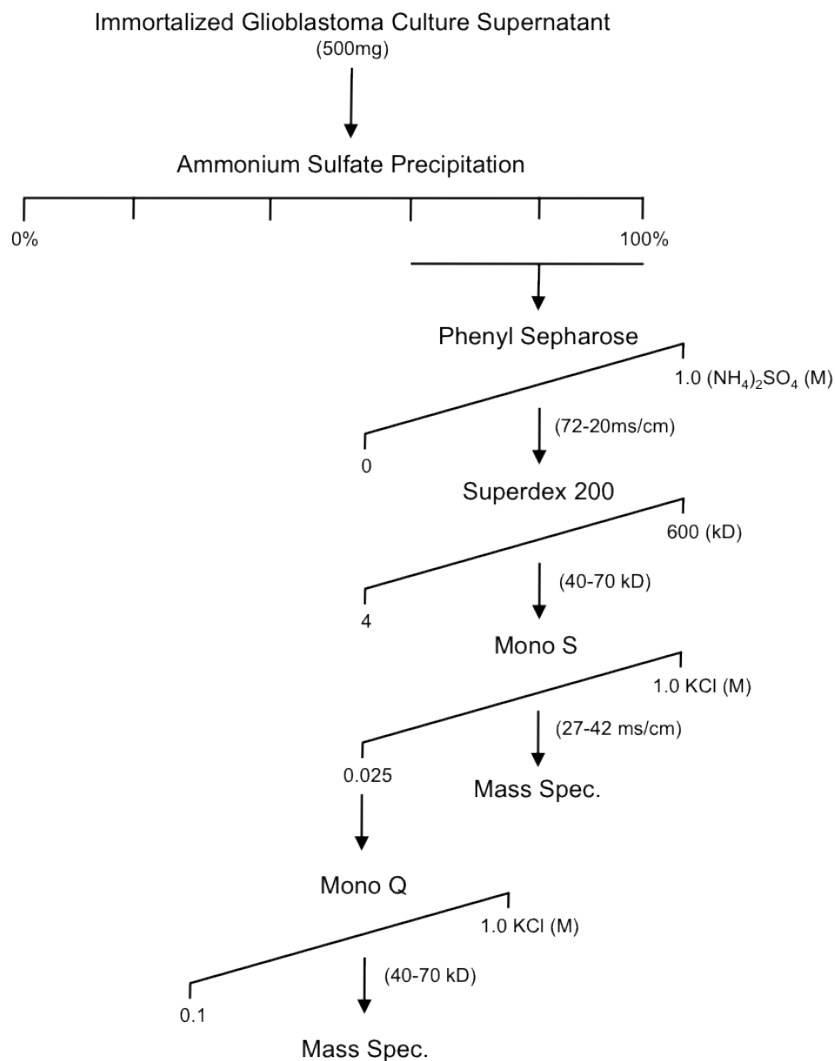


**Fig. 6.4.** Purification scheme of glioblastoma secreted factor responsible for NK cell ligand upregulation on primary monocytes.

Supernatant from cultured U-87 cells, grown in 5% serum, was collected daily. The presence of ligand-inducing activity is measured by incubating the U-87 supernatant with isolated primary monocytes. Ligand upregulation is measured by qPCR with primers specific to MICA/B and ULBP1. The ligand-inducing activity is then precipitated based on its hydrophobicity by the addition of ammonium sulfate (ammonium sulfate cut). The target precipitates at 60-

100% ammonium sulfate saturation. This sample is then further separated using a Phenyl Sepharose column (Fig 6.5). Sample complexity is further decreased approximately 50% by the gel filtration column (Superdex 200)(Fig. 6.6). The ligand-inducing fraction is separated by protein charge using the MonoS (ion exchange) column. Interestingly, this column reveals two separate activities with differing effects on MICB and ULBP1. The factor that does not bind to the matrix strongly induces MICB (MICB-heavy or MICBh), while the other induces ULBP1 strongly and MICB moderately (ULBP-heavy or ULBP1h)(Fig 6.7). In the final step of our purification scheme, we used another ion exchange column (MonoQ) to further isolate the factor present in the flow through of the MonoS column (Fig. 6.8).

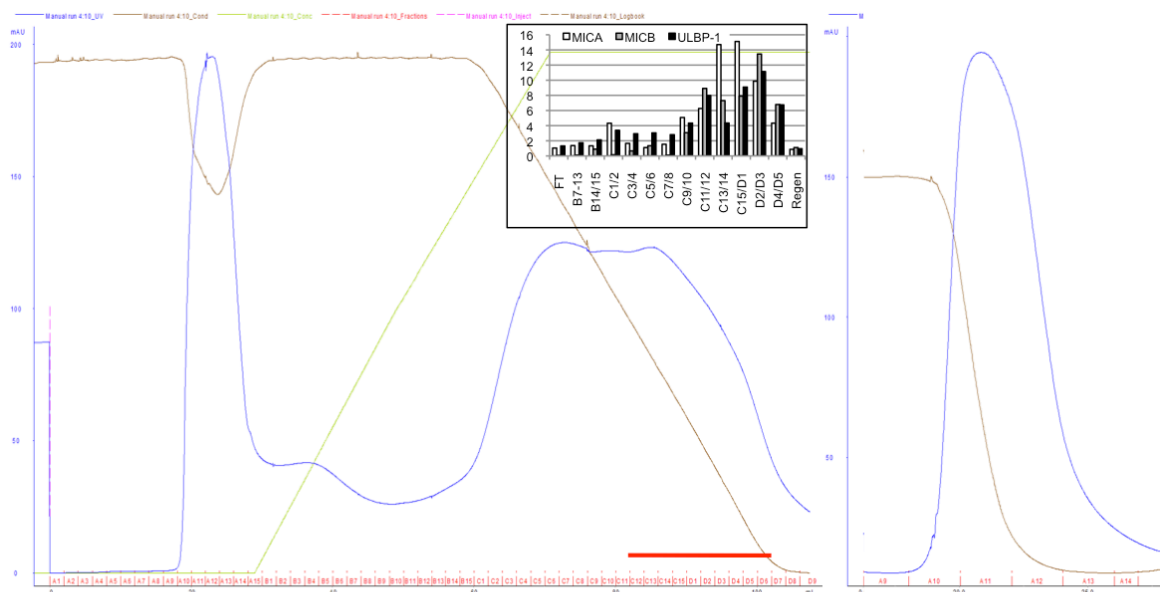


**Fig. 6.5.** Biochemical separation of NK cell ligand-inducing factor by Hydrophobicity on a Phenyl Sepharose oolumn. Presence of target detected in fractions C12-D6 (72-20 ms/cm) by qPCR activity assay.

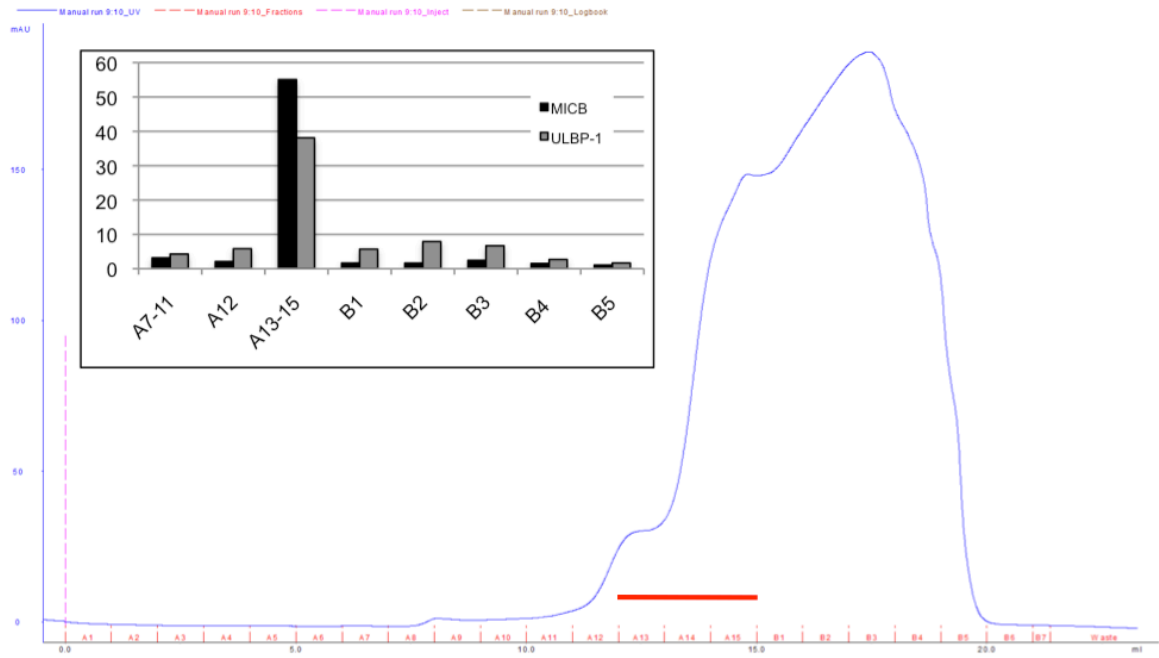


**Fig. 6.6.** Biochemical separation of ligand-inducing factor by molecular size on a superdex200 gel filtration column. Presence of target detected in fractions A13-A15 by qPCR activity assay.

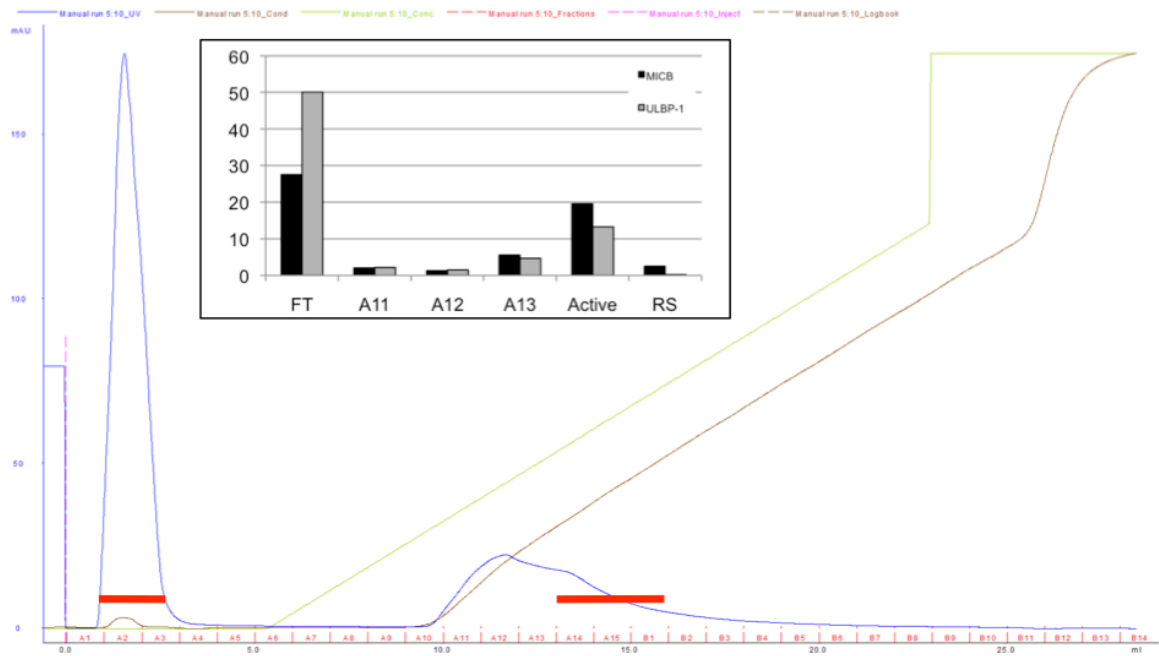


**Fig. 6.7.** Biochemical purification of ligand-inducing factor by protein charge using a MonoS ion exchange column. Presence of target detected in the flow through and fractions A14-B1 by qPCR activity assay.

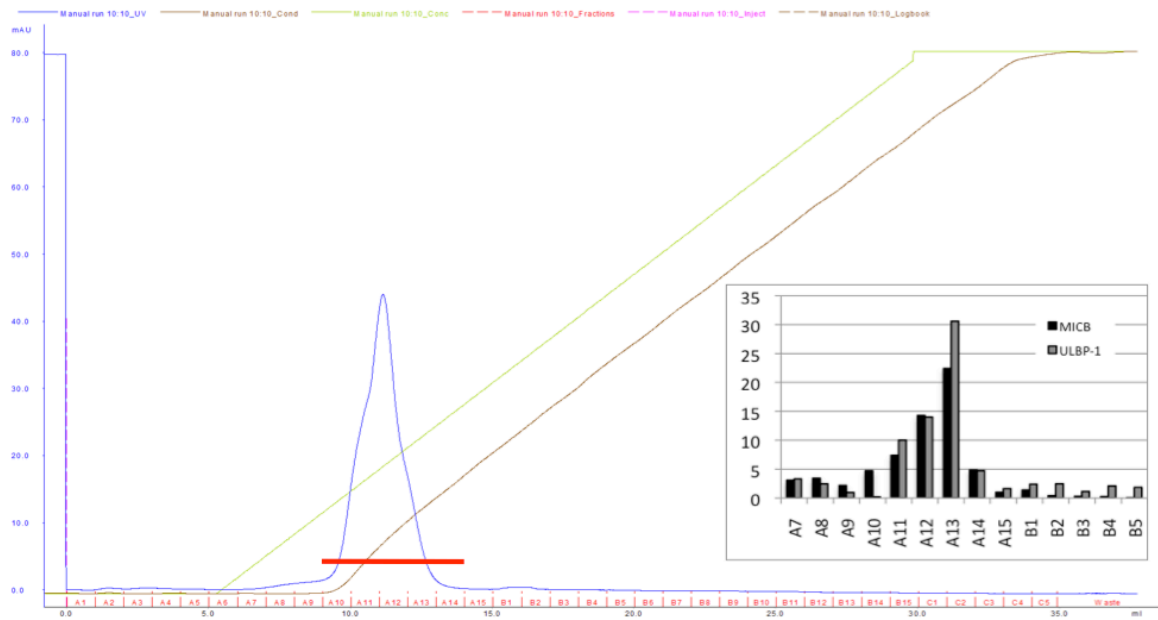


**Fig. 6.8.** Biochemical separation of ligand-inducing factor by protein charge using MonoQ ion exchange column. Presence of target detected in fractions A10-A14 by qPCR activity assay.

We did not get much more separation, as the activity was present in the major peak bound to the column. Using this purification strategy we have purified our target from ~97% of the starting material and concentrated our activity at least 100 fold (Table 6.2). This conclusion is further supported by silver stain analysis of the complexity of the purified sample. We detect only 3 or 4 distinct proteins present in the Flow through fraction of the MonoS. The silver stain analysis of the activity-containing fraction from the MonoQ reveals a similar complexity with a few more minor species detected (Fig. 6.9). These final fractions were split, with one half sent in-solution for mass spectrometric analysis and the other stained by silver. Sections were cut from the silver stained gel for mass spectrometric analysis (Fig. 6.9).

Step	Percent Starting Material	Activity Dilutions
<b>A.S.</b>	40	2
<b>Phen Seph</b>	6.8	10
<b>S200</b>	3.6	500
<b>MonoS</b>	0.64	50
<b>MonoQ</b>	2.34	100

**Table 6.2.** Purification and concentration of our target protein at each step of Purification #1.

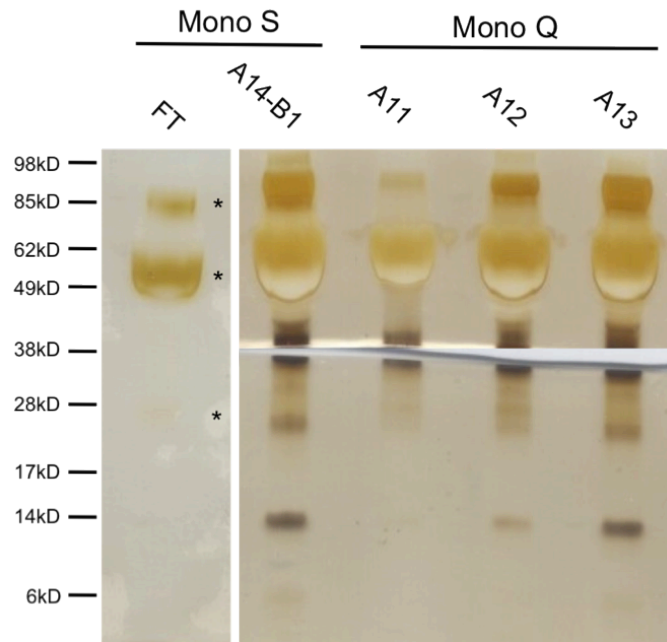


**Fig. 6.9.** Silver stain of final purified fractions containing ligand-inducing activity. Mono S Flow Through (FT) contains 1/10 of total sample prior to being purified on Mono Q. Loaded half of final Mono S A14-B1 and Mono Q sample volume.

Unfortunately, mass spectrometric analysis of the purified NKG2D ligand-inducing fractions identified bovine serum albumin as the predominant protein species, with minimal other promising candidates. This required the



implementation of additional purification steps to remove serum components and therefore, a redesign of the purification scheme.

Bovine serum albumin (BSA) has previously been shown to bind Hydroxyapatite matrix in 0.02M Sodium acetate and efficiently eluted in 0.33M  $\text{Na}_2\text{HPO}_4$ , 0.02M Sodium Acetate(19). Under these conditions, our targets also bound to the matrix (Fig. 6.10). A gradient using 0.11M  $\text{Na}_2\text{HPO}_4$ , 0.02M Sodium acetate permitted BSA and the majority of protein to flow through the matrix, while one target (ULBP1h) bound. We then eluted ULBP1h with 0.33M  $\text{Na}_2\text{HPO}_4$ , 0.02M Sodium acetate (Fig. 6.12). Unfortunately, the target that preferentially upregulates MICB (MICBh) does not bind the matrix under these conditions (Fig. 6.11). Using these described Hydroxyapatite conditions we were able to separate ~98% of the BSA in the sample from the ULBP1-upregulating target (ULBP1h), while coordinately reducing the complexity of our protein sample.

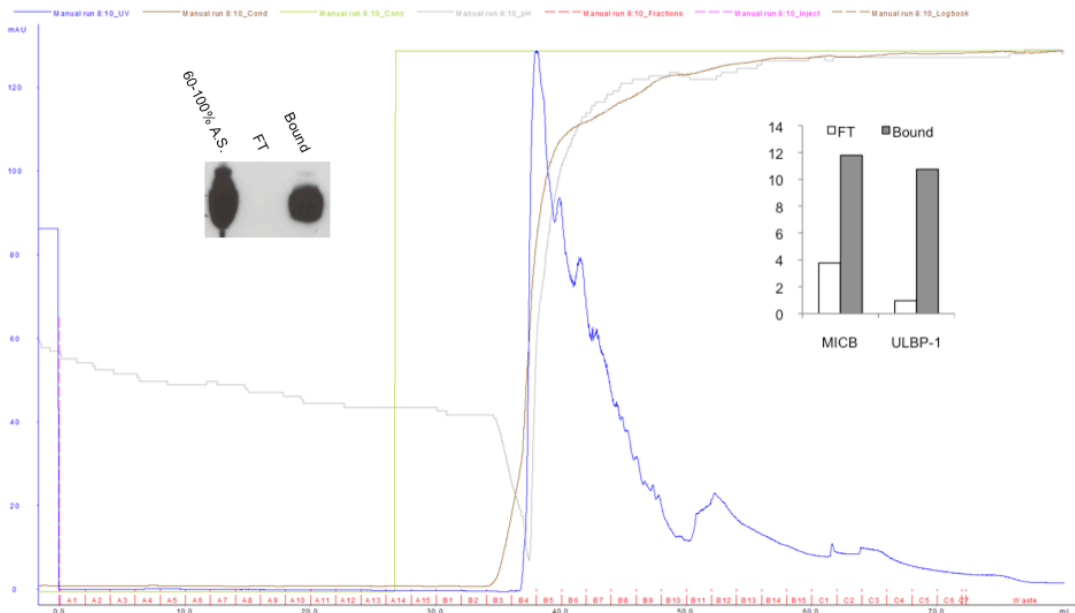


**Fig. 6.10.** Biochemical separation of NK cell ligand-inducing factor on a Hydroxyapatite column to determine conditions for efficient BSA removal. Presence of target and BSA detected in bound fraction.

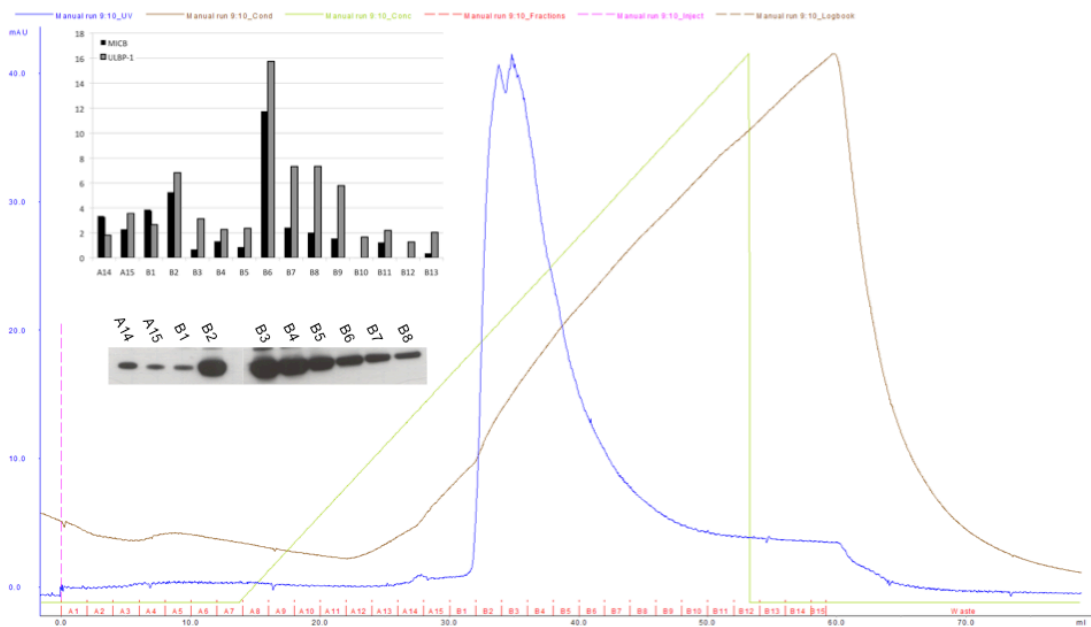


**Fig. 6.11.** Gradient separation of NK cell ligand-inducing factor on a Hydroxyapatite column to determine conditions for efficient BSA removal. Majority of BSA in separate fractions from one of the activities (ULBP-1). MICB activity separates with majority of BSA.

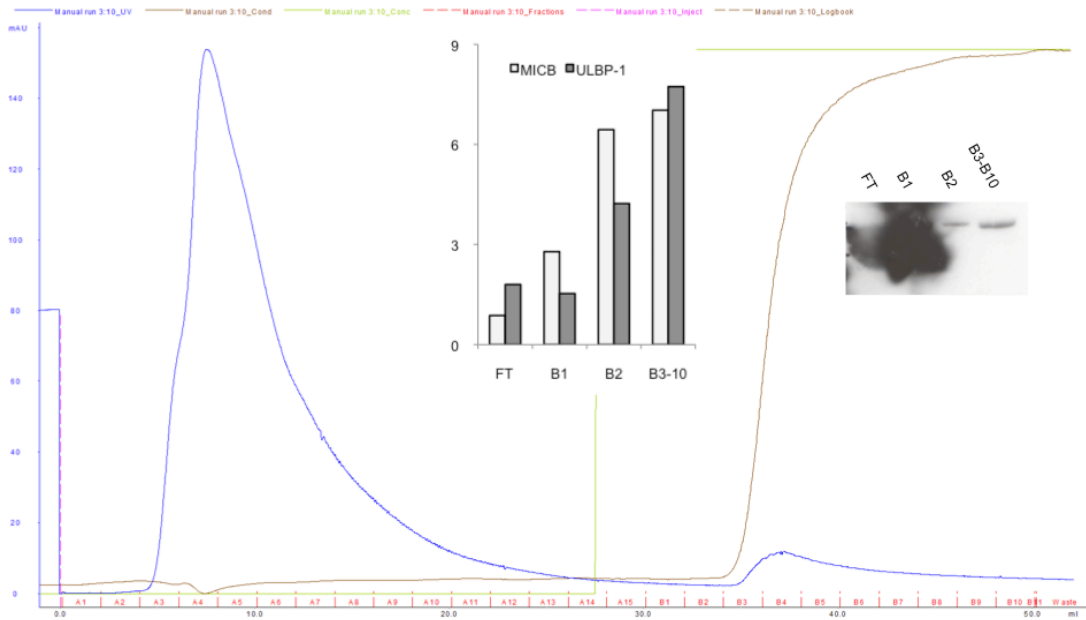


**Fig. 6.12.** Verification of Hydroxyapatite conditions for efficient BSA removal. >99% of BSA removed using these conditions: binding buffer = 0.11M Na<sub>2</sub>HPO<sub>4</sub> 0.02M Sodium Acetate, elution buffer = 0.33M Na<sub>2</sub>HPO<sub>4</sub> 0.02M Sodium Acetate.

Once the new purification conditions were established (Fig. 6.13), 30 liters of U87 media were collected and concentrated ~10 fold, performed an ammonium sulfate cut as described in purification #1. The pellets were resuspended in 110ml of water. This large volume required us to load the Hydroxyapatite 18 individual times with 10ml of material in 0.11M Na<sub>2</sub>HPO<sub>4</sub>, 0.02M Sodium Acetate. ULBP1h was eluted from the column twice using 0.33M Na<sub>2</sub>HPO<sub>4</sub>, 0.02M Sodium Acetate (Fig. 6.14). To ensure maximum removal of BSA, a third Hydroxyapatite column was run on the previous two eluents (Fig. 6.15). The Hydroxyapatite purification step removed approximately 98% of protein and concentrated our activity 100 fold. We further purified ULBP1h from 75% of total protein and concentrated our activity a further three fold on an ion exchange column (MonoQ)(Fig. 6.16). ULBP1h eluted in three fractions of

varying protein complexity (judged by the mAU profile). The remaining BSA was present in varying degrees in these fractions. One third of fraction B3 was silver stained (Figure 6.17) and sent for analysis by mass spectrometry at the UCSF core facility. Unfortunately, despite the removal of over 99% of the contaminating proteins, the predominant species present in the final fraction (B3) remains bovine (Table 6.2). However, we did obtain two human-specific candidates from the analysis. L-lactate dehydrogenase (LDH) was of particular interest. LDH isoenzyme, LDH5, is used as a marker for late stage tumor diagnosis and is known to be secreted by a number of different tumor types (6, 8, 10, 16, 20).

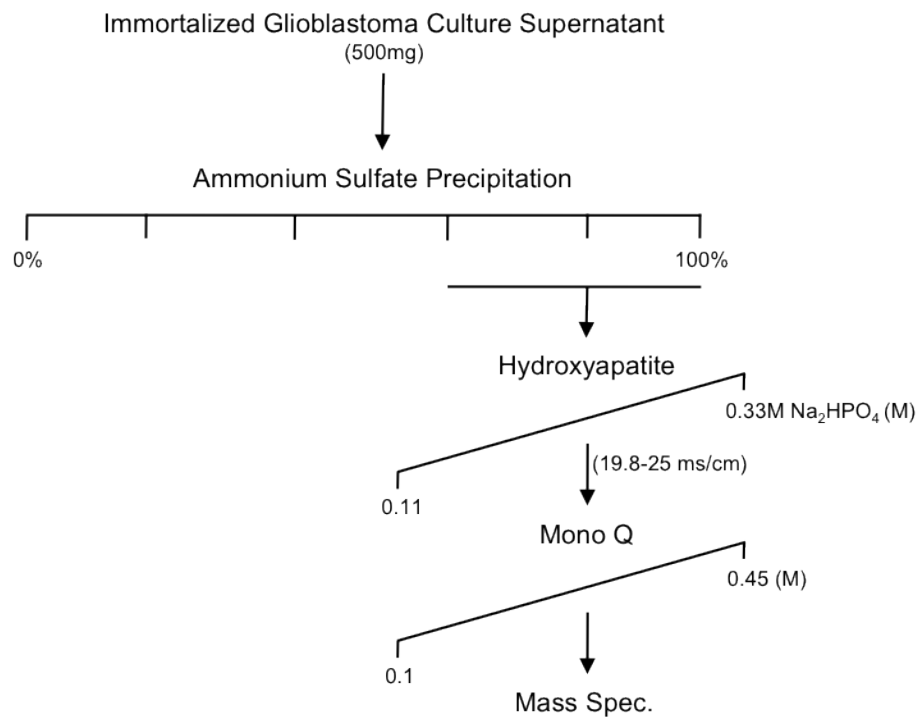


**Fig. 6.13.** Purification scheme for secreted glioblastoma factor responsible for NK cell ligand ULBP1 upregulation on primary monocytes.

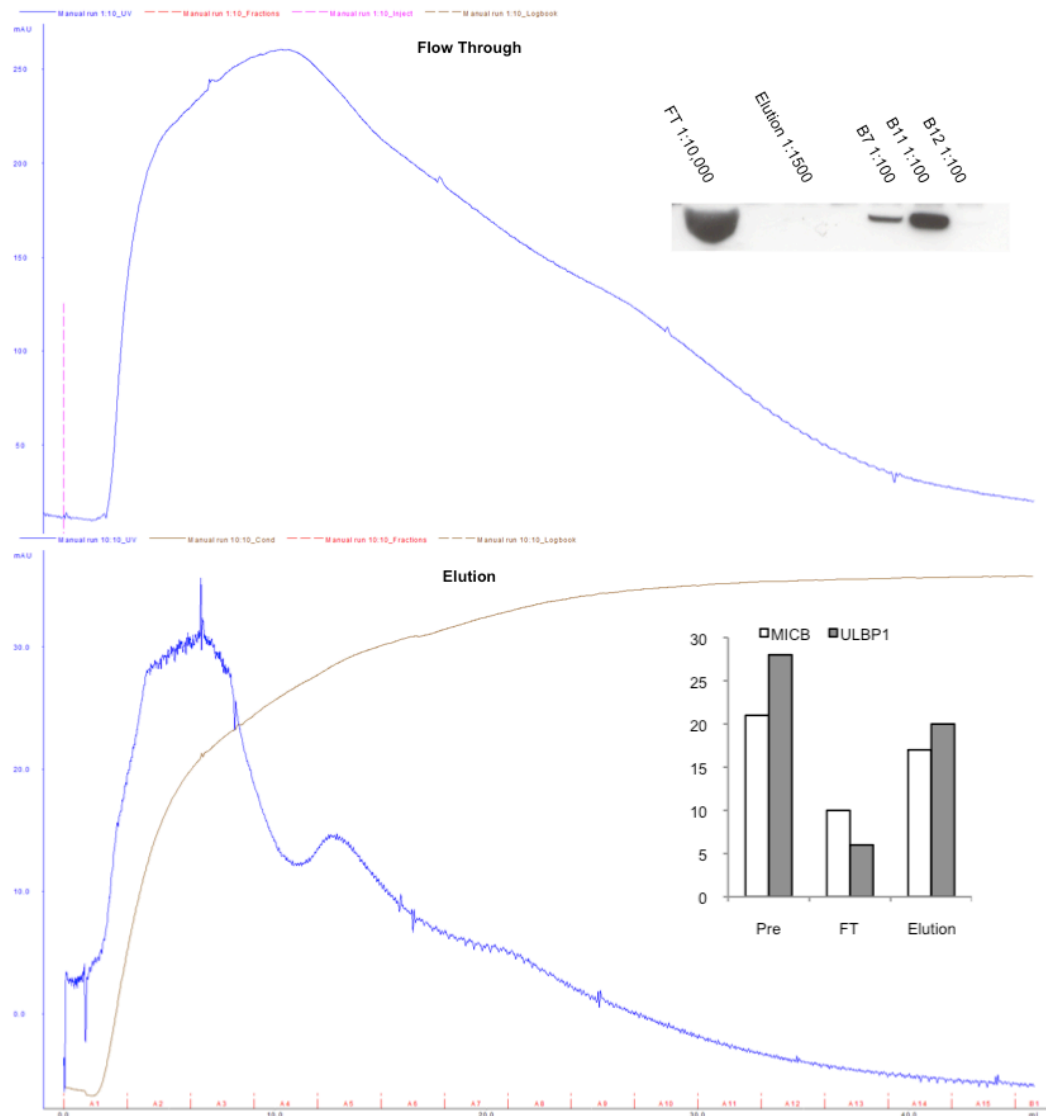


**Fig. 6.14.** BSA removal on the Hydroxyapatite column (purification step #2). Flow Through (FT) pictured is a representative profile of the 18 FTs completed and Elution is representative of the 3 elutions completed.

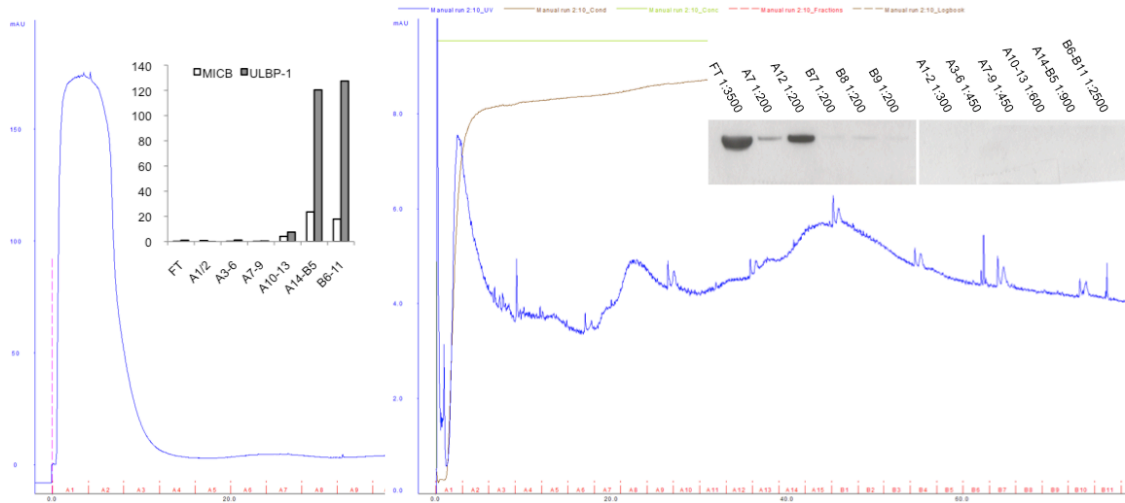


**Fig. 6.15.** Final BSA removal on the Hydroxyapatite column (purification step #3). Two previous hydroxyapatite elutions from purification step #2 were rerun to further remove remaining BSA.

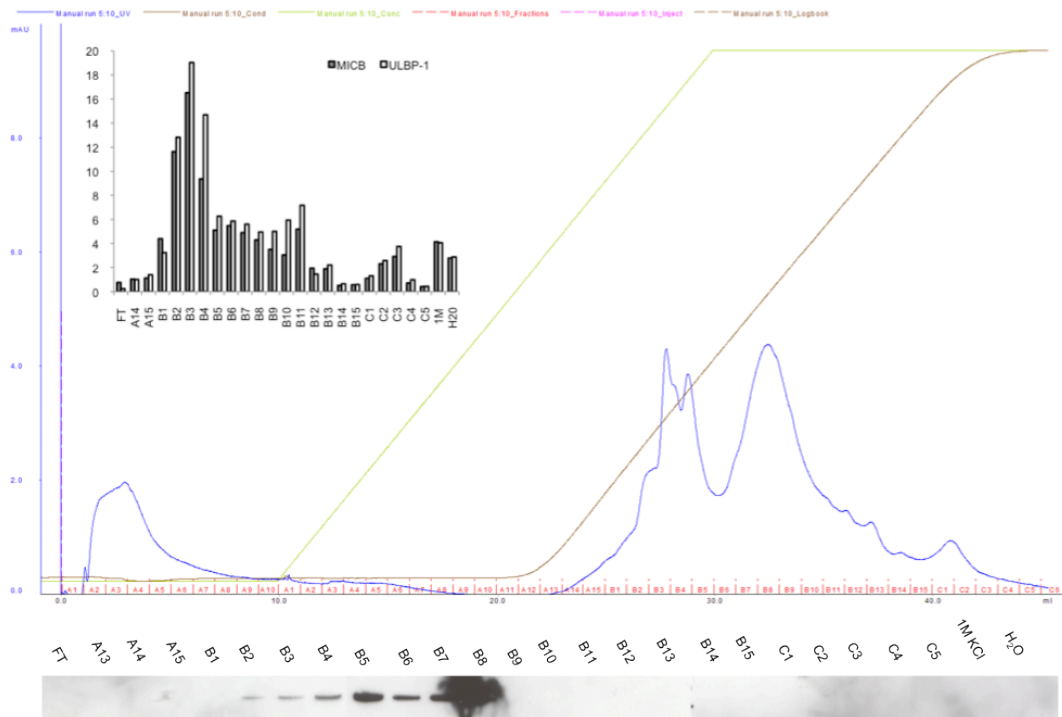


**Fig. 6.16.** MonoQ Gradient (purification step #4). Removal of BSA and further purification of ULBP1 activity. All fractions run on western at 1:50 dilution.

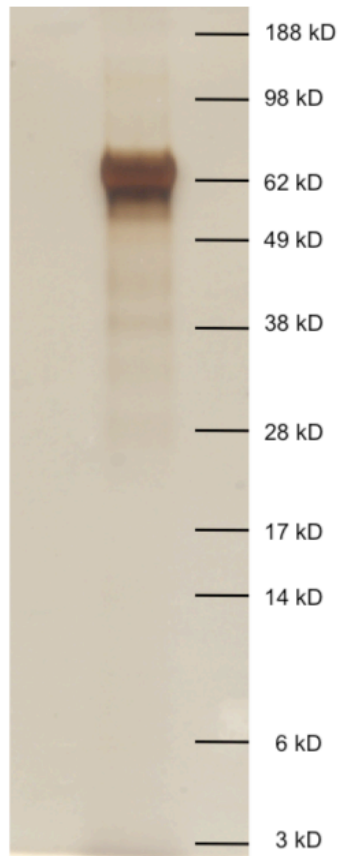


**Fig. 6.17.** Silver stain of 1/3 of MonoQ gradient (purification step #4) fraction B3.

# Unique Peptides	% Coverage	Species	Protein Name
74	83.9	BOVIN	Serum albumin
15	30.2	BOVIN	Alpha-fetoprotein
11	28.8	BOVIN	Alpha-1-antiproteinase
13	32.7	BOVIN	Pigment epithelium-derived factor
14	30.1	BOVIN	Antithrombin-III
8	38.6	BOVIN	Alpha-1-acid glycoprotein
6	21.8	BOVIN	Plasma serine protease inhibitor
7	11	BOVIN	Complement factor I
6	21.9	BOVIN	Serum amyloid P-component
3	19.7	BOVIN	Transthyretin
3	7.6	BOVIN	Vitamin D-binding protein
1	6	<b>HUMAN</b>	L-lactate dehydrogenase A chain
1	6.8	BOVIN	40S ribosomal protein S6
3	3	BOVIN	Thrombospondin-1
2	5.5	BOVIN	Serpin peptidase inhibitor, member 2
3	7	BOVIN	Uncharacterized protein
2	4.8	BOVIN	Endopin 2
3	7.1	BOVIN	Serpin A3-2
1	31.1	BOVIN	Haptoglobin
3	1.2	<b>HUMAN</b>	Collagen alpha-1(V) chain
1	4.8	BOVIN	40S ribosomal protein S2
1	1.4	BOVIN	Complement factor B
1	2	BOVIN	Plasma kallikrein
2	4.9	BOVIN	Betaine--homocysteine S-methyltransferase 1
1	9	BOVIN	Hemoglobin subunit beta
1	20	BOVIN	Pancreatic elastase inhibitor
1	4.6	BOVIN	Proliferation-associated protein 2G4
4	4.8	BOVIN	Serotransferrin
1	3.5	BOVIN	Heterogeneous nuclear ribonucleoprotein K
1	2.5	BOVIN	Plasminogen activator inhibitor 1
1	0.7	BOVIN	Collagen alpha-1(I) chain
1	4.9	BOVIN	Uncharacterized protein
2	1.1	BOVIN	Collagen alpha-1(II) chain
1	3.1	BOVIN	Vitamin K-dependent protein C (Fragment)
1	0.6	BOVIN	Complement factor H

**Table 6.3.** Proteins detected in the silver stain of Purification #2 MonoQ B3 fraction.



The main intracellular function of LDH is to catalyze the interconversion of pyruvate and lactate with concomitant interconversion of NADH and NAD<sup>+</sup>. Under oxygen-poor conditions LDH converts pyruvate, the final product of glycolysis, to lactate (Fig. 6.18). It then performs the reverse reaction during the Cori cycle in the liver. Therefore, it is not surprising that in the anaerobic tumor environment this enzyme would be upregulated and abundant.

Its normal subcellular localization is the mitochondrion and it is thought that LDH is only non-specifically released into the extracellular environment as a consequence of cytotoxicity and rupture of the cell membrane. Our observations from the unbiased purification of ULBP1h, suggest there may be another more specific mechanism of extracellular release of LDH by tumor cells. We do not observe any cytopathic effects in the U87 culture. Furthermore, we have observed low complexity and low protein abundance in the serum-free culture of these cells, indicating there is likely little to no lysis and consequent non-specific emptying of cellular contents into the media. These observations suggest that glioma cells, and likely other tumor types, are selectively secreting LDH into the extracellular environment. Interestingly, a correlation has been observed between elevated LDH secretion in breast cancer patients and NK cell dysfunction (12). Again, the authors suggest the release of LDH into the serum is a result of cell membrane permeabilization, but perhaps it is instead due to the increased secretion of LDH by the tumor cells, which could directly result in NK cell exhaustion and dysfunction.

There are 5 isoenzymes of LDH; LDH1, LDH2, LDH3, LDH4, LDH5. These isoenzymes are comprised of hetero or homo tetramers of M or H subunits. The M chain is encoded by the *ldha* gene, while the H chain is encoded by the *ldhb* chain. The abundance of each isoenzyme is tissue specific (Table 6.4). Astrocytes, which give rise to glioblastoma, contain both LDH1 and LDH5 (1). To determine if NK cell ligand upregulation is a novel function of LDH, we obtained purified, native LDH1 and LDH5 and tested these active enzymes in our NK cell ligand-upregulating assay. To control for the stress/toxicity the presence of a large amount of protein might induce, we used an enzyme known to be secreted by glioma cells, recombinant matrix metallo-protease 9 (MMP9)(11, 18). To our gratification, both LDH1 and LDH5 induce MICB and ULBP1 upregulation, while MMP9 had no effect. Furthermore, the induction profile mirrors the activity of ULBP1h, preferentially upregulating ULBP1 in comparison to MICB (Fig. 6.19). These results suggest that we have identified LDH as the factor secreted by glioma cells.

Future studies will be needed to further confirm this finding through inhibition of LDH in glioma supernatant and in primary patient serum samples. It will also be interesting to determine the specific LDH isoenzymes responsible for the glioma cell secreted activity and the mechanism by which it is inducing the ligand upregulation. LDH inhibitor, Oxamate, specifically targets the active site of LDH1 and LDH5. This tool will help to confirm the discovery that LDH is responsible for the ULBP1 upregulating activity and narrow the isoenzyme candidates. If oxamate inhibits ULBP1h activity in our samples, we will be able

to further differentiate between LDH1 and LDH5 utilizing the LDH5-specific inhibitor, silver nitrate. This chemical specifically binds and inactivates the alpha chain of LDH and therefore inhibits LDH2, LDH3, LDH4, and LDH5, but not LDH1, which is comprised of four B chains. These findings will provide novel tools with which to study NKG2D ligands and their specific functions as well as provide much needed insight into the immune evasion mechanism of glioblastoma and possibly many other LDH-secreting tumors.

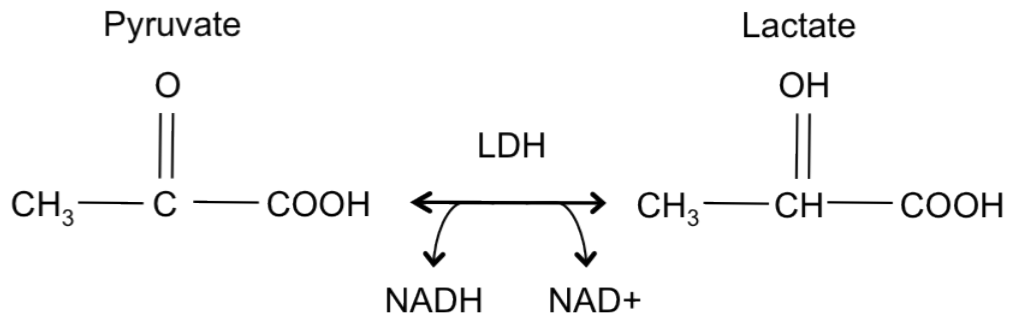


**Fig. 6.18.** Enzymatic conversion of pyruvate conversion to lactate catalyzed by L-lactate dehydrogenase.

<b>Isoenzyme</b>	<b>Localization</b>
LDH1	Heart, red blood cells
LDH2	Reticuloendothelial system
LDH3	Lungs
LDH4	Kidneys, placenta, pancreas
LDH5	Liver, striated muscle

**Table 6.4.** Tissue abundance of LDH isoenzymes

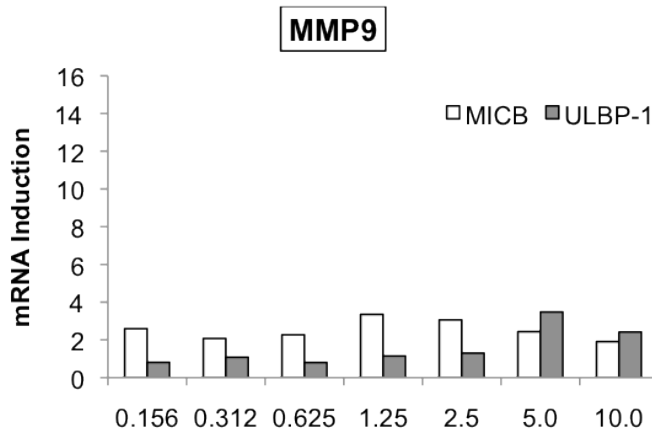
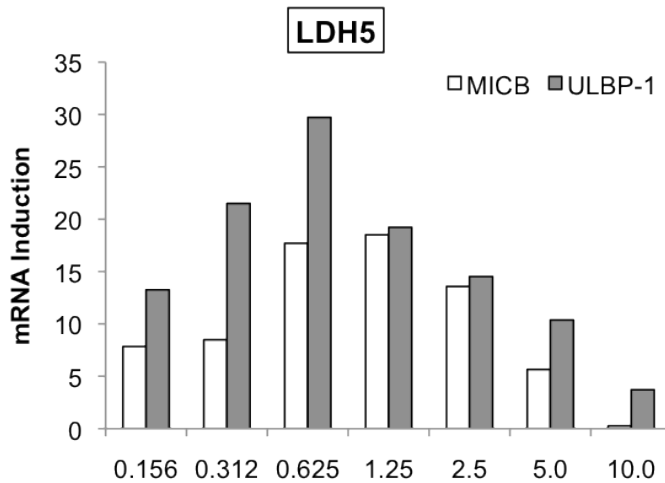
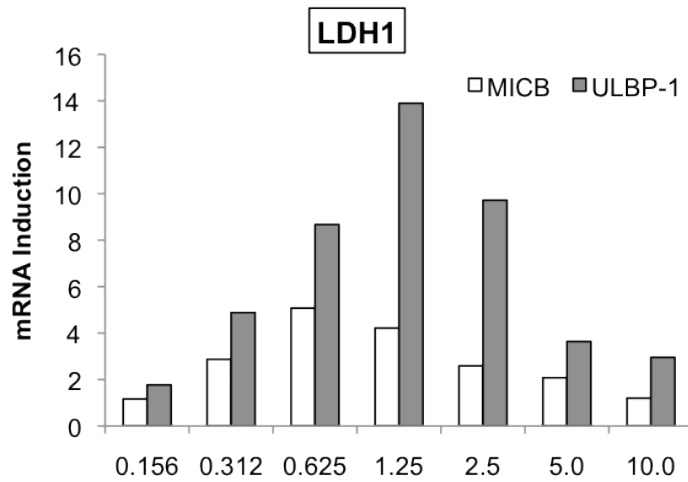


**Fig. 6.19. Purified LDH1 and LDH5 ( $\mu\text{g/ml}$ ) contains NK cell ligand-upregulating activity. The preferential upregulation of ULPB-1 mirrors the activity profile of the activity purified and analyzed by mass spec. This is in contrast to the lack of activity from a known purified secreted protein, r.MMP9.**

The identity of MICBh, the second NKG2D ligand-inducing activity, remains to be identified. Due to the nature of its separation on the Hydroxyapatite column (eluting with ~99% of bovine albumin and other serum components), we were unable to identify that activity using this biochemical purification scheme. By switching to serum-free conditions, we are still able to separate the two activities and can develop a new purification scheme specifically for MICBh (Fig. 6.20). However, because there are 5 LDH isoenzymes, it may be possible that they display different NK cell ligand upregulating activities. To rule out the possibility that MICBh is also an LDH isoenzyme we probed MICBh-containing fractions with an LDH-specific antibody. Surprisingly, LDH seems to correlate with the fractions containing MICBh activity when separated on the MonoS ion exchange column (Fig 6.21). While suggestive, these results will need to be verified using an LDH inhibitors, Oxamate and silver nitrate, to confirm if the MICBh activity is also due to LDH. If the MICBh activity remains in the presence of the LDH inhibitors, we will utilize the serum-free purification scheme to identify the protein responsible for this second activity.

The discovery of this novel function of LDH has many implications for glioblastoma and the many other tumor types where LDH upregulation and secretion are observed. LDH inhibition may effectively target tumor cells through two mechanisms; (1) selectively target metabolically impaired cells dependent on LDH's enzymatic function in the anaerobic tumor environment and (2) improve

the NK cell response to these aberrant cells and consequently increasing the effectiveness of immune therapy against these tumor types.

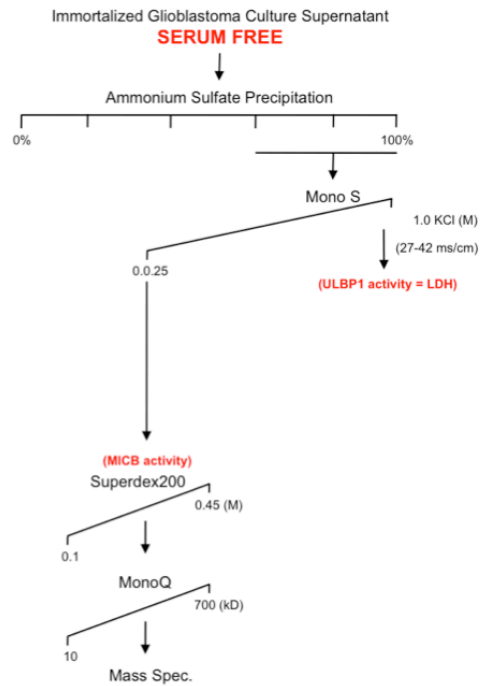


**Fig. 6.20.** Purification scheme for secreted glioblastoma factor (MICBh) responsible for NK cell ligand MICB upregulation on primary monocytes.

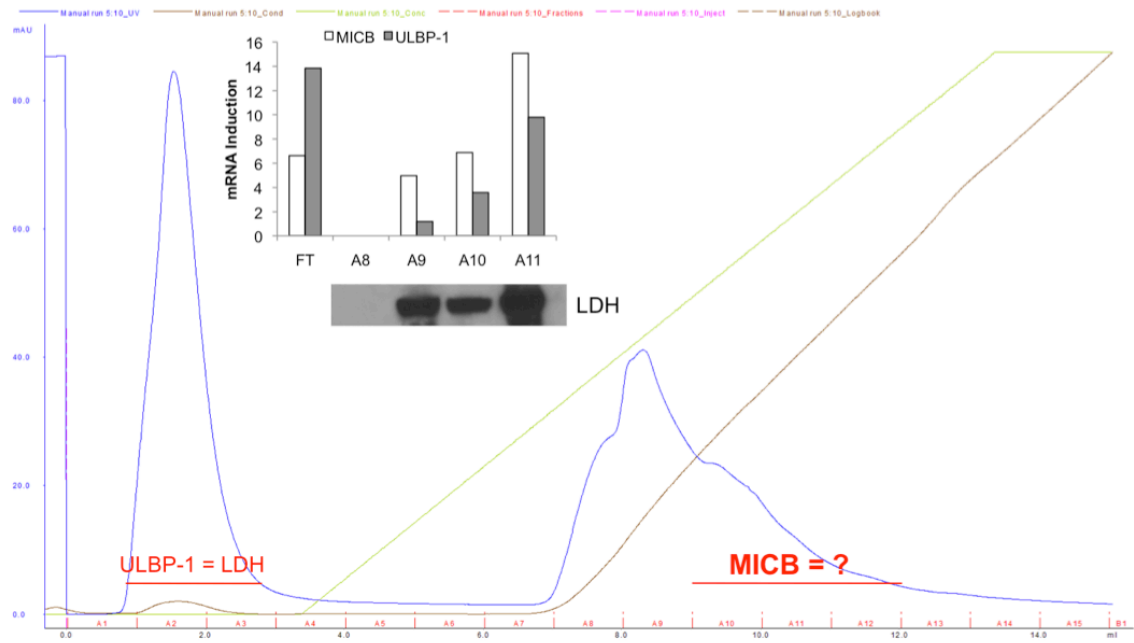


**Fig. 6.21.** Fractions from the MonoS purification step of the serum-free purification scheme, targeting MICBh isolation, probed for NK cell ligand-upregulating activity and the presence of LDH by western blot. Previously identified LDH/ULBP-1h does not bind to the MonoS and is therefore present in the Flow Thru (FT) fraction.



## Materials and Methods

**Cell Culture and Reagents.** Immortalized U87 glioblastoma cell line cultured in 5% bovine serum DMEM. LDH antibody (Abcam) used for western blot. Sybrgreen mix (Invitrogen) was used for detection of MICA, MICB, and ULBP-1 mRNA in primary monocytes. Mass Spectrometry compatible Silver stain (Pierce) was done according to manufacturer's instruction. The FPLC used was a GE Healthcare AKTA FPLC™. All FPLC columns were provided by GE Healthcare.

**NK cell ligand-upregulation Assay.** 50ul of test solution is incubated with  $1 \times 10^3$  isolated primary monocytes isolated from healthy anonymous donors (obtained from the Blood Centers of the Pacific) for 18h. mRNA is isolated from primary monocytes using a Qiagen RNeasy kit. RT-qPCR is performed using Invitrogen Sybrgreen and a BIO-RAD 4300 RT-qPCR machine. Fold induction of NK cell ligands is calculated using the Pfaffel method.

**Purification #1 Conditions.** Twelve liters of U87 media supernatant were concentrated 10 fold, then ~75% of protein was removed using an Ammonium Sulfate Cut. The activity precipitated in the 60-100% saturated ammonium sulfate fraction. This fraction was then further purified on the Phenyl Sepharose Column using a binding buffer of, 1M ammonium sulfate, 100mM  $\text{Na}_5\text{HPO}_4$ , and an elution buffer of, 100mM  $\text{Na}_2\text{HPO}_4$ . The active fraction was then separated in

Phosphate buffered saline on a gel filtration column (Superdex 200). The active fraction obtained from the gel filtration column was purified on an ion exchange column (MonoS) using the binding buffer, 25mM KCl, 50mM sodium acetate, pH 5.0, and the elution buffer, 1M KCl, 50mM sodium acetate, pH 5.0.

**Purification #2 Conditions.** Twelve liters of U87 media supernatant were concentrated 10 fold, then ~75% of protein was removed using an Ammonium Sulfate Cut. The activity precipitated in the 60-100% saturated ammonium sulfate fraction. The majority of bovine serum albumin was removed using the Hydroxyapatite column under conditions in which albumin did not bind, but the ULBP1h target does; binding buffer, 0.11M Na<sub>2</sub>HPO<sub>4</sub>, 0.02M sodium acetate, pH 6.8, elution buffer, 0.33M Na<sub>2</sub>HPO<sub>4</sub>, 0.02M sodium acetate, pH 6.8. This column was run at room temperature to avoid buffer precipitation. The ion exchange (MonoQ) gradient was the final step of purification using the binding buffer, 0.1M KCl, and elution buffer, 0.45M KCl.

## **Acknowledgements**

We would like to thank Courtney Crane, Ph.D. for being an amazing collaborator and for discovering this exciting phenotype. We would also like to thank Lewis Lanier, M.D. for his helpful scientific advice.

## References

1. **Bittar, P. G., Y. Charnay, L. Pellerin, C. Bouras, and P. J. Magistretti.** 1996. Selective distribution of lactate dehydrogenase isoenzymes in neurons and astrocytes of human brain. *J Cereb Blood Flow Metab* **16**:1079-1089.
2. **Buckner, J. C., P. D. Brown, B. P. O'Neill, F. B. Meyer, C. J. Wetmore, and J. H. Uhm.** 2007. Central nervous system tumors. *Mayo Clin Proc* **82**:1271-1286.
3. **Cerwenka, A., and L. L. Lanier.** 2001. Natural killer cells, viruses and cancer. *Nat Rev Immunol* **1**:41-49.
4. **Cerwenka, A., and L. L. Lanier.** 2003. NKG2D ligands: unconventional MHC class I-like molecules exploited by viruses and cancer. *Tissue Antigens* **61**:335-343.
5. **Champsaur, M., and L. L. Lanier.** 2010. Effect of NKG2D ligand expression on host immune responses. *Immunol Rev* **235**:267-285.
6. **Chen, Y., H. Zhang, A. Xu, N. Li, J. Liu, C. Liu, D. Lv, S. Wu, L. Huang, S. Yang, D. He, and X. Xiao.** 2006. Elevation of serum l-lactate dehydrogenase B correlated with the clinical stage of lung cancer. *Lung Cancer* **54**:95-102.
7. **Crane, C. A., S. J. Han, J. J. Barry, B. J. Ahn, L. L. Lanier, and A. T. Parsa.** 2010. TGF-beta downregulates the activating receptor NKG2D on NK cells and CD8+ T cells in glioma patients. *Neuro Oncol* **12**:7-13.
8. **Dimopoulos, M. A., B. Barlogie, T. L. Smith, and R. Alexanian.** 1991. High serum lactate dehydrogenase level as a marker for drug resistance and short survival in multiple myeloma. *Ann Intern Med* **115**:931-935.
9. **Dix, R. D., E. R. Podack, and S. W. Cousins.** 2003. Loss of the perforin cytotoxic pathway predisposes mice to experimental cytomegalovirus retinitis. *J Virol* **77**:3402-3408.
10. **Gonzalez-Billalabeitia, E., R. Hitt, J. Fernandez, E. Conde, F. Martinez-Tello, R. Enriquez de Salamanca, and H. Cortes-Funes.** 2009. Pre-treatment serum lactate dehydrogenase level is an important prognostic factor in high-grade extremity osteosarcoma. *Clin Transl Oncol* **11**:479-483.
11. **Komatsu, K., Y. Nakanishi, N. Nemoto, T. Hori, T. Sawada, and M. Kobayashi.** 2004. Expression and quantitative analysis of matrix metalloproteinase-2 and -9 in human gliomas. *Brain Tumor Pathol* **21**:105-112.
12. **Konjevic, G., V. Jurisic, and I. Spuzic.** 2001. Association of NK cell dysfunction with changes in LDH characteristics of peripheral blood lymphocytes (PBL) in breast cancer patients. *Breast Cancer Res Treat* **66**:255-263.
13. **Lanier, L. L.** 2001. On guard--activating NK cell receptors. *Nat Immunol* **2**:23-27.
14. **Moretta, A., G. Pantaleo, L. Moretta, J. C. Cerottini, and M. C. Mingari.** 1983. Direct demonstration of the clonogenic potential of every human peripheral blood T cell. Clonal analysis of HLA-DR expression and cytolytic activity. *J Exp Med* **157**:743-754.
15. **Smyth, M. J., D. I. Godfrey, and J. A. Trapani.** 2001. A fresh look at tumor immunosurveillance and immunotherapy. *Nat Immunol* **2**:293-299.

16. **Suguro, M., Y. Kanda, R. Yamamoto, A. Chizuka, T. Hamaki, T. Matsuyama, N. Takezako, A. Miwa, and A. Togawa.** 2000. High serum lactate dehydrogenase level predicts short survival after vincristine-doxorubicin-dexamethasone (VAD) salvage for refractory multiple myeloma. *Am J Hematol* **65**:132-135.
17. **Van Meir, E. G., C. G. Hadjipanayis, A. D. Norden, H. K. Shu, P. Y. Wen, and J. J. Olson.** 2010. Exciting new advances in neuro-oncology: the avenue to a cure for malignant glioma. *CA Cancer J Clin* **60**:166-193.
18. **Wang, M., T. Wang, S. Liu, D. Yoshida, and A. Teramoto.** 2003. The expression of matrix metalloproteinase-2 and -9 in human gliomas of different pathological grades. *Brain Tumor Pathol* **20**:65-72.
19. **Wassell, D. T., R. C. Hall, and G. Embery.** 1995. Adsorption of bovine serum albumin onto hydroxyapatite. *Biomaterials* **16**:697-702.
20. **Yuce, K., C. Baykal, C. Genc, A. Al, and A. Ayhan.** 2001. Diagnostic and prognostic value of serum and peritoneal fluid lactate dehydrogenase in epithelial ovarian cancer. *Eur J Gynaecol Oncol* **22**:228-232.

## CHAPTER 7

### Summary

#### **Novel components of the ER stress-induced apoptotic pathway**

CRK is a novel pro-apoptotic BH3-only protein activated upon irremediable ER stress (see Chapter 2). This finding challenges the conventional idea that BH3-only proteins are designed to specifically mediate apoptosis. It is possible cellular biology has evolved in response to terminal damage to convert a molecule critical to many aspects of cellular function into an executor of apoptosis. CRK has previously only been known as an adaptor molecule facilitating a number of different cellular functions, including cell morphology, movement, proliferation, and differentiation (1). In Figure 7.1 we present a model of the mechanism of CRK activation upon irremediable ER stress. In addition, we have identified that an upstream cysteine protease is responsible for activating the pro-apoptotic BH3-only CRK. This cysteine protease is not caspase 2, which we previously demonstrated is activated upon irremediable ER stress (2). Surprisingly, preliminary data indicate that cathepsin B plays a likely role in CRK cleavage (see Chapter 3). This discovery suggests an exciting and previously unknown role for lysosomal components in ER stress-induced apoptosis. Further studies are necessary to confirm the role of Cathepsin B in

this pathway and the mechanism of its activation. These findings provide much needed insight into this critical pathway.

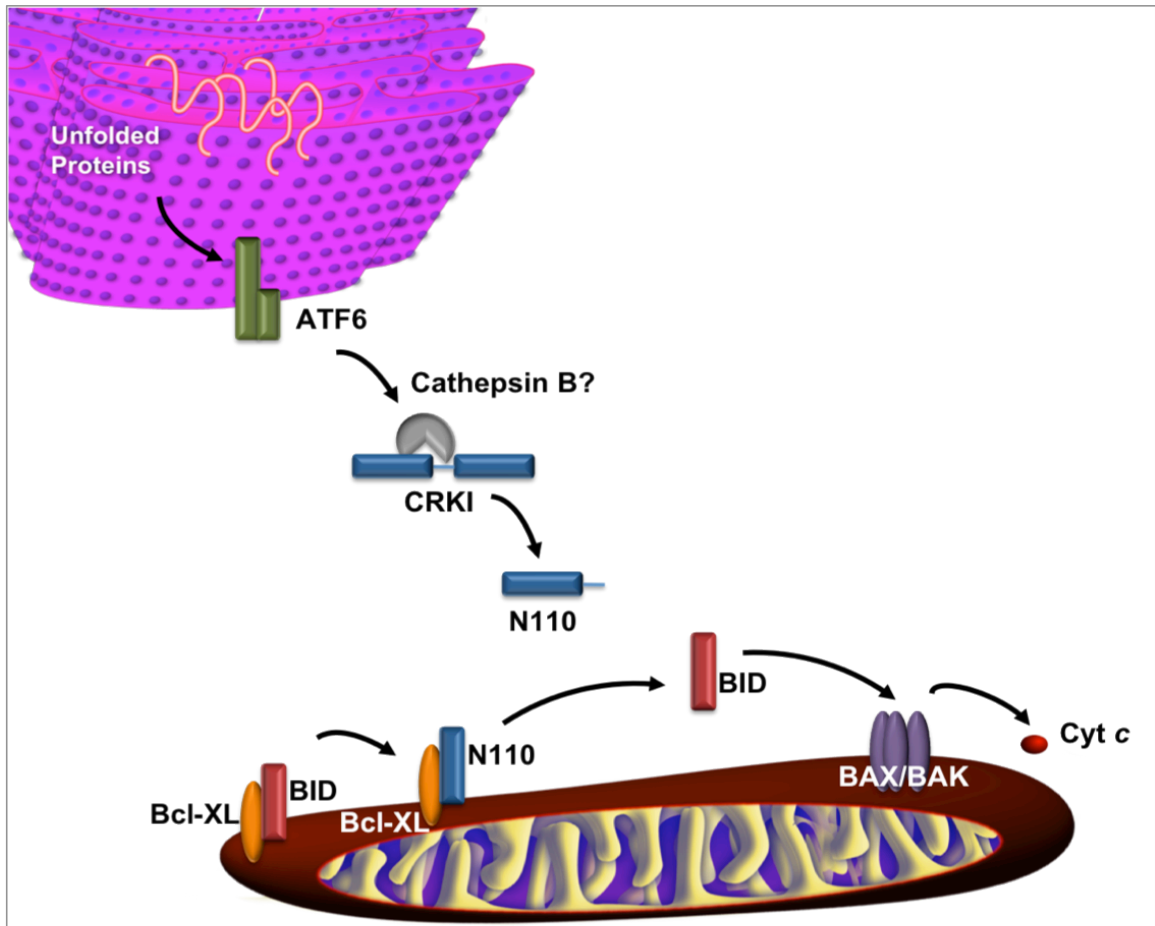


**Fig. 7.1. Model of pro-apoptotic CRK mechanism.** ATF6 senses unfolded proteins within the ER, then through an unknown mechanism activates a cysteine protease, potentially Cathepsin B. This cysteine protease then cleaves CRKI or CRKII (CRKI represented in model) at D110. This creates an N-terminal fragment (N110) which contains a sensitizing BH3-only domain. N110 binds anti-apoptotic Bcl-XL at the mitochondria, displacing activating BH3-only BID. Bid then binds BAX/BAK, inducing oligomerization and cytochrome c release.

## **KSHV manipulation of the UPR**

The study of viral manipulation of host machinery has historically provided great insight into cellular biology. Here, we have utilized the large DNA virus, Kaposi's sarcoma-associated herpesvirus, to further understand the cytoprotective/cytotoxic threshold of the unfolded protein response pathway (UPR)(Chapter 4). While determining the usefulness of UPR knockout MEFs in our study, we have provided much needed insight into the possibility of the development of a murine model of KSHV infection by identifying the multiple defects in viral replication in this species (Chapter 5).

By monitoring the state of the IRE1/XBP1 branch of the UPR, we discovered that lytically replicating KSHV actively inhibits splicing of the XBP1 transcript. This splicing event allows for translation of an active transcription factor, XBP1, which is responsible and required for ER expansion. This observation led to the finding that despite the absence of XBP1, the host ER expands significantly during the KSHV lytic cycle. This is likely in response to the acute influx of viral proteins that need to be folded and modified during viral replication. These findings led to the identification of two novel phenotypes of KSHV; (1) KSHV encodes an inhibitor of XBP1 splicing and (2) KSHV utilizes an XBP1-independent mechanism of ER expansion. While initial attempts to define the XBP1-independent ER expansion mechanism were unsuccessful, we have provided a model of two likely possibilities (Fig. 7.2).

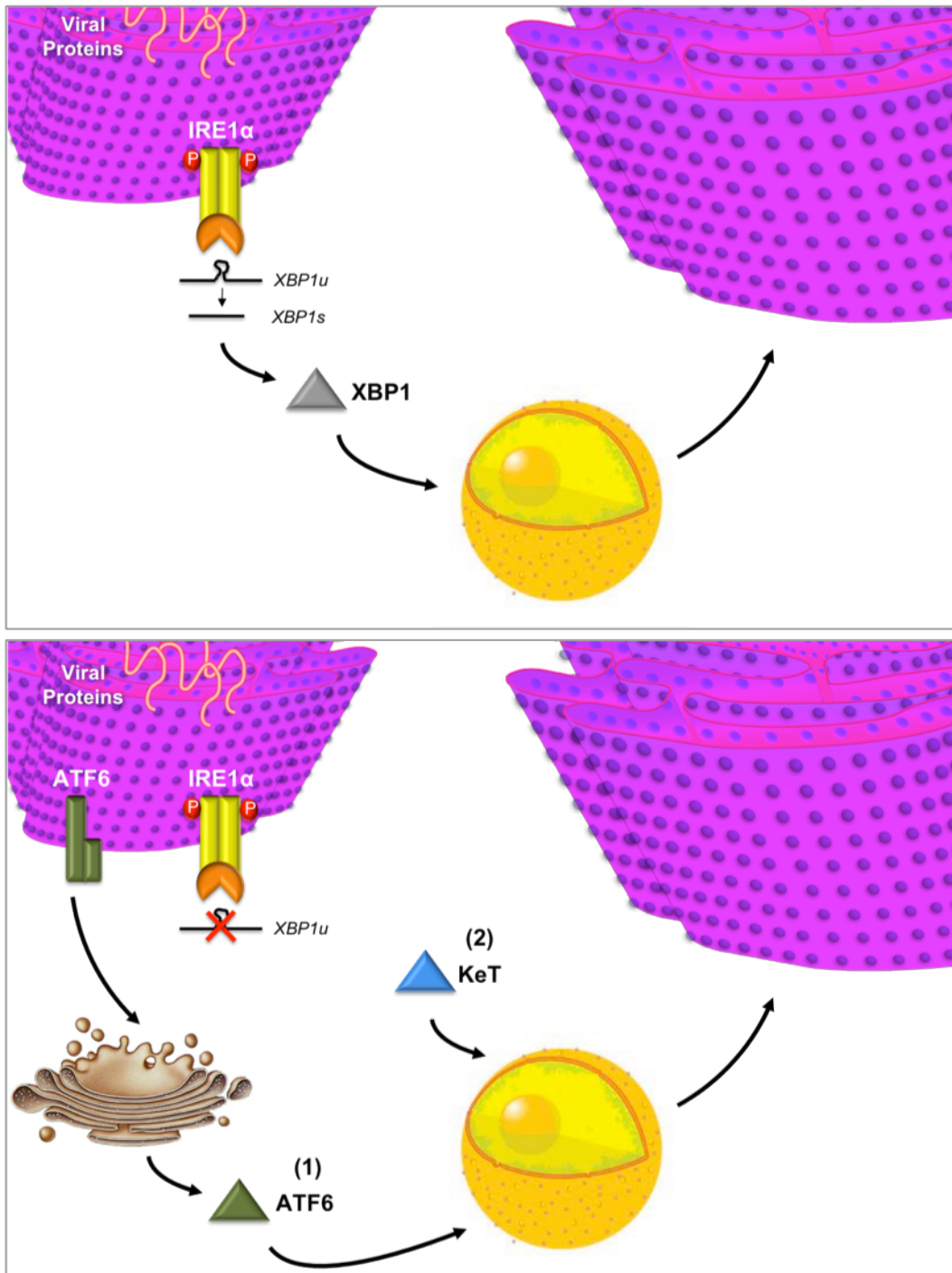


**Fig. 7.2. Model of potential XBP1-independent ER expansion mechanisms.** A) Normally, IRE1 $\alpha$  facilitates splicing of the *XBP1* transcript, resulting in a transcription factor responsible for ER expansion. B) During KSHV lytic replication, XBP1 splicing is inhibited. Two possible mechanisms of XBP1-independent ER expansion; 1) Utilize ER expansion potential of ATF6 2) KSHV encodes “substitute” transcription factor (KeT).



## **Identification of a novel function of LDH and its role in GBM immune evasion**

Using an unbiased biochemical approach, we have identified a novel function of L-lactate dehydrogenase. LDH plays an important role in the immune evasion mechanism of glioblastoma (GBM) cells. GBM cells secrete LDH into the extracellular environment resulting in the upregulation of NKG2D ligands, MICB and ULBP1, on tumor infiltrating monocytic myeloid cells. This results in the retargeting of Natural Killer (NK) cells to these monocytic myeloid cells. NK cells then exhaust their cytotoxic potential on the decoy monocytic cells, preventing them from then lysing the tumor cells (Fig. 7.3).

This discovery expands the known function of LDH, primarily thought to only have metabolic enzymatic activity and provides a unique biochemical tool to further dissect the differences between the signaling outcomes of the eight human NKG2D ligands. In addition, this finding provides a promising therapeutic target for this aggressive and deadly tumor type. Immunotherapy is a very promising therapeutic approach for this disease and identifying a way to increase a patient's innate immune response could have an enormous impact on the efficacy of this promising treatment.

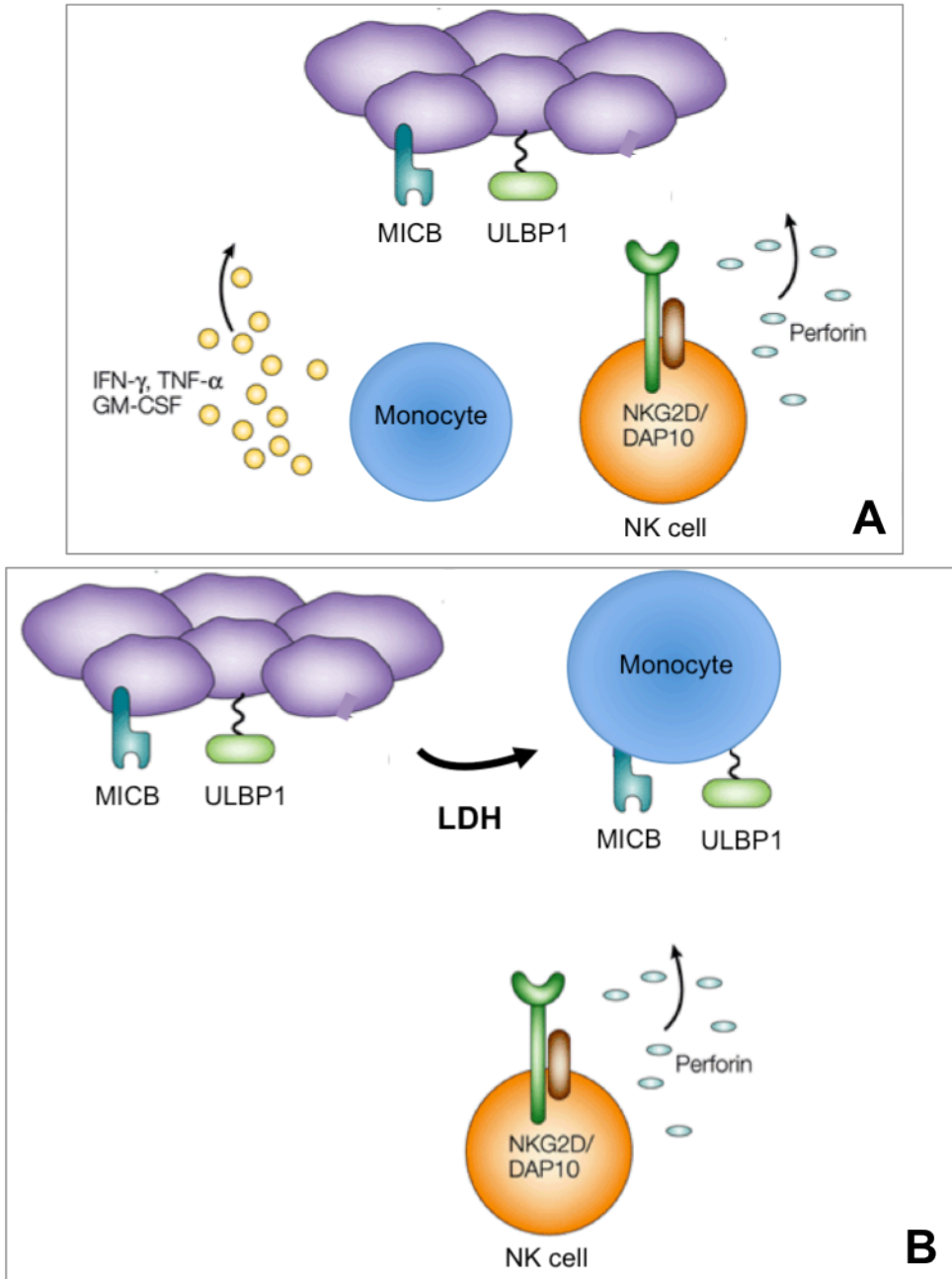


**Fig. 7.3. Model of LDH mechanism in GBM NK cell evasion.** A) In the absence of immune evasion tactics, NK cells and monocytes target tumor cells with cytolytic perforin and immunosuppressive cytokines. B) GBM cells secrete LDH, which upregulates NKG2D ligands on monocytic myeloid cells. This results in NK cells exhausting their killing potential on these “decoy” cells.

## References

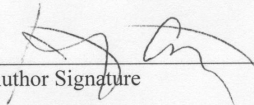
1. **Feller, S. M.** 2001. Crk family adaptors-signalling complex formation and biological roles. *Oncogene* **20**:6348-6371.
2. **Upton, J. P., K. Austgen, M. Nishino, K. M. Coakley, A. Hagen, D. Han, F. R. Papa, and S. A. Oakes.** 2008. Caspase-2 cleavage of BID is a critical apoptotic signal downstream of endoplasmic reticulum stress. *Mol Cell Biol* **28**:3943-3951.

**Publishing Agreement**

*It is the policy of the University to encourage the distribution of all theses, dissertations, and manuscripts. Copies of all UCSF theses, dissertations, and manuscripts will be routed to the library via the Graduate Division. The library will make all theses, dissertations, and manuscripts accessible to the public and will preserve these to the best of their abilities, in perpetuity.*

**Please sign the following statement:**

*I hereby grant permission to the Graduate Division of the University of California, San Francisco to release copies of my thesis, dissertation, or manuscript to the Campus Library to provide access and preservation, in whole or in part, in perpetuity.*

  
\_\_\_\_\_  
Author Signature

November 15, 2011

\_\_\_\_\_  
Date